FINAL REPORT ~ FHWA-OK-22-05

ODOT RADAR SYSTEM FOR REAL-TIME TRAFFIC FLOW MONITORING

Hazem Refai, Ph.D.
Mohamed Ali Habib
School of Electrical and Computer Engineering (ECE)
The University of Oklahoma

Joshua Qiang Li, Ph.D., P.E.
Wenyao Liu
School of Civil and Environmental Engineering
Oklahoma State University

December 2022

OKLAHOMA
Transportation

The Oklahoma Department of Transportation (ODOT) ensures that no person or groups of persons shall, on the grounds of race, color, sex, religion, national origin, age, disability, retaliation or genetic information, be excluded from participation in, be denied the benefits of, or be otherwise subjected to discrimination under any and all programs, services, or activities administered by ODOT, its recipients, sub-recipients, and contractors. To request an accommodation please contact the ADA Coordinator at 405-521-4140 or the Oklahoma Relay Service at 1-800-722-0353. If you have any ADA or Title VI questions email ODOT-ada-titlevi@odot.org.

The University of Oklahoma herein certifies that, as of the date of submission to the Oklahoma Department of Transportation, the electronic version of this report meets all federal and state online accessibility requirements pertaining to:

United States Code Title 29, Section 794d vocational rehabilitation rights to access technology, and Oklahoma State Statutes Title 62, Section 34.20 duties relating to communications systems.

and is ready for posting online.

The contents of this report reflect the views of the author(s) who is responsible for the facts and the accuracy of the data presented herein. The contents do not necessarily reflect the views of the Oklahoma Department of Transportation or the Federal Highway Administration. This report does not constitute a standard, specification, or regulation. While trade names may be used in this report, it is not intended as an endorsement of any machine, contractor, process, or product.

ODOT RADAR SYSTEM FOR REAL-TIME TRAFFIC FLOW MONITORING

FINAL REPORT ~ FHWA-OK-22-05
ODOT SPR2 ITEM NUMBER 2315

Submitted to:

Office of Research and Implementation
Oklahoma Transportation

Submitted by:

Hazem Refai, Ph.D.
Mohamed Ali Habib
School of Electrical and Computer Engineering (ECE)
The University of Oklahoma

Joshua Qiang Li, Ph.D., P.E.
Wenyao Liu
School of Civil and Environmental Engineering
Oklahoma State University

December 2022

TECHNICAL REPORT DOCUMENTATION PAGE

1. REPORT NO.	2. GOVERNMENT ACCESSION NO.	3. RECIPIENT'S CATALOG NO.
FHWA-OK-22-05		

4. TITLE AND SUBTITLE	5. REPORT DATE
ODOT Radar System for Real-Time Traffic Flow Monitoring	Dec 2022
	6. PERFORMING ORGANIZATION CODE
7. AUTHOR(S): Hazem Refai, Ph.D. and Mohamed Ali Habib, Joshua Qiang Li, Ph.D., and Wenyao Liu	8. PERFORMING ORGANIZATION REPORT Click here to enter text.
9. PERFORMING ORGANIZATION NAME AND ADDRESS The University of Oklahoma 660 Parrington Oval, Norman, OK. 73019	10. WORK UNIT NO.
	11. CONTRACT OR GRANT NO. ODOT SPR Item Number 2314
12. SPONSORING AGENCY NAME AND ADDRESS Oklahoma Transportation Office of Research and Implementation 200 N.E. 21st Street, Rm. 3A7 Oklahoma City, OK 73105	13. TYPE OF REPORT AND PERIOD COVERED Final Report Oct 2021 - Sep 2022
	14. SPONSORING AGENCY CODE

15. SUPPLEMENTARY NOTES

16. ABSTRACT

This report presents research results and experiments that were designed to compare four traffic systems: Radar, AVC, HERE, and INRIX in terms of speed, volume, and travel time. The first three chapters introduce the systems, related studies, data collection procedures, and preprocessing techniques. The second three chapters detail the comparison results. Machine learning models that utilize radar speed data for travel time estimation are introduced in chapter 7. Chapter 8 presents the geospatial and temporal analysis experiment results.

17. KEY WORDS	18. DISTRIBUTION STATEMENT
Travel Time, Speed, Analysis, Radar, AVC, HERE, INRIX, Estimation Models	No restrictions. This publication is available from the Office of Research and Implementation, Oklahoma DOT.

19. SECURITY CLASSIF. (OF THIS REPORT)	20. SECURITY CLASSIF. (OF THIS PAGE)	21. NO. OF PAGES	22. PRICE
Unclassified	Unclassified	73	N/A

Form DOT F 1700.7 (08/72)

SI* (MODERN METRIC) CONVERSION FACTORS

APPROXIMATE CONVERSIONS TO SI UNITS

SYMBOL	WHEN YOU KNOW	MULTIPLY BY	TO FIND	SYMBOL
		LENGTH		
in	inches	25.4	millimeters	mm
ft	feet	0.305	meters	m
yd	yards	0.914	meters	m
mi	miles	1.61	kilometers	km
		AREA		
in^2	square inches	645.2	square millimeters	mm^2
ft^2	square feet	0.093	square meters	m^2
yd^2	square yard	0.836	square meters	m^2
ac	acres	0.405	hectares	ha
mi^2	square miles	2.59	square kilometers	km^2
		VOLUME		
fl oz	fluid ounces	29.57	milliliters	m
gal	gallons	3.785	liters	L
ft^3	cubic feet	0.028	cubic meters	L
yd^3	cubic yards	0.765	cubic meters	m^3
	NOTE: volumes greater than 1000 L shall be shown in m^3			m^3
		MASS		
oz	ounces	28.35	grams	g
lb	pounds	0.454	kilograms	kg
T	short tons (2000 lb)	0.907	megagrams (or "metric ton")	Mg (or "t")
		TEMPERATURE (exact degrees)		
°F	Fahrenheit	5 (F-32)/9 or (F-32)/1.8	Celsius	°C
		ILLUMINATION		
fc	foot-candles	10.76	lux	lx
fl	foot-Lamberts	3.426	$candela/m^2$	cd/m^2
		FORCE and PRESSURE or STRESS		
lbf	poundforce	4.45	newtons	N
lbf/in^2	poundforce per square inch	6.89	kilopascals	kPa

APPROXIMATE CONVERSIONS FROM SI UNITS

SYMBOL	WHEN YOU KNOW	MULTIPLY BY	TO FIND	SYMBOL
		LENGTH		
mm	millimeters	0.039	inches	in
m	meters	3.28	feet	ft
m	meters	1.09	yards	yd
km	kilometers	0.621	miles	mi
		AREA		
mm^2	square millimeters	0.0016	square inches	in^2
m^2	square meters	10.764	square feet	ft^2
m^2	square meters	1.195	square yards	yd^2
ha	hectares	2.47	acres	ac
km^2	square kilometers	0.386	square miles	mi^2
		VOLUME		
mL	milliliters	0.034	fluid ounces	fl oz
L	liters	0.264	gallons	gal
m^3	cubic meters	35.314	cubic feet	ft^3
m^3	cubic meters	1.307	cubic yards	yd^3
		MASS		
g	grams	0.035	ounces	oz
kg	kilograms	2.202	pounds	lb
Mg (or "t")	megagrams (or "metric ton")	1.103	short tons (2000 lb)	T
		TEMPERATURE (exact degrees)		
°C	Celsius	1.8C+32	Fahrenheit	°F
		ILLUMINATION		
lx	lux	0.0929	foot-candles	fc
cd/m^2	$candela/m^2$	0.2919	foot-Lamberts	fl
		FORCE and PRESSURE or STRESS		
N	newtons	0.225	poundforce	lbf
kPa	kilopascals	0.145	poundforce per square inch	lbf/in^2

*SI is the symbol for the International System of Units. Appropriate rounding should be made to comply with Section 4 of ASTM E380. (Revised March 2003)

Table of Contents

List of Figures

List of Tables

Chapter 1: Project Introduction and its Objectives

1.1 Background

The Oklahoma Department of Transportation (ODOT) Strategic & Performance Management (SAPM) Division has completed the deployment of 162 Houston Radar sites on major interstate and state highways in Oklahoma. Most sites are installed in the Oklahoma City (OKC) and Tulsa metropolitan areas. Eighty radar sites are collocated with current ODOT automatic vehicle classifiers (AVC). However, unlike daily transmitted AVC traffic data, radar site data are communicated to and stored on a cloud server every five minutes, making information available for sharing with other systems. Radar units are equipped with high-definition cameras to capture roadway traffic and determine if/when traffic patterns become atypical. Video feeds can also be live-streamed from each of these sites. Cameras can be programmed to acquire pictures of road traffic and store data automatically and periodically on the cloud server for future examination. Additionally, the radar units are equipped with power and thermal sensors to measure battery voltage and ambient temperature.

AVC and radar units collect individual lane traffic data, including vehicle volume, speed, and classification. Data are submitted monthly to the Federal Highway Association (FHWA) and used to calculate annual average daily traffic (AADT), among other traffic parameters. When combined with FHWA's monthly National Performance Management Research Data Set (NPMRDS), the state's passenger and freight travel reliability performance measurements can be calculated as part of the national highway system (NHS). Travel time (TT) and speed data are supplied by the INRIX company using probe-based techniques. Oklahoma's NHS is divided into roughly 5000 traffic message channels (TMC) segments, with speed data reported every five minutes.

The HERE company also supplies data to ODOT. Unlike SAPM's mandatory compliance with annual and monthly FHWA submission requirements, ODOT's Maintenance Division depends on real-time speed data to monitor traffic conditions and update TTs on overhead displays located on major road segments. Accordingly, ODOT's Maintenance Division maintains an annual subscription with HERE to receive roadway traffic speed data every five minutes. Like INRIX data, HERE data is collected using GPS-based probe vehicle travel information.

Given this availability of radar-detected average speed, vehicle volume, and class data collected at various locations every five minutes, this project aimed to develop an interface for comparing, and validating radar traffic data with data received from INRIX and HERE. Furthermore, radar data will be evaluated for use to calculate real-time TT of several ODOT-selected routes. If proven usable, models could then be constructed by incorporating radar data for predicting TTs within the OKC and Tulsa metropolitan areas.

1.2 Project Objectives

The project's research and development activities were focused on four areas: 1) developing schemes to evaluate radar data validity; 2) conducting speed comparison among various data sets (i.e., AVC, radar, HERE, and NPMRDS), and then quantifying the accuracy of each system; 3) conducting volume comparison among various data sets (e.g., AVC and radar); and 4) developing

machine learning-based models using radar data to determine TTs on major highways within the OKC and Tulsa metropolitan areas.

The first objective was developing mechanisms for collecting vehicle data from each of the four systems, namely AVC, radar, INRIX, and HERE, to preprocess each data set for validation, detect, and remove noise and outliers, and format data into an appropriate shape for analyses.

The second objective was studying speed measurements reported by radar, INRIX, and HERE systems. Knowing that speed data reported by INRIX and HERE are based on probe techniques, OU researchers were able to evaluate the differences and determine any spatial or temporal dependencies among the three systems. Notably, the AVC system was used as ground truth for accuracy analysis.

The third objective was developing models using radar data to determine TTs for ODOT-selected highway segments in the OKC and Tulsa metropolitan areas. Radar sites in both regions are reasonably dense and well distributed among major interstate highways coming into and out of the cities. The novel models will use road capacity (i.e., number of lanes), passenger vehicle and freight volume, and average speed to determine TTs.

The fourth objective was developing a statistical scheme and machine learning models leveraging radar data to accurately predict TT on ODOT-selected highway segments and cross-sections in the OKC and Tulsa metropolitan areas.

1.3 Summary of Results

During peak and off-peak hours, the average difference among the radar, INRIX, and HERE speed measurements is 7 MPH. TTs calculated for selected roadways using radar versus HERE have shown a difference of two minutes during these times. TT estimation using radars reports a one-minute difference, on average, from that of HERE during free flow. The difference could be up to four minutes, however, for a flow speed of less than 50 MPH. During slow traffic of 40 MPH or less, radars do not provide accurate speed measurements.

Chapter 2: Related Work

2.1 Introduction

Travel time (TT) estimation is a well-studied topic in ground transportation. Many studies investigated various methods for measurements, estimation, and prediction including 1) License plate matching using computer vision techniques; 2) GPS-based probe-data (INRIX); 3) Inductive loop detectors; 4) Various wireless MAC address matching by transceiver devices; and many more. This project collects vehicle flow data from four systems two of which are probe-based, and another two are sensor-based to compare.

The study referenced in [1] detailed the use of Iowa DOT (Wavetronix) radar units for calculating TT. Four radar units were deployed along a stretch of I-235 and separated by a mile or less. Calculated TT by their developed model was compared to that provided by INRIX (ground truth). The obtained mean squared error (MSE) was 0.03, 0.18, and 0.23 respectively for 1, 5, and 10 minutes of INRIX data aggregation. In [6] the authors illustrated radar highway placements along the highways to achieve accurate TT calculations.

The authors in [2] evaluate four speed-based models using data collected from two roadways in Australia. The study experimented on two segments of 4 and 8.5 mile-long. Using data collected from inductive loop detectors, the researchers estimated travel time for the selected segment. Camera-based license plate detection system was used as the ground truth. They proposed four models for TT estimations: an instantaneous model, a time slice model, a dynamic time slice model, linear model. The study results reported little difference (less than 1%) in the travel time estimation error across the models which were all found to underestimate actual travel times. Three error metrics were used to measure the performance, measures are: 1) mean absolute error (MAE) 2) root mean squared error (RMSE) 3) mean absolute relative error (MARE). The models trained on inductive loop data had about 7% of error in the off-peak periods and up to 15% in the peak periods.

The authors in [3] use a large dataset collected of 173 million taxi trips to estimate travel time between two points. They experimented on two datasets, namely, NYC Taxi and Shanghai Taxi data. Their approach outperformed available approaches, including online map services offered by Bing and Baidu. The proposed approach estimates travel time for a requested trip by examining past trips of similar characteristics regardless of the specific trajectory or path which is taken from the origin to the destination. This is adopted under the assumption that with a large amount of data, there will be enough similar data samples or trips to be used by the model to achieve stable performance. For example, given an origin point, destination point, and departure time (a query trip), the approach finds similar (neighboring) trips with similar properties and aggregates their travel time to estimate the total travel time for the queried trip. Error metrics include mean absolute error (MAE) and median absolute error (MedAE). The study compared several models to estimate travel time including but not limited to linear regression, neighbor average (AVG), and other proposed temporally weighted neighbor models. MAE error ranged from 142 seconds up to 381 seconds for the NYC dataset and from 92 up to 130 seconds for the Shanghai Taxi data. The paper proposes a baseline method that estimates travel time using some averaging techniques of similar trips. The analysis conducted in this study shows that the mean value of the travel time is a practical performance metric, even if it is estimated using other trips.
The authors in [4], performed short-time prediction on a heavily congested freeway in the Netherlands. The study proposes an online learning model whose weights or parameters, which are used for prediction, are updated at each new incoming data point; the model keeps learning after

deployment. The model consists of a 2-layer recurrent neural network (RNN) with the use of an extended Kalman Filtering (EKE). Speed data is collected using dual-loop detectors embedded in roadways every 500m (or 1640 ft) along 7km (or 4.3 miles) of a freeway, totaling 13 detector sites. Data was selected during regular congestion periods between 14:00 and 20:00. The study compared the performance of their proposed model against two other models acting as baseline models: 1) instantaneous model which sums up section-level travel time estimations to calculate the route travel time using average speed measured at the upstream and downstream detectors of each of the sections. 2) day-to-day average travel time. Error measures included: 1) root mean squared error (RMSE) 2) bias 3) root residual error (RRE) 4) squared correlation coefficient (R^2). Results reported that the proposed model and the instantaneous model both outperformed the baseline averaging model. Reported errors showed that the proposed neural network outperformed other models with an RMSE of 100 seconds while the instantaneous model had an RMSE of 167 seconds and the averaging model had an RMSE of 274 seconds.

The authors in [5] evaluate the performance of three travel time estimation methods using speed data collected per lane from dual loop detectors for a real-time display. Probe data is considered as ground truth and was obtained from FasTrak in San Francisco Bay Area with a 5-min resolution. The authors selected a 15-mile section of the EB I-80 freeway for the experiment. Different temporal periods were used for evaluation: 1) morning off-peak (12:00 AM to 7:00 AM), 2) morning peak (7:00 AM to 10:00 AM), 3) midday (10:00 AM to 3:00 PM), 4) afternoon peak (3:00 PM to 7:00 PM), and 5) afternoon off-peak (7:00 PM to 12:00 AM). Due to the significant amount of found outliers and wrong measurements in the data, the authors proposed an outlier removal method to improve the quality of the data called the local mean absolute deviation (LMM) method which is an improved scheme for the median absolute deviation (MAD) method by applying MAD in a moving window setting, the window size was set to 10 minutes, to capture the time-dependent trend in data. Three statistical models were used for travel time estimation: 1) instantaneous model: total travel time is the sum of TT estimations of individual segments or links of the highway route; this model assumes that traffic conditions such as speed remain unchanged from the time a vehicle enters a route until it exists it. 2) Dynamic Route: a model which uses speed from a future timestep in segment-level travel time calculation; therefore, this model requires future traffic information or data 3) Linear Regression. The instantaneous and linear regression models are suitable for real-time application deployment unlike the dynamic route model unless the future speed data need for link-level estimations are interpolated using some method like a forecasting model trained on historical data, however, this introduces another model which makes the dynamic route model an ensemble of two models: the original and a forecasting model, thus, increasing the complexity of the system. Error metrics include 1) Relative Error: measured as the absolute difference between the model's estimate and the median travel time from the ground truth data divided by this median. 2) Accuracy Index: which will have a value of one when the loop-based model travel time lies in an interval bounded by the 15^{th} and 85^{th} percentile travel times of the probe data and 0 otherwise. Evaluations of the proposed dynamic travel times had relative errors of 0.02, 0.13, 0.10, 0.05, and 0.07 and accuracy indices of 1.0, 0.16, 0.56, 0.31, and 0.55 for the periods: morning off-peak, morning peak, midday, afternoon peak, afternoon off-peak respectively for all lanes. The authors reported minimal difference in their findings between the performance of all the used models when the route travel time is relatively short and the transition from free-flow traffic to maximum congestion is slow and suggested the use of the instantaneous model due to its simplicity.

Chapter 3: Data Collection & Preprocessing

This section discusses the following: 1) introduction to the four systems utilized for the project, namely radar, HERE, AVC, and INRIX; 2) data format per system, as well as collection methods; 3) preprocessing algorithms and techniques for validating systems, and 4) formatting data for comparison and model development.

3.1 Systems:

As previously mentioned, this project utilized data from four systems—radar, AVC, INRIX, and HERE—for statistical analysis and machine learning model development to estimate instantaneous TT. These systems can be classified into two categories: **sensor-based** (AVC & radar) – acquire traffic data (speed and volume) via underground or highway roadside **physical sensors**, and **probe-based** (INRIX and HERE) – acquire traffic data from **cell phones** located in passenger vehicles or via in-vehicle transponders installed in commercial vehicles.

3.1.1 Radar

In January 2021, ODOT's Strategic Asset & Performance Management (SAPM) Division introduced 139 microwave radar sites (e.g., Houston Tetryon) along the interstate and major highways in Oklahoma, primarily in the Oklahoma City and Tulsa metropolitan areas. Since then, the number has increased to 147, including those for this project. Radar sensors collected traffic data, including vehicle speed, volume, and occupancy, for vehicles traveling in each direction.

Figure 3.1 illustrates the way in which a radar system collects traffic data. Radar devices are typically located on a highway shoulder or roadway median. When vehicle motion is detected, the frequency of the reflected signal changes, indicating the presence and speed of passing vehicles. Vehicles are counted via transmitting microwave signals. Because smaller vehicles are likely to be blocked by trucks or larger vehicles as they pass a radar system, speed accuracy and volume data quality could be affected. It is important to note that this problem is typical for all radar systems.

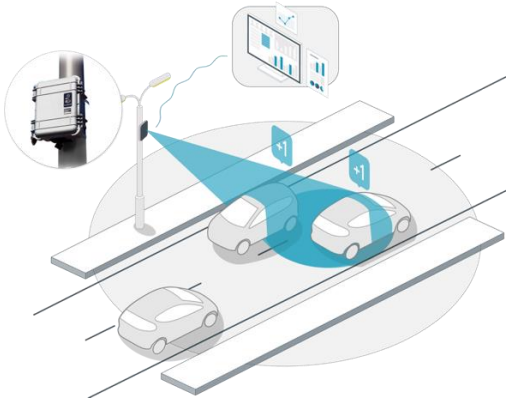

Figure 3.1. Radar station traffic monitoring.

Collected data is stored in a database on a cloud server with real-time access via the Tetryon software through http://oktrafficradar.org/. The software provides both images and a portal for accessing graphical traffic data reports from the radars. Data is also gathered and stored on a cloud server and made available for viewing through http://oktrafficradar.org/radar/data. The GUI (graphical user interface) of the website provides an interactive map (see Figure 3.2) with the state of each radar site (e.g., connected, not connected, no data, no camera snapshot). Reports for speed and class histograms can also be downloaded.

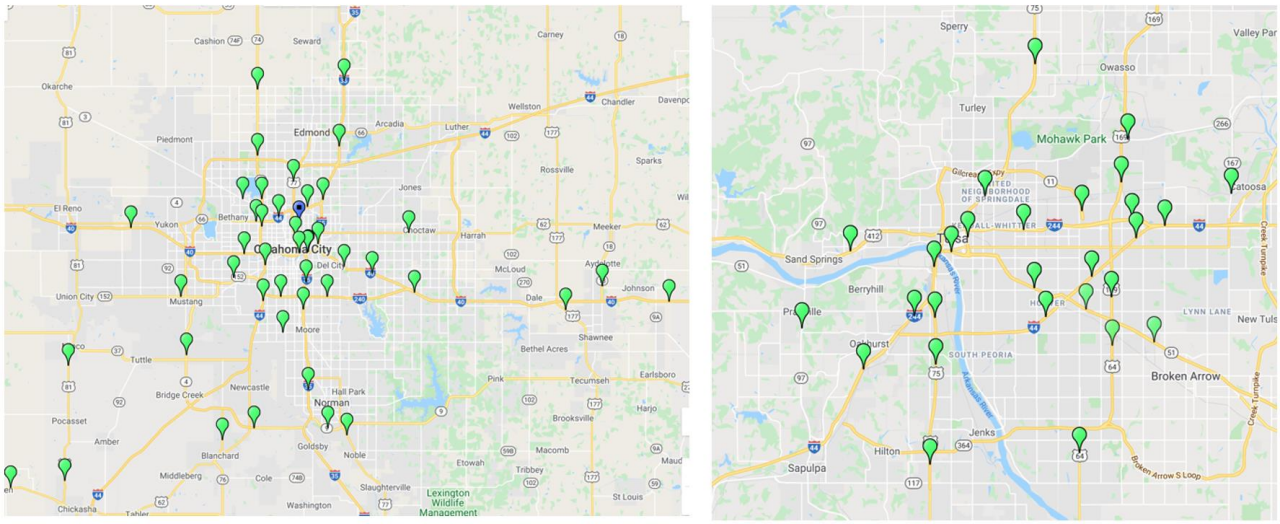

Figure 3.2. An interactive map showing radar sites in OKC and Tulsa, accessible through http://oktrafficradar.org/radar/data.

Speed data is provided in two forms: 1) average speed and 2) binned speed. Average speed incorporates all vehicles and lanes in each direction along the highway and then provides one value. Binned speed is defined over 17 speed-bins. Sensors provide vehicle counts in each speed bin. The width of each speed bin is 5 MPH, except for the lowest (i.e., all vehicles driving less than 20 MPH) and the highest (i.e., all vehicles driving faster than 95 MPH). Note that it is possible to determine an estimate of average speed using the speed bins by selecting a mid-point (i.e., value) per bin, multiplying by the number of vehicles, and then summing over all bins. We experimented with both speed types and found minimal differences between them. An average speed was used to compare and model stages for two reasons: 1) higher agreement with speed measured by other systems and 2) consistency, as other systems provide one numeric value for speed, rather than bins, except for AVC.

Data are provided per site by a separate CSV format file, each with time-stamped traffic data for vehicles traveling in both directions on the highway. The sampling interval was 15 minutes to align with AVC data. It is important to note that radar can provide traffic data at finer and coarser resolutions (e.g., 1, 5, 15, 30, and 60 minutes, etc.). Figure 3.3 shows an example of raw data for radar 811001.

```
"NAME","VOLUME","Occu-
pancy(%)","Speed
(MPH)","85%
Speed
(MPH)","0ft - 9ft","9ft - 20ft","20ft - 32ft","32ft - 43ft","43ft - 46ft","46ft - 60ft","60ft - 80ft",">80ft","HEADWAY (ms)","GAP (ms)","MM/DD/YYYY","Starting HH:MM:SS","Inter-
 val(sec)","SP1
<20mph","SP2
20mph - 25mph","SP3
25mph - 30mph","SP4
30mph - 35mph","SP5
35mph - 40mph","SP6
40mph - 45mph","SP7
45mph - 50mph","SP8
50mph - 55mph","SP9
55mph - 60mph","SP10
60mph - 65mph","SP11
65mph - 70mph","SP12
70mph - 75mph","SP13
75mph - 80mph","SP14
80mph - 85mph","SP15
85mph - 90mph","SP16
90mph - 95mph","SP17
>95mph",
00811001EB,24,0.3,49,55,0,21,3,0,0,0,0,0,31321,31163,08/01/2022,00:00:00,900,0,0,0,1,0,4,7,9,2,0,1,0,0,0,0,0,0
00811001WB,18,0,49,56,0,17,1,0,0,0,0,0,56567,56419,08/01/2022,00:00:00,900,0,0,0,3,0,1,5,6,3,0,0,0,0,0,0,0,0
00811001EB,13,0,49,54,0,12,1,0,0,0,0,0,22342,22214,08/01/2022,00:15:00,900,0,0,0,0,0,0,4,2,6,1,0,0,0,0,0,0,0,0
00811001WB,19,0,46,52,0,17,1,0,1,0,0,0,60690,60480,08/01/2022,00:15:00,900,0,0,0,1,1,4,9,3,1,0,0,0,0,0,0,0,0
00811001EB,9,0,50,55,0,7,2,0,0,0,0,0,55312,55198,08/01/2022,00:30:00,900,0,0,0,0,0,0,0,2,6,1,0,0,0,0,0,0,0,0
00811001WB,11,0,45,52,0,11,0,0,0,0,0,0,61402,63247,08/01/2022,00:30:00,900,0,0,0,0,0,1,3,4,3,0,0,0,0,0,0,0,0,0
```

Figure 3.3. An example of raw data for a radar site 811001.

Appropriate data preprocessing techniques were applied to the raw data for extracting useful information and shaping it into a convenient format used later for statistical analysis. Figure 3.4 shows the preprocessed output data format obtained after applying data processing on raw data files. This format was used to convert raw data from other systems, as well.

```
timestamp,speed,dir,radar,volume
2021-08-01 00:00:00,49,EB,811001,27
2021-08-01 00:00:00,50,WB,811001,24
2021-08-01 00:15:00,49,EB,811001,26
2021-08-01 00:15:00,47,WB,811001,24
2021-08-01 00:30:00,49,EB,811001,30
...
```

Figure 3.4. Preprocessed data format.

Finally, Figure 3.5 shows all ODOT radar sites located in the state of Oklahoma.

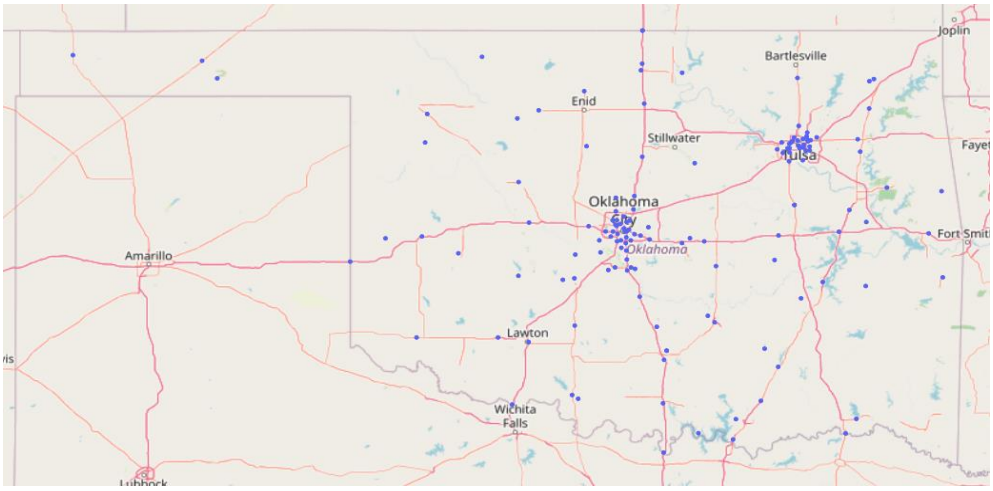

Figure 3.5. ODOT radar sites (purple dots) in Oklahoma.

3.1.2 Automatic Vehicle Classifier (AVC)

The automatic vehicle classifier (AVC) system utilizes underground, lane-specific, loop-piezo-loop detectors with PEEK ADR 2000 controllers for counting passing vehicles and collecting speed and volume data. ODOT manages 94 AVC sites throughout the state, 92 of which are collocated with radar sites.

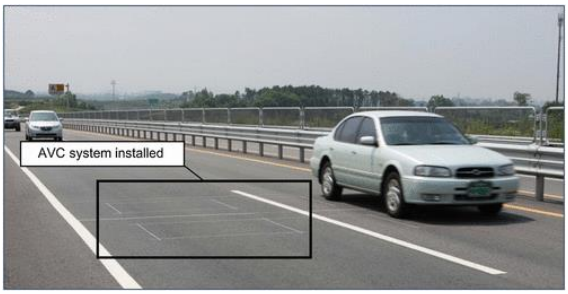

Figure 3.6. An example of an AVC site installed on an Oklahoma highway. AVC provides traffic data using inroad traffic sensors (e.g., inductive loop and piezo) and detecting the front and back wheels of passing vehicles,

Data is provided per site and separated into a CSV formatted file. Each file has time-stamped traffic data per lane per day for an entire month. Figure 3.7 shows the raw data format for an AVC site.

Figure 3.7. An example of raw traffic data for AVC site 810001.

AVC traffic data is collected daily at a sampling rate of 15 minutes. Figure 3.9 shows the speed calculation procedure for an AVC site using the 12 pre-defined speed bins. For calculations, bin mid-points are selected, and then multiplied by the number of vehicles. Sum over the bins is used to obtain an overall, average speed estimate for each timestamp. This process can be described more specifically, as follows. Let $m = \{m_1, \dots, m_{12}\}$ be a column vector that contains the mid-points for the bins and $v = \{v_1, \dots, v_{12}\}$ be the column vector containing the number of vehicles per bin. Speed can be estimated by determining the dot product of these two vectors:

$$s = m^T \cdot v$$

Figure 3.8 Average speed calculation equation for AVC raw data

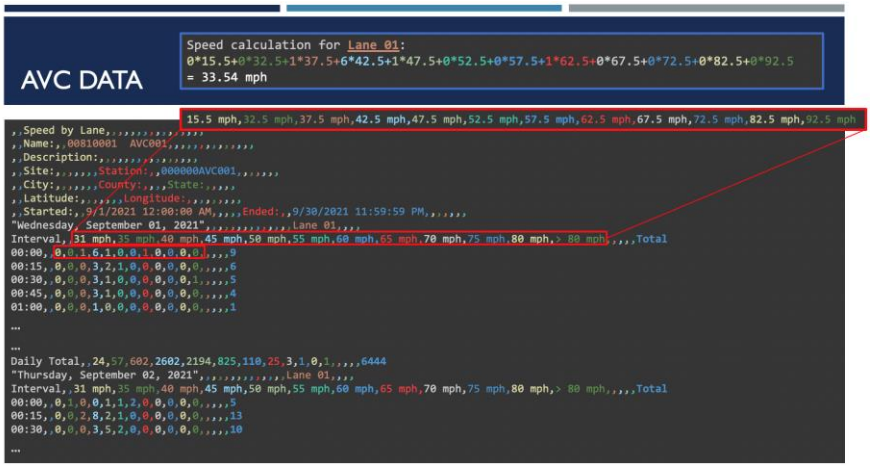

Figure 3.9. Speed calculation using bins (mid-point) for an AVC site.

AVC raw data provides information only about lanes, not vehicle direction. was used to extract directional information using lane numbering. For example, for a 2-lane NB/SB highway, lane no. 2 will be considered the NB direction, and lane no. 1 will be the SB direction.

Table 3.1
Lane-to-direction Mapping for AVC

No. of lanes	Highway directions	Direction	Lanes
2	Northbound/Southbound	Northbound	2
2	Northbound/Southbound	Southbound	1
2	Eastbound/Westbound	Eastbound	2

No. of lanes	Highway directions	Direction	Lanes
2	Eastbound/Westbound	Westbound	1
4	Northbound/Southbound	Northbound	3, 4
4	Northbound/Southbound	Southbound	1, 2
4	Eastbound/Westbound	Eastbound	3, 4
4	Eastbound/Westbound	Westbound	1, 2
6	Northbound/Southbound	Northbound	4, 5, 6
6	Northbound/Southbound	Southbound	1, 2, 3
6	Eastbound/Westbound	Eastbound	4, 5, 6
6	Eastbound/Westbound	Westbound	1, 2, 3
8	Northbound/Southbound	Northbound	5, 6, 7, 8
8	Northbound/Southbound	Southbound	1, 2, 3, 4
8	Eastbound/Westbound	Eastbound	5, 6, 7, 8
8	Eastbound/Westbound	Westbound	1, 2, 3, 4

Appropriate data preprocessing techniques were applied to clean and merge data from all months into a shape similar to the target shape shown in Figure 3.4.

AVC *volume data* has a different raw data format than that previously presented in Figure 3.7. See Figure 3.10. Data was used for statistical comparison with the radar system to determine volume accuracy; data is available from January 2022 to August 2022. After preprocessing, volume data were merged with data extracted from the previously presented AVC speed spanning August 2021 to December 2021, as shown in Figure 3.7. The final AVC volume dataset spans a full year from August 2021 to August 2022.

```
SITE_ID,COUNT_DATE_TIME,COUNT_TYPE,COUNT_INTERVAL,COUNT_LANE,COUNT_DIRECTION,CLASS_1,CLASS_2,CLASS_3,CLASS_4,CLASS_5,CLASS_6,CLASS_7,CLASS_8,CLASS_9,CLASS_10,CLASS_11,CLASS_12,CLASS_13,CLASS_14,CLASS_15,VOLUME
00810001,1/1/2022 12:00:00 AM,1,15,1,W,0,12,2,0,0,0,0,0,0,0,0,0,0,0,14
00810001,1/1/2022 12:00:00 AM,1,15,2,W,0,8,3,0,0,0,0,0,0,0,0,0,0,0,11
00810001,1/1/2022 12:00:00 AM,1,15,2,E,0,16,5,0,0,0,0,0,0,0,0,0,0,0,21
00810001,1/1/2022 12:00:00 AM,1,15,1,E,0,8,1,0,1,0,0,0,0,0,0,0,0,0,10
00810001,1/1/2022 12:15:00 AM,1,15,1,W,0,26,7,0,0,0,0,0,0,0,0,0,0,0,33
00810001,1/1/2022 12:15:00 AM,1,15,2,W,0,15,6,0,0,0,0,0,0,0,0,0,0,0,21
00810001,1/1/2022 12:15:00 AM,1,15,2,E,0,13,2,0,0,0,0,0,0,0,0,0,0,0,15
00810001,1/1/2022 12:15:00 AM,1,15,1,E,0,14,7,0,2,0,0,0,0,0,0,0,0,0,23
00810001,1/1/2022 12:30:00 AM,1,15,1,W,0,29,4,0,0,0,0,0,0,0,0,0,0,0,33
00810001,1/1/2022 12:30:00 AM,1,15,2,W,0,18,6,0,1,0,0,0,0,0,0,0,0,0,25
00810001,1/1/2022 12:30:00 AM,1,15,2,E,0,26,5,0,1,0,0,0,0,0,0,0,0,0,32
00810001,1/1/2022 12:30:00 AM,1,15,1,E,0,20,5,0,1,0,0,0,0,0,0,0,0,0,26
```

Figure 3.10. Revised AVC volume data.

3.1.3 HERE

HERE is a commercial company providing real-time, probe-based traffic data accumulated from in-vehicle transponders located in commercial vehicles or from cell phones located in passenger vehicles. HERE, like other GPS probe-based systems, such as INRIX, divides highways and streets into segments (i.e., TMCs). However, probe-based systems define the individual segments differently, meaning that a HERE TMC might have different starting and ending points on a highway than INRIX TMC. therefore, different lengths. HERE TMCs tend to be longer than INRIX's. Consequently, a highway route (or corridor) will have fewer HERE TMCs than INRIX TMCs.

HERE provides real-time traffic data, including speed, confidence levels, and TT. The ODOT's Maintenance Division uses HERE speed data to monitor traffic conditions and update TTs displayed on DMS (Dynamic Message Signs) displays located on major road segments (see Figure 3.11).

Figure 3.11. An example of a Dynamic Message Sign (DMS) showing estimated TT to nearby highway intersections.

Data is received every 5 minutes. An application programming interface (API) was developed to fetch raw data provided by HERE in XML format, and then store it in a database on a cloud server. This information can be accessed via SSH (Secure Shell) or Remote Desktop Connection. Figure 3.12 shows a real-time XML data stream provided by HERE.

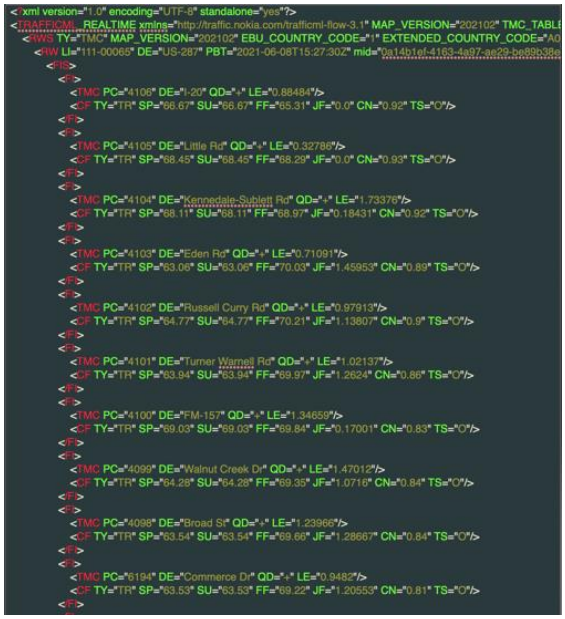

Figure 3.12. Real-time HERE raw XML data stream.

A website GUI has been developed to make HERE data accessible for viewing and downloading through https://speed.tulsa.ou.edu/npmrdsv1/data.

Figure 3.13 shows HERE raw data downloaded from the database. Notice that the developed API continuously populates the data feed streaming directly from HERE, and each TMC is defined by a specific ID. TMCs were collocated using GPS data provided by the TMC identification file, shown in Figure 3.14. Existing radar and AVC site information are used later for statistical comparison.

```
id,created_timestamp,tmc,sub_segment,length,type,confidence,speed,uncapped_speed,ff_speed,jam_factor,traversability_state
1055,2021-08-12 16:55:00-05,111N07442,-1,5.94767,TR,0.99,59.09,60.174,58.84,0,0
1109,2021-08-12 16:55:00-05,111N07496,-1,2.52026,TR,0.972,50.95,50.95,55.99,0.719626,0
1115,2021-08-12 16:55:00-05,111N07503,-1,9.69672,TR,0.824,58.272,58.272,58.66,0.052754,0
1147,2021-08-12 16:55:00-05,111N07540,-1,1.26282,TR,0.99,65.24,71.364,65.24,0,0
1185,2021-08-12 16:55:00-05,111N07656,-1,5.89437,TR,0.98,64.5,67.002,64.25,0,0
1211,2021-08-12 16:55:00-05,111N07733,-1,3.78441,TR,0.968,53.006,53.006,52.38,0.00327,0
1276,2021-08-12 16:55:00-05,111N08132,-1,1.5462,TR,0.99,34.008,34.008,48.9,2.436926,0
1289,2021-08-12 16:55:00-05,111N08146,-1,10.70713,TR,0.964,57.748,57.748,56.61,0,0
1305,2021-08-12 16:55:00-05,111N08200,-1,10.84377,TR,0.98,60.46,65.232,60.34,0,0
```

Figure 3.13. HERE raw data format downloaded.

HERE data include these TMC identification files which provide metadata regarding the HERE segments or TMCs (e.g., starting and ending GPS coordinates, TMC length, direction, road name and number, and others) describing all TMC segments.

Figure 3.14. HERE TMC identification metadata file.

Since HERE data is provided every 5 minutes, appropriate resampling was applied to raw data for converting the sampling rate to 15 minutes to align with other systems and compare stages. Notably, HERE raw data files have different time zones, which were accounted for during preprocessing. After collocating TMCs with existing radar/AVC sites, appropriate traffic directions were acquired.

The *uncapped speed* column was used in statistical analysis and TT estimation for comparison and modeling.

3.1.4 INRIX

Like HERE, INRIX is a commercial company that provides traffic data as a service for consumers, like ODOT. INRIX data is available for download one week after the end of each month from a database stored at the Regional Integrated Transportation Information System (RITS). Data includes three types of speed—speed, average speed, reference speed; TT; density (indicated by letters); segment/TMC; epoch, representing time, 288/day, every 5 minutes; and date indicating the day of the year. Figure 3.15 shows an example of an INRIX raw data file.

```
Date,Epoch,Segment,Speed,Average Speed,Reference Speed,Travel Time,Data Density
08012021,0,111-05446,65,37,62,23.81,A
08012021,0,111+04974,54,56,64,5.41,A
08012021,0,111N05156,68,66,72,26.39,A
...
```

Figure 3.15. INRIX raw data.

We have experimented, analyzed, and compared the three-speed types and selected the *speed* column for final comparison and machine learning model development for estimating TT. INRIX, like HERE, provides a metadata file for all TMCs, as shown in Figure 3.16.

Data preprocessing includes creating timestamps by merging data from the *date* and *epoch* columns, mapping each TMC to the corresponding ODOT radar/AVC site, and extracting the direction of each segment/TMC using INRIX's TMC Identification file. Data is resampled every 15 minutes to align with other systems. Timestamps are created for comparison. The final data shape is shown in Figure 3.4.

Figure 3.16. INRIX TMC Identification metadata file.

A website GUI (see Figure 3.17) has been developed to make INRIX data accessible for viewing and downloading through https://speed.tulsa.ou.edu/npmrdsv2/data. INRIX provides two types of traffic data: *trucks* and *trucks & passengers*; the latter was used in this project.

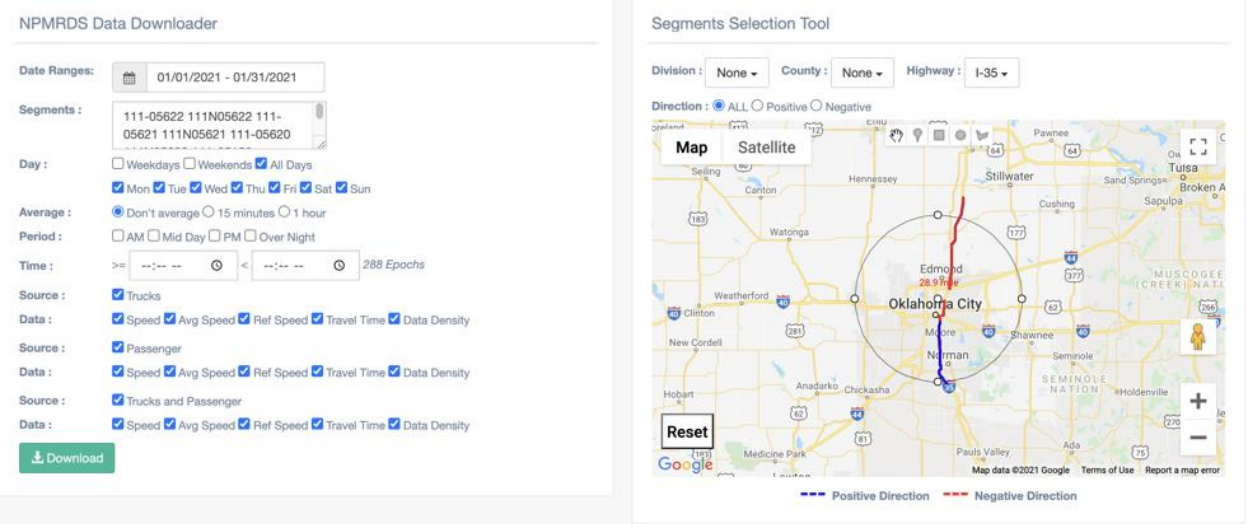

Figure 3.17. INRIX website GUI.

3.2 Summary

Table 3.2 summarizes the systems and the type of traffic data provided.

Table 3.2
Systems Data Description

System	Type	Sampling Rate	Data availability	Speed	Source
Radar	Sensor	1 min	Real-time	17 bins	ODOT
AVC	Sensor	15 min	Daily	12 bins	ODOT
INRIX	Probe	5 min	Monthly	Average	Outsourced
HERE	Probe	5 min	Real-time	Average	Outsourced

This section introduced the four systems utilized in this project. Raw data and used preprocessing techniques used to convert data into the appropriate format will be described in the next few sections. Statistical analysis will highlight differences in the way the systems measure speed and model development to estimate TT, starting from a DMS display to a nearby intersection across multiple routes in the OKC and Tulsa metropolitan areas.

Chapter 4: Speed Analyses per System

This section introduces the setup implemented and the empirical results of the speed comparison across the systems for quantifying the accuracy of speed measurements in MPH using different metrics (e.g., mean absolute error [MAE], mean squared error [MSE]).

The goal of this phase was to highlight the agreement and discrepancies in speed measurement between systems. This includes utilizing data from collocated sites, determining spatial speed error (per direction and site) across all systems, selecting free-flow data, analyzing temporal error analysis (per direction and site over time) across the systems, investigating, faulty locations flagged with "relatively higher error than most sites", and quantifying overall error difference using metrics (e.g., MSE, MAE),

4.1 Comparison setup

Speed comparison results are demonstrated across all four systems, namely: AVC vs. radar, AVC vs. HERE, AVC vs. INRIX, radar vs. INRIX, radar vs. HERE, and INRIX vs. HERE.

Each of the four systems provides its data as a table indexed by time using a 15-minute interval. To compare speed across systems, we need to join and align datasets of different systems based on timestamps and time-matching. Furthermore, to maximize sample size (i.e., the number of data rows), we joined timestamp, site ID, and direction datasets independently rather than joining them all into only one dataset. In other words, joining all four tables into one table using time-matching may result in fewer data samples, thus, less information than if each two data tables are joined and compared separately. Doing so helped magnify the difference and/or agreement between each couple of systems more clearly.

Rows with zero-valued speed were removed after joining the data – to avoid biasing the difference values. For example, if comparing AVC and radar, the dataset table will have columns (e.g., *timestamp*, *site ID*, *direction*, *AVC speed*, and *radar speed)* and rows with zero values for speed for both AVC and radar. These were removed.

4.2 Spatial error analysis

Inspecting speed error per site and direction for speed aided in discovering sites with relatively larger errors (e.g., speed difference) than most sites – errors can be due to faulty data or other issues related to the site or data collection. Speed was compared using metrics like MAE, MSE, and root mean squared error (RMSE).

The following list of 13 sites had significant differences across all systems: *810006, 810008, 810009, 810013, 810017, 810023, 810024, 810034, 810054, 810081, 810089, 810511, 810521*. Removing these sites from comparison drastically reduced error metrics (see Figure 4.7, where removing two sites reduces the maximum MSE (Mean Squared Error) from ~900 MPH^2 to ~250 MPH^2). The deviation of MSE between sites becomes much less prominent, thus, most sites had comparable MSE.

The sites that had relatively higher speed differences between AVC vs. radar: *[810034, 810023, 810017, 810008],* as shown in Figure 4.1. For AVC vs. HERE: *[810034, 810024, 810023, 810054, 810009],* see Figure 4.2. For AVC vs. INRIX: *[810006, 810009, 810013, 810017, 810023, 810511, 810521],* see Figure 4.3. For Radar vs. INRIX: *[810006, 810013, 810081, 810089, 810511]*, see

Figure 4.4. For Radar vs. HERE: *[810024, 810054]*, see Figure 4.5. For INRIX vs. HERE: *[810024, 810054]*, see Figure 4.6.

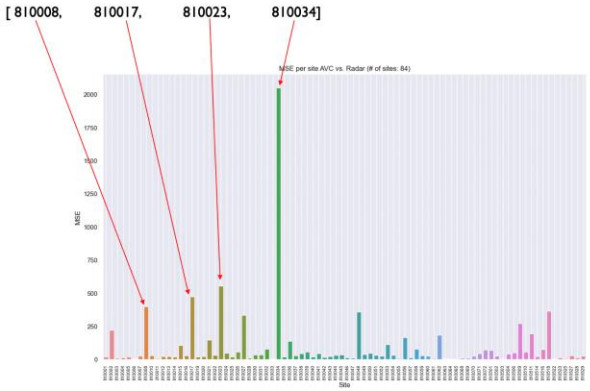

Figure 4.1. AVC vs. radar speed MSE per site, highlighting sites with relatively high differences.

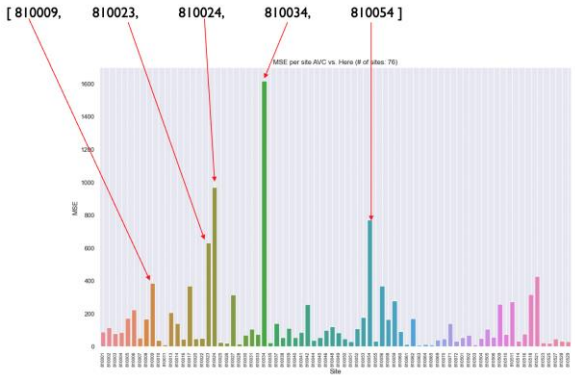

Figure 4.2. AVC vs. HERE speed MSE per site, highlighting sites with relatively high differences.

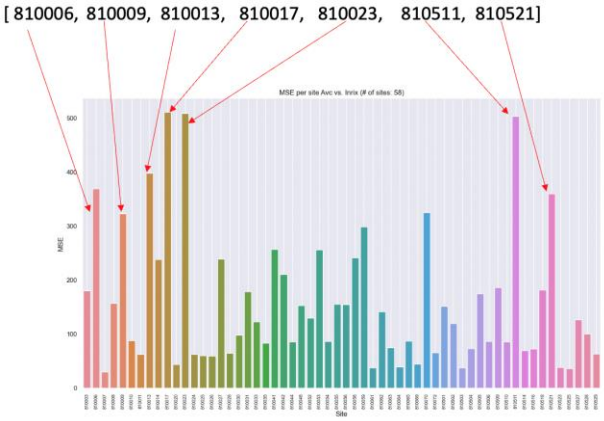

Figure 4.3. AVC vs. INRIX speed MSE per site, highlighting sites with relatively high differences.

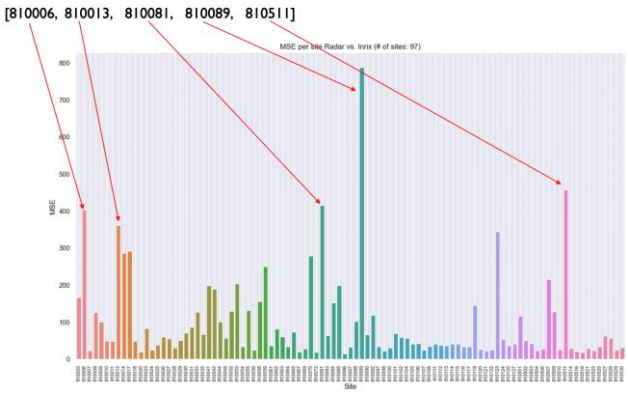

Figure 4.4. Radar vs. INRIX speed MSE per site, highlighting sites with relatively high differences.

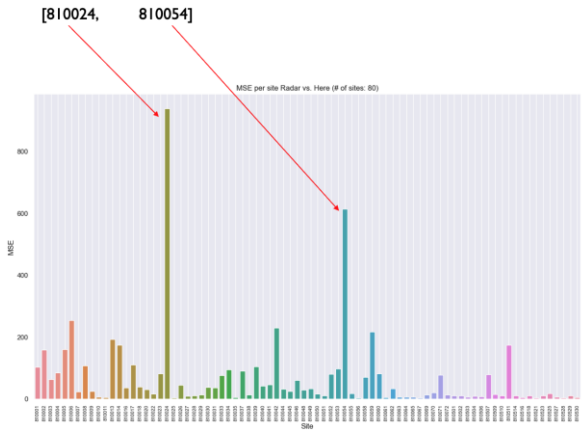

Figure 4.5. Radar vs. HERE speed MSE per site, highlighting sites with relatively high differences.

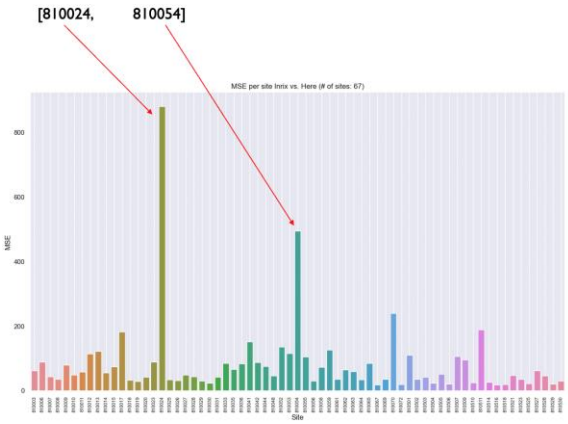

Figure 4.6. INRIX vs. HERE speed MSE per site, highlighting sites with relatively high differences.

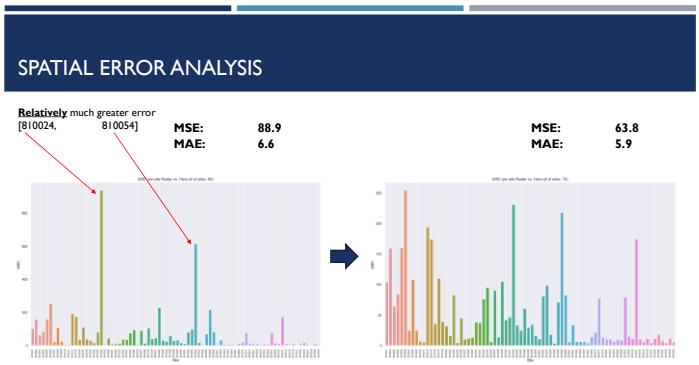

Figure 4.7. Example showing the effect of removing "faulty" site on speed MSE between radar and HERE.

To determine why some sites have higher differences, we investigated the data more deeply and inspected the speed distribution of *"faulty"* sites to discover reasons or patterns. We found data distributions were different at those sites. For example, Figure 4.8 and Figure 4.9 show the speed histograms for four ignored sites for AVC vs. radar in each direction. From this, we can clearly see that radar and AVC have noticeable discrepancies. One reason for this phenomenon is that speed calculation for AVC is based on chosen mid-points of speed bins, which, of course, has some effect on the error. Figure 4.10 provides another example, showing speed histograms for AVC and radar speed measurements for three sites and both directions.

Note that in Figure 4.8 the default bin size was determined using a reference rule dependent upon sample size and variance – this rule is known as the Freedman-Diaconis rule which uses the interquartile range and sample size to calculate the bin width. While this selection works well in many cases (i.e., with "well-behaved" data), it fails in others. Given that the bin is too large, many important features might be erased. Given that the bin is too small, random variability might dominate, obscuring the shape of the true underlying distribution. For this reason Figure 4.9 shows the result of setting the bin size to a selected value (5 in this case) to ensure data aligns with that shown in Figure 4.8.

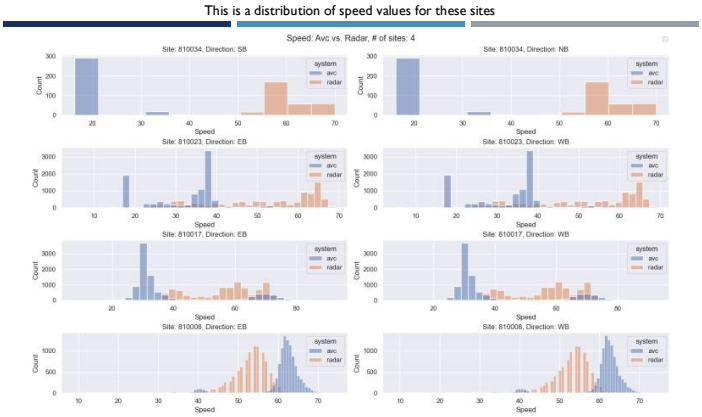

Figure 4.8. AVC vs. radar "faulty" sites speed distribution.

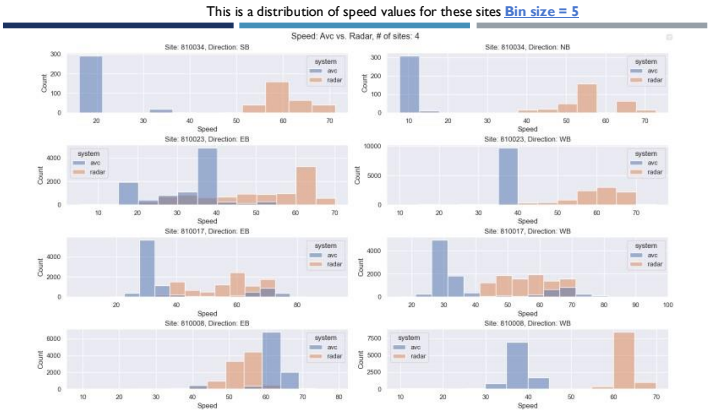

Figure 4.9. Speed distribution at AVC vs. radar "faulty" sites, where bin size=5.

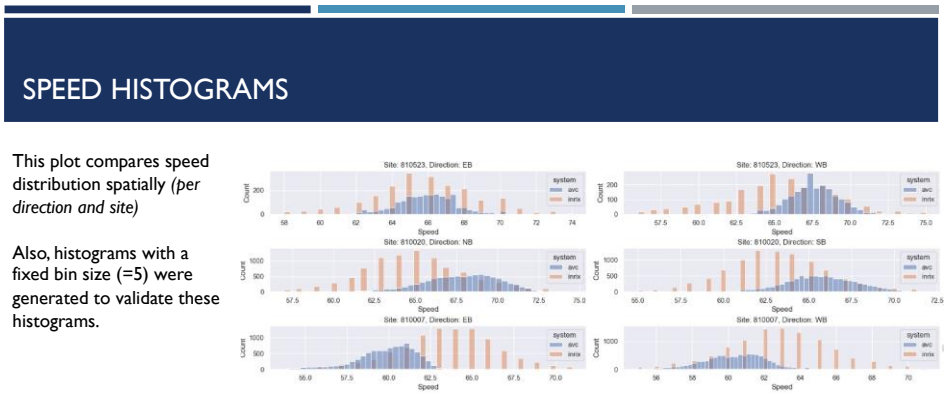

Figure 4.10. AVC vs. INRIX speed histogram per site and direction.

4.3 Removing outliers (free-flow data selection)

Outliers, in this report, are data values that are different from free-flow speed data as well as any values that don't fit in the distribution. In this case, we identify "outliers" in speed values and remove them. Doing so corresponds with choosing data in the **free-flow range**. We used the following policy for detecting and removing outliers.

$$Q_3 + 1.5\,IQR$$

Figure 4.11 Free-flow data selection (upper bound)

$$Q_1 - 1.5\,IQR$$

Figure 4.12 Free-flow data selection (lower bound)

where Q_1 is the first quartile, Q_3 is the third quartile, and IQR is the interquartile range defined as the difference between the 75th and 25th percentiles of the data, as follows:

$$IQR = Q3 - Q1$$

Figure 4.13 Interquartile range equation

The equation in Figure 4.13 describes the measure of statistical dispersion, which is the spread of speed data, also known as the interquartile range.

Figure 4.14 is a graphical explanation showing the outlier removal method with upper and lower bounds.

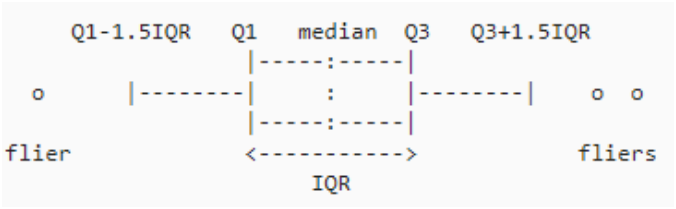

Figure 4.14. Interquartile custom method, where fliers are considered outliers.

Figure 4.15 shows an example of outlier removal (i.e., free-flow data selection) for both directions for site 810032. The first two plots display AVC speed data as a histogram with the defined upper Figure 4.11 and lower Figure 4.12 bounds, as well as other scalars, such as the data mean and median. We can see clearly that the method eliminates anomalies (i.e., "outliers") while retaining the majority of the data. In this example, we can also see how the method focuses on free-flow speed ranges, due to the nature of traffic data since most data typically lies in the free-flow range.

One issue worth noting is that the radar system is not as efficient as a system like AVC in lower speed ranges. Note we can see that the in the histogram, AVC data bars (upper two) in the 20-40 MPH range are detected while radar (lower two) are not detected. This will be reflected later in TT estimation. Figure 3.1 and Figure 4.19 show that where we plot histograms of speed data per site and direction for AVC (see Figure 3.1) and radar (see Figure 4.19), speed values are in the lower range for AVC, but not for radar (see red circles).

Figure 4.15. Free-flow data selection.

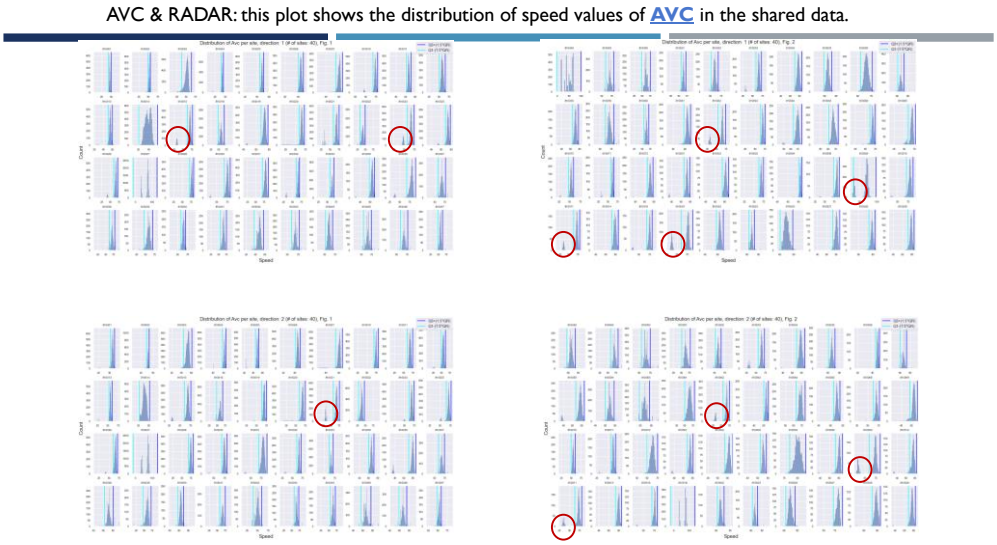

Figure 4.16. AVC speed histograms per site and direction.

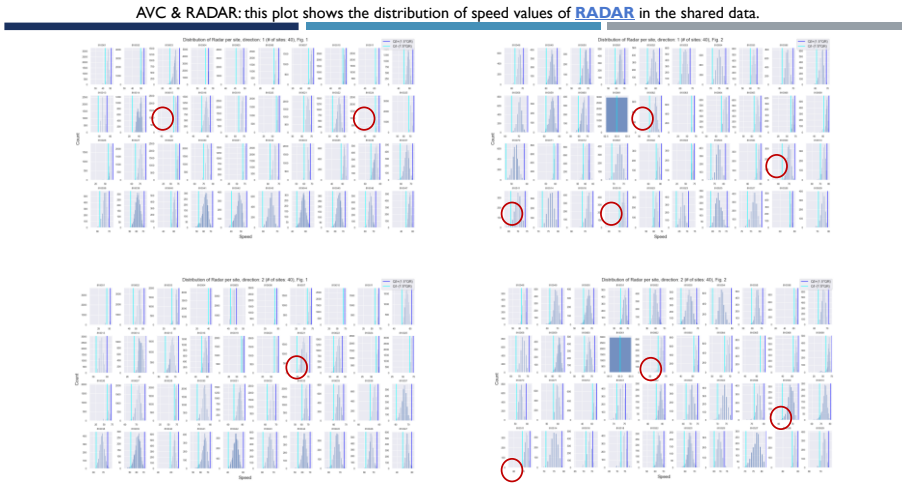

Figure 4.17. Radar speed histograms per site and direction.

4.4 Temporal error analysis

The goal of inspecting speed differences over time (e.g., daily) is uncovering temporal patterns in error. For example, Figure 4.18 and Figure 4.19 show daily MSE for speed between AVC and radar per site and direction for the top and bottom five sites. Note that these sites have the highest and lowest speed errors when utilizing results from clean or free-flow data (i.e., after removing outliers and zero-valued speeds). In spite of noticeable patterns (e.g., site 810027 EB), there were no significantly recognizable patterns across all sites. Figure 4.20 shows another example of the best (i.e., right) and worst (i.e., left) five sites when examining daily MSE in both directions.

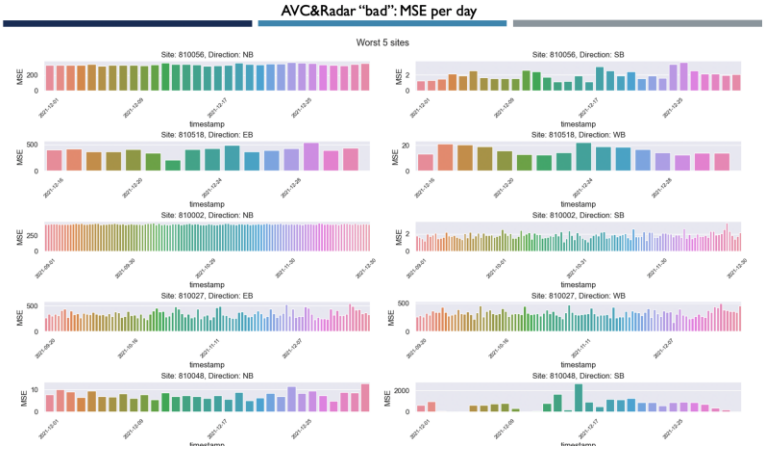

Figure 4.18. AVC vs. radar daily MSE for top five sites (i.e., highest overall MSE in clean data).

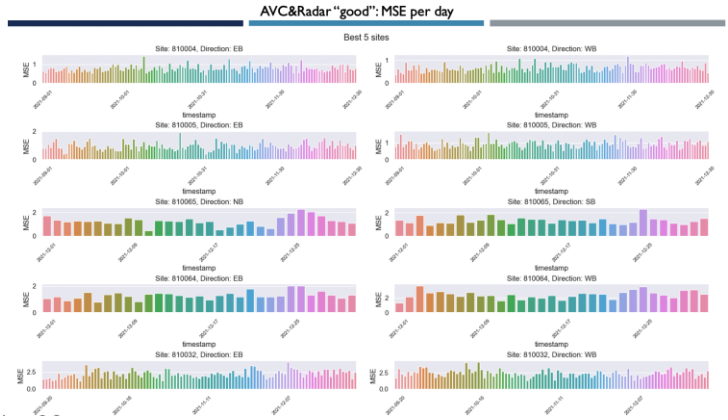

Figure 4.19. AVC vs. radar daily MSE for lowest five sites i.e., (lowest overall MSE in clean data).

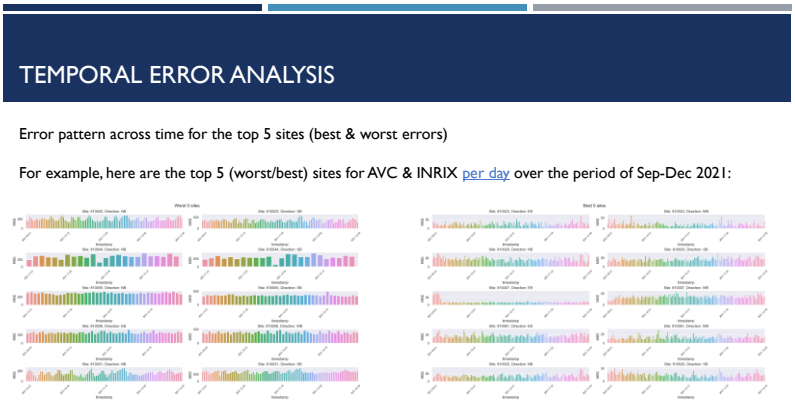

Figure 4.20. Daily MSE for sites with highest and lowest overall MSE (i.e., AVC vs. INRIX).

4.5 Results

Speed comparison results are discussed below.

Table 4.1 shows speed comparison results for sites over the period spanning from August to December 2021. The table shows MAE, the percentage of time in which one system measured lower speed, the average positive difference (i.e., average values when designated system reported higher speed), and the average negative difference (i.e., the average value of all lower measurements). Note that the AVC difference was slightly higher than other systems due to the speed calculation of AVC. Recall that radar and AVC define speeds within 5 MPH ranges, we use

the number of cars within each speed range and multiply it with the midpoint of the corresponding bin to calculate the average speed at each time step. This will intrinsically have an impact resulting in some margin of error in the speed MAE of sensors (radar and AVC) compared to probes (INRIX and HERE).

Table 4.2 shows speed comparison results from data collected between August 2021 and July 2022. Note that AVC is measured only from August to December 2021, thus the reason AVC data is not included in this table. Notice that the results over the longer period align with the results shown in Table 4.1, for instance, radar and INRIX had 5.6 MPH MAE in Table 4.1 and 5.24 MPH MAE in Table 4.2.

Also, in Table 4.1 and Table 4.2, radar tends to overestimate speed most of the time when compared to probe-based systems (e.g., INRIX and HERE). Speed was underestimated when compared to AVC. Overall, INRIX tends to underestimate speed when compared to HERE.

Table 4.1
Speed comparison results for selected sites from August to December 2021.

Systems	**MAE** (MPH)	**Time with lower speed (%)**	**Avg. pos diff** (MPH)	**Avg. neg diff** (MPH)
AVC vs. RADAR	**3.02**	Radar was **60.22%** of the time lower than AVC	3.66 (radar is higher)	2.61 (radar is lower)
AVC vs. HERE	**6.7**	HERE was **77.8%** of the time lower than AVC	6.77 (HERE is higher):	6.69 (HERE is lower):
AVC vs. INRIX	**7.1**	INRIX was **84.1%** of the time lower than AVC	5.37 (INRIX is higher)	7.45 (INRIX is lower)
Radar vs. INRIX	**5.6**	Radar was **16%** of the time lower than INRIX	6.0 (radar is higher)	3.86 (radar is lower)
Radar vs. HERE	**5.7**	Radar was **26.52%** of the time lower than HERE	6.65 (radar is higher)	3.44 (radar is lower)
INRIX vs. HERE	**4.5**	INRIX was **70.77%** of the time lower than HERE	3.67 (INRIX is higher)	4.87 (INRIX is lower)

Table 4.2
Speed comparison results for selected sites from August 2021 to July 2022.

Systems	**MAE** (MPH)	**Time with lower speed (%)**	**Avg. pos diff** (MPH)	**Avg. neg diff** (MPH)
Radar vs. INRIX	**5.24**	Radar was **18.74%** of the time lower than INRIX	5.39 (radar is higher)	4.58 (radar is lower)
Radar vs. HERE	**5.08**	Radar was **27.82%** of the time lower than HERE	5.69 (radar is higher)	3.5 (radar is lower)
INRIX vs. HERE	**4.35**	INRIX was **70.37%** of the time lower than HERE	3.54 (INRIX is higher)	4.7 (INRIX is lower)

Table 4.3 shows comparison results for the same configuration for lower speeds ranging from 0 to 40 MPH.

Table 4.3
Speed comparison results for selected sites over the period (August to December of 2021) 0-40MPH

Systems	**MAE** (MPH)	**Time with lower speed (%)**	**Avg. pos diff** (MPH)	**Avg. neg diff** (MPH)
AVC vs. RADAR	**3.36**	Radar was **13.05%** of the time lower than AVC	3.35 (radar is higher)	3.39 (radar is lower)
AVC vs. HERE	**8.77**	HERE was **56.39%** of the time lower than AVC	7.13 (HERE is higher)	10.04 (HERE is lower)
AVC vs. INRIX	**12.6**	INRIX was **88.71%** of the time lower than AVC	6.54 (INRIX is higher)	13.83 (INRIX is lower)
Radar vs. INRIX	**11.89**	Radar was **7.94%** of the time lower than INRIX	12.6 (radar is higher)	3.73 (radar is lower)
Radar vs. HERE	**9.79**	Radar was **11.6%** of the time lower than HERE	10.54 (radar is higher)	3.44 (radar is lower)
INRIX vs. HERE	**5.55**	INRIX was **72%** of the time lower than HERE	4.13 (INRIX is higher)	6.11 (INRIX is lower)

Speed comparison results shown in Table 4.1, Table 4.2, and Table 4.3 are for a selected set of sites distributed across Oklahoma. Speed range was filtered using the outlier removal policy, where most data is in the normal or free-flow range. Data samples were not selected within specific hours, the analysis includes data samples from all available time periods throughout the day.

Looking at the speed analysis results that are presented in Table 4.3 for lower speeds in Table 4.1 for free-flow, we notice that the MAE grows approximately by 1.1, 1.3, 1.7, 2.1, 1.7, 1.2 folds for AVC vs. Radar, AVC vs. HERE, AVC vs. INRIX, Radar vs. INRIX, Radar vs. HERE, and INRIX vs. HERE, respectively. Consequently, the radar is less practical at lower speeds (<40 MPH) compared to HERE and INRIX – this could be a result of the following factors: the radar's tendency, shown in the previous tables, to overestimate speed measurements compared to INRIX and HERE, traffic congestion in which vehicles, especially larger ones, near the radar block other cars on the road resulting in less accurate average speed calculation – this can be the reason that speed distribution for the radars missing values at lower speeds when compared to AVC as was shown in Figure 4.16 and Figure 4.17.

4.6 Summary

In this section, we presented the speed comparison setup, data manipulation, and cleaning techniques, as well as experimental error analysis. Empirical results showed that radar has a 5 MPH difference in speed measurement when compared to probe-based systems, like INRIX and HERE. The difference between INRIX and HERE is 4.5 MPH. Results also demonstrated a less than 7 MPH average difference in speed measurement among all systems.

Chapter 5: Travel Time Comparison

Subsequent to analyzing the speed difference between systems, the goal is to compare TT estimation. In this regard, we are interested in finding out the difference between systems relevant to individual segments (i.e., links), as well as routes (i.e., corridors). Additionally, it is important to validate radar-system data against probe-system data for TT estimation using only radar, HERE, and INRIX data.

TT comparison requires calculating and comparing system measures of TT. While some systems, like INRIX, provide estimation as a scalar value out-of-the-box in just seconds, systems like radar and HERE do not. Hence, we used speed and link distance (i.e., segment length) to arrive at an estimate. All necessary unit conversions to minutes were made. For routes, TT estimation represents the total sum of TT estimations of individual segments. Distance (in miles) was calculated per segment using GPS starting and ending coordinates via the geodesic distance (WGS-84), which considers the spherical shape of the earth. Using the sum of individual segment distances (i.e., lengths) using each segment's corresponding starting and ending coordinates was more accurate than using the starting and ending coordinates of the entire route for calculating distance.

5.1 Travel time estimation for a segment

Since probe-based systems divide highways into segments that have start (entry) and end (exit), TT calculation is accomplished by dividing the distance over the measured speed, as in Figure 5.1:

$$tt_i = \frac{d_i}{s_i}$$

Figure 5.1 TT calculation for a segment

where tt_i is the TT estimation *(minutes*) for segment i; s_i is the measured speed *(MPH)*; and d_i is the length *(miles)* of the segment (see Figure 5.2).

$$d_i = Geodesic(start_i, end_i)$$

Figure 5.2 Segment distance of a segment using the geodesic distance

where $start_i$ is the GPS coordinate (latitude and longitude) of the entering point of the segment/TMC i, and end_i is the GPS coordinate of the exit.

Calculating radar is different since radar stations are located at a point on a highway, thus, without a start and end point (i.e., no distance). However, since we are comparing TT for a group of the selected individual segments that have a start and end defined by the probe-based systems, we can use distance from these systems with radar-measured speed to estimate TT. This is justified, since radar is being independently compared to other systems (e.g., INRIX and HERE) and segment length difference is not an issue. Also, the overall objective is to estimate TT for routes. Recall that we experimented with different methods for calculating route length for radar. This is discussed in detail below.

5.2 Travel time estimation for routes

Since we have determined a TT estimation per segment, we can then sum TTs to obtain an overall estimate for the route at some timestep. Hence, the total estimate of route TT *(in minutes)* will be

$$tt_{route} = \sum tt_i$$

Figure 5.3 TT route equation

Figure 5.4 graphically demonstrates TT estimation for INRIX and HERE.

To increase statistical confidence and granularity of data (i.e., number of data samples) in the estimate, we eliminated data samples in which data was available for only less than half of the segment. In other words, to estimate TT for a route, at least half of the segments must have a TT estimate. Given there is data for more than half but not all segments, interpolation can be implemented to estimate TT for segments with missing data by calculating the average TT of segments with data. For example, in Figure 5.4, data is available for segments *tmc1, tmc2, tmc4, and tmc5*; however, segment *tmc3* has no data for some timestep *t*. TT estimation of *tmc3* will be *(TTtmc1+TTtmc2+ TTtmc4+ TTtmc5)/4*, and the estimate for the route can be calculated using Figure 5.3. Note that TT for individual TMCs can be calculated using the equation shown in Figure 5.1.

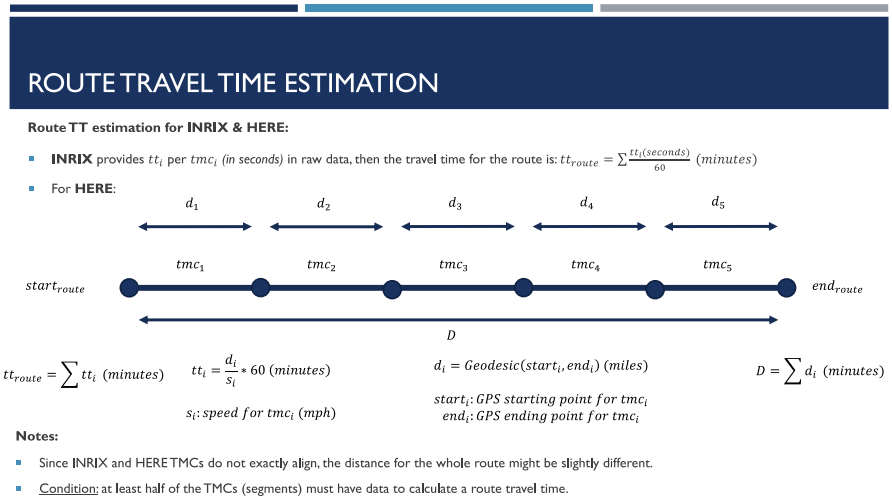

Figure 5.4. Route TT estimation for INRIX and HERE.

The TT calculation procedure for the radar system is as follows.

5.2.1 Total distance calculation for radar

INRIX and HERE define highway segments (or TMCs) differently relative to length. Routes used in this research were selected based on the total length of the route defined by both INRIX and HERE to minimize the effect of route length on results. To obtain a route length estimate for the radar system, we explored the following options. First, use average route distance (i.e., length) utilizing both INRIX and HERE. (see Figure 5.5). Second, use the route length of INRIX when comparing radar to INRIX. (see Figure 5.7). Third, use the route length of HERE when comparing radar to HERE. (see Figure 5.8).

$$D_{radar} = \frac{D_{HERE} + D_{INRIX}}{2}$$

Figure 5.5 Average route distance equation

Where D_{HERE} and D_{INRIX} is the total length of the route calculated using:

$$D_{route} = \sum d_i$$

Figure 5.6 Route distance summation equation

where d_i is calculated using the equation presented in Figure 5.2.

$$D_{radar} = D_{INRIX}$$

Figure 5.7 Radar route distance using INRIX distance

$$D_{radar} = D_{HERE}$$

Figure 5.8 Radar route distance using HERE distance

5.2.2 Total travel time calculation for radar

Figure 5.9 shows the details of TT estimation for a route with 3 radars. Radars are indicated by purple stars at points on the highway. After calculating the total distance of the whole route using one of the options discussed in the section entitled "Total distance calculation for radar," we must use it to obtain the distance per individual segment. Then, the measured speed and distance per individual segments along the route can be used in TT estimations for these segments, as in the equation shown in Figure 5.1. Finally, the total speed would be the sum of TTs of these hypothetical segments (or radars, technically speaking) using the equation shown in Figure 5.3.

Similarly, we can apply the condition that requires at least half of the radar segments to have speed data to ensure TT calculations are possible. Data interpolation was used as needed for radars missing data – for instance, in Figure 5.9, if two of the three radars have speed measurements then TT can be calculated for both of them and the average TT will be assigned for the last radar that is, in this case, missing data (at some time step; data row in the data table), and finally, the route TT can be calculated by summing the TTs for the three radars.

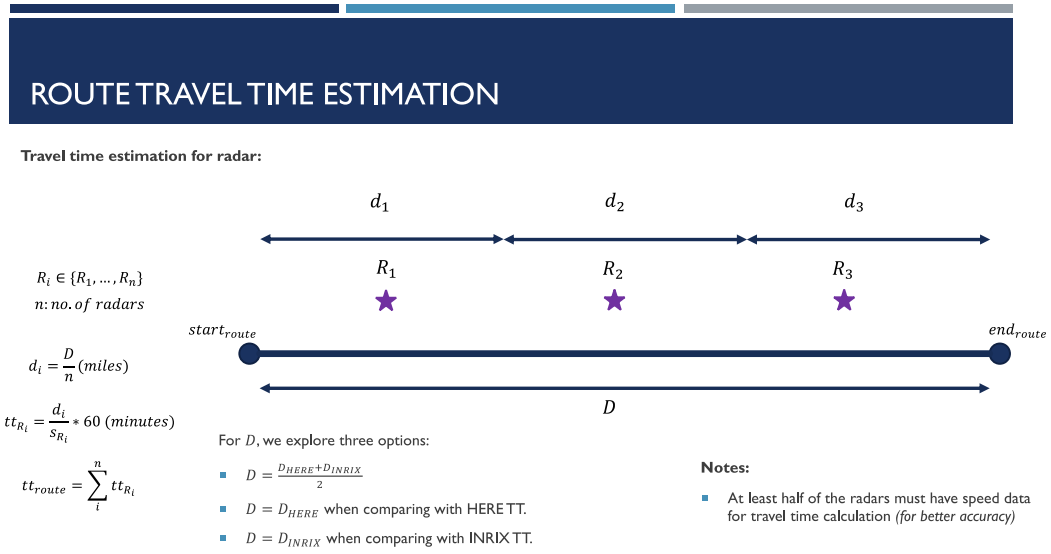

Figure 5.9. Route TT estimate for radar.

5.2.3 Routes

Specific routes (i.e., corridors) were studied for this report. Most are located in the Oklahoma City and Tulsa metropolitan areas along interstate and major highways. Routes start near a DMS display that ODOT uses to show TT estimates; they end at a nearby intersection or exit. Most routes have 1 to 3 radars units and different lengths, ranging from two to 12 miles.

Routes meta-data is listed below:

Route 1 (see Figure 5.10): City: OKC, Highway: I-35, Displays (DMS): *['I-35 NB @ S 19th Moore', 'I-35 NB @ S 89th']*, Radars: *[811007, 811072, 811109]*, INRIX TMCs: *['111P04906', '111P04907', '111P04908', '111P04909', '111P04910', '111P04911', '111P04912']*, HERE TMCs: *['111P04906', '111P04907', '111P04908', '111P04909', '111P04910', '111P04911', '111P04912']*.

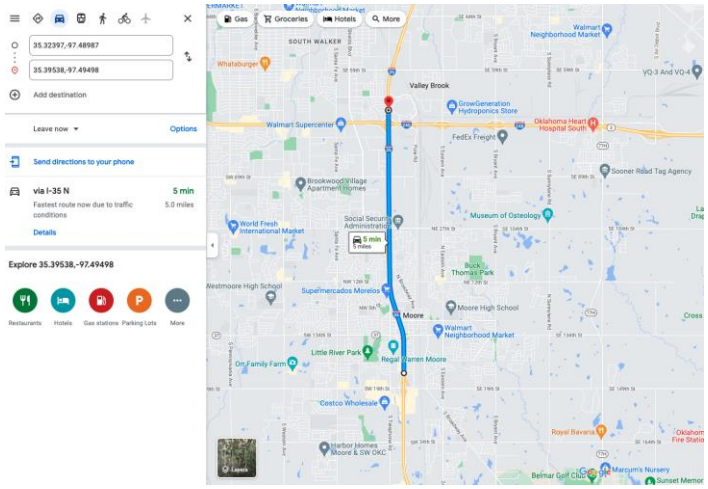

Figure 5.10. Route 1 (5 miles long on I-35).

Route 2 (see Figure 5.11): City: OKC, Highway: I-40, Displays (DMS): ['I-40 EB @ Meridian','I-40 EB AND Western'], Radars: *[811007, 811072, 811109]*, INRIX TMCs: *['111-04946', '111N04946', '111-04945', '111N04945', '111-04944', '111N04944', '111-04943', '111N04943', '111-04942', '111N04942', '111-04941', '111N04941', '111-04940', '111N04940', '111-04939', '111N04939', '111-04938', '111N04938', '111-04937', '111N04937', '111-04936', '111N04936', '111-04935', '111N04935', '111-04934', '111N04934', '111-04933', '111N04933', '111-04932', '111N04932', '111P04929', '111+04930', '111P04930', '111+04931', '111N04974']*, HERE TMCs: *['111N04946', '111N04945', '111N04944', '111N04943', '111N04942', '111N04941', '111N04940', '111N04939', '111N04938', '111N04937', '111N04936', '111N04935', '111N04934', '111N04933', '111N04932', '111P04929', '111P04930', '111P04931', '111N04974']*,

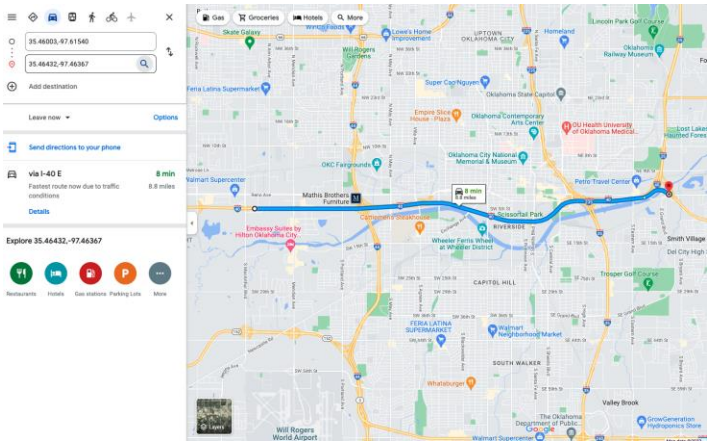

Figure 5.11. Route 2 (9 miles long on I-40).

Route 3 (see Figure 5.12): City: OKC, Highway: I-40, Displays (DMS): ['I-40 EB @ Meridian','I-40 NB @ S 25th'], Radars: *[811007, 811023]*, INRIX TMCs: *['111-04946', '111N04946', '111-04945', '111N04945', '111-04944', '111-05130', '111N05130', '111-05129', '111N05129', '111-05128', '111N05128', '111-05127', '111N05127', '111-05126', '111N05126', '111-05125', '111P05171']*, HERE TMCs: *['111N04946', '111N04945', '111P18853', '111N05130', '111N05129', '111N05128', '111N05127', '111N05126', '111N05125', '111P05171']*.

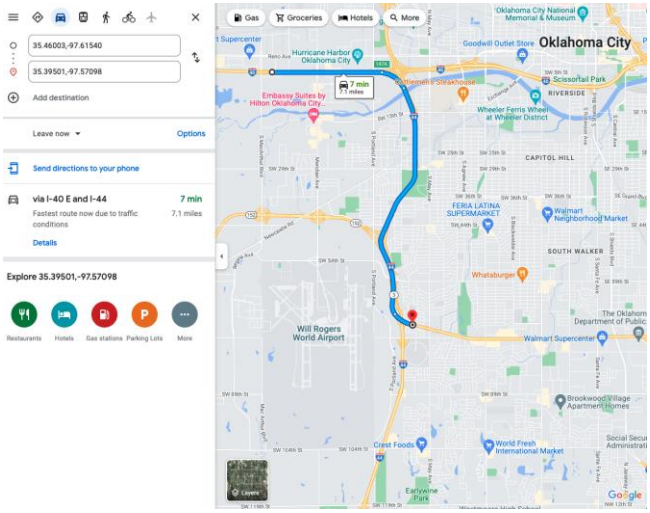

Figure 5.12. Route 3 (7 miles long on I-40).

Route 4 (see Figure 5.13): City: OKC, Highway: I-40, Displays (DMS): ['I-40 WB @ Choctaw','I-40 WB @ Post','I-40 WB @ Sooner'], Radars: [811067, 811117, 811008], INRIX TMCs: ['111+04962', '111P04962', '111+04963', '111P04963', '111+04964', '111P04964', '111+04965', '111P04965', '111+04966', '111P04966', '111+04967', '111P04967', '111+04968', '111P04968', '111+04969', '111P04969', '111+04970', '111P04970', '111+04971', '111P04971', '111+04972', '111P04972', '111+04973', '111P04973'], HERE TMCs: ['111P04962', '111P04963', '111P04964', '111P04965', '111P04966', '111P04967', '111P04968', '111P04969', '111P04970', '111P04971', '111P04972', '111P04973']

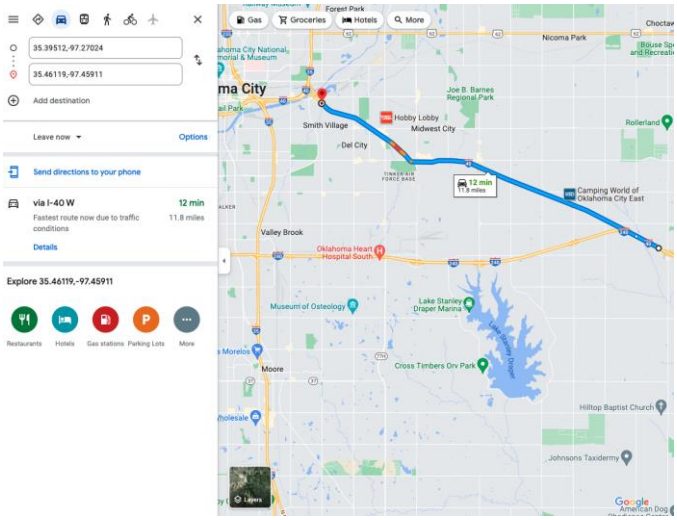

Figure 5.13. Route 4 (12 mile long on I-40).

Route 5 (see Figure 5.14): City: OKC, Highway: I-44, Displays (DMS): ['I-44 EB @ S 96th'], INRIX TMCs: ['111+05123', '111P05123', '111+05124', '111P05124'], HERE TMCs: ['111P05123', '111P05124'], Radars: [811114].

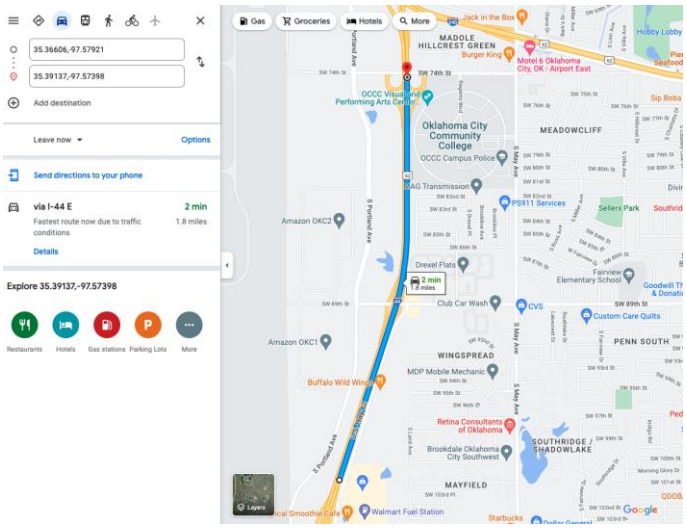

Figure 5.14. Route 5 (2 miles long on I-44).

Route 6 (see Figure 5.15): City: OKC, Highway: I-44, Displays (DMS): ['I-44 EB @ S 96th'], INRIX TMCs: ['111+05123', '111P05123', '111+05124', '111P05124', '111+05125', '111P05125', '111+05126', '111P05126', '111+05127', '111P05127', '111+05128', '111P05128', '111+05129', '111P05129', '111+05130', '111P05130'], HERE TMCs: ['111P05123', '111P05124', '111P05125', '111P05126', '111P05127', '111P05128', '111P05129', '111P05130'], Radars: [811114, 811023].

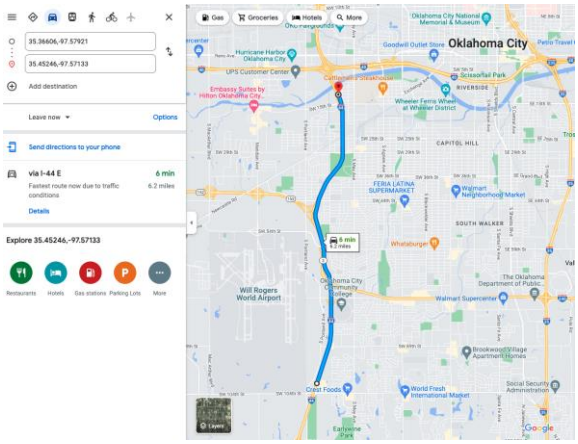

Figure 5.15. Route 6 (6 miles long on I-44).

Route 7 (see Figure 5.16): City: Tulsa, Highway: I-44, Displays (DMS): ['I-44 WB @ E 145th'], INRIX TMCs: ['111-04998', '111N04998', '111-04997', '111N04997', '111-04996', '111N04996', '111-04995', '111N04995'], HERE TMCs: ['111N04998', '111N04997', '111N04996', '111N04995'], Radars: [811105, 811019].

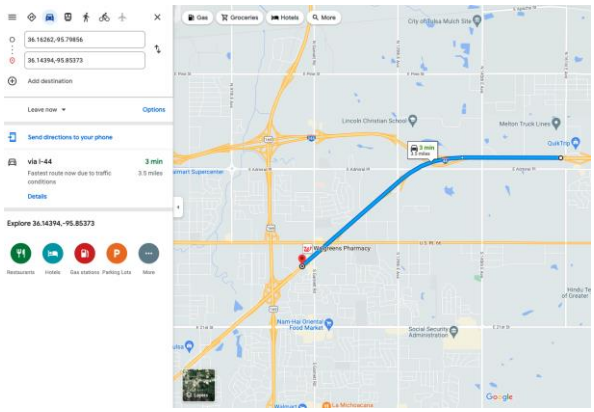

Figure 5.16. Route 7 (4 miles long on I-44).

Route 8 (see Figure 5.17): City: Tulsa, Highway: I-44, Displays (DMS): ['I-44 EB @ Harvard'], INRIX TMCs: ['111+04988', '111P04988', '111+04989', '111P04989', '111+04990', '111P04990', '111+04991', '111P04991', '111+04992', '111P04992', '111+04993', '111P04993', '111+04994', '111P04994', '111+04995', '111P04995', '111+04996', '111P04996', '111+04997', '111P04997'], HERE TMCs: ['111P04988', '111P04989', '111P04990', '111P04991', '111P04992', '111P04993', '111P04994', '111P04995', '111P04996', '111P04997'], Radars: [811098, 811097, 811019].

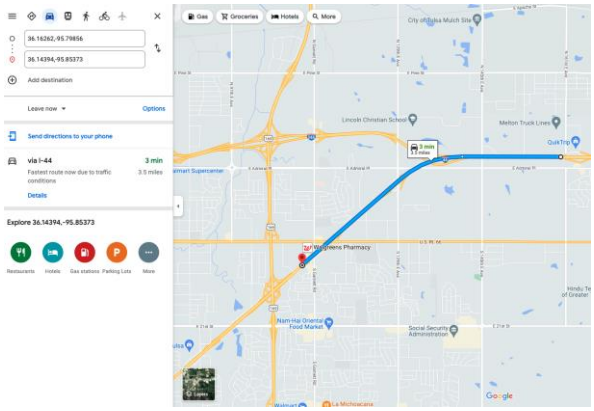

Figure 5.17. Route 8 (9 miles long on, I-44).

Route 9 (see Figure 5.18): City: Tulsa, Highway: SH-51, Displays (DMS): ['SH-51 WB @ E 129th'], INRIX TMCs: ['111P05091', '111+05092', '111P05092', '111+05093', '111P05093', '111+05094', '111P05094', '111P05075', '111+05076', '111P05076', '111+05077', '111P05077'], HERE TMCs: ['111P05091', '111P05092', '111P05093', '111P05094', '111P05075', '111P05076', '111P05077'], Radars: [811025, 811104].

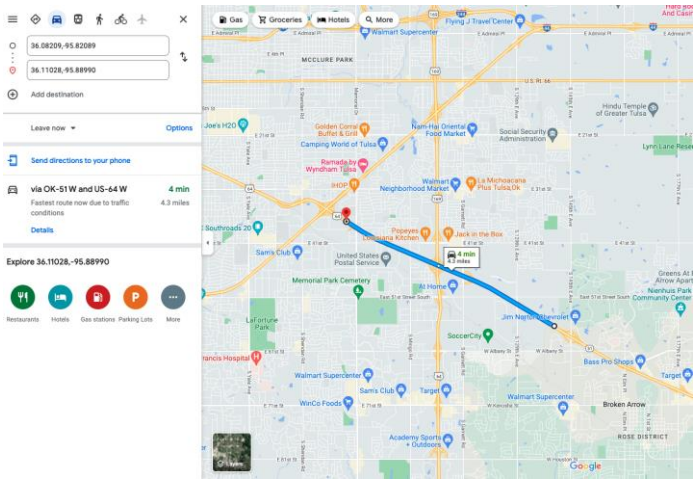

Figure 5.18. Route 9 (4 miles long on SH-51).

Acquiring data for these routes' radars, INRIX, and HERE TMCs involved collecting data and applying various preprocessing techniques to convert each into the format used to determine TT. Appropriate code was developed to convert and preprocess data, distance, and TT calculation, as well as compare results.

5.3 Experiments

Since TT is not the same in all traffic conditions and for all time periods, we designed a set of experiments to compare TT and quantify the difference between systems under investigation during different time periods and in various traffic states. These "experiments" are meant to highlight the differences and agreements between radar, HERE, and INRIX under a set of traffic conditions including peak and off-peak hours as well as low speeds and free flow.

Time periods: 1) All hours: include data from all day hours without applying a time-related filter, **2) 8 AM to 6 PM, 3) Peak:** ODOT defined "peak" periods: (6 AM to 10 AM, and 4 PM to 8 PM) **4) Off-Peak:** Compliment of peak periods (10 AM to 4 PM, and 8 PM to 6 AM)
Speed: Speed filters will control various traffic conditions. **1) Outlier policy: Free-flow** data using the outlier elimination method defined in "Removing outliers (free-flow data selection)" **2) No filter:** include data from all speed ranges without restrictions **3) 0-40 MPH** and **4) 0-50 MPH** for low-speed range data.

Designed experiments include each time period at all speed ranges, resulting in a total of **16 experiments (tests)**. It is important to note that there are two peak-hour ranges and two low-speed ranges.

5.4 Results

Table 5.1 show results for the TT comparison of individual TMCs that correspond to ODOT radar sites. Speed comparison results for these sites were presented in the previous section. Results span from August to December 2021. Table 5.2 shows comparison results for segments with low-speed

ranges. Approximate difference increase, respectively, by: 3, 1.69, and 1.74 at lower speeds (<40 MPH).

Table 5.1
TT comparison results for selected segments.

Selected TMCs	MSE (in minutes)	MAE (in minutes)
INRIX vs. radar	0.62	0.38
HERE vs. radar	0.44	0.43
INRIX vs. HERE	0.74	0.47

Table 5.2
TT comparison results for selected segments (0-40 MPH).

Selected TMCs	MSE (in minutes)	MAE (in minutes)
INRIX vs. radar	3.2	1.15
HERE vs. radar	1.29	0.73
INRIX vs. HERE	9.52	0.82

Of greater interest is TT estimation for routes whose results are presented below.

Table 5.5 shows the summary of comparison results for all 16 experiments comparing radar and probe-based systems. Results are averaged over the results from all 9 routes and are shown for two cases: 1) when the total route length for radar is the average route length of both INRIX and HERE, and 2) when the total route distance is simply INRIX route length compared to INRIX and HERE route length when compared to HERE. Each row corresponds to an experiment with speed and time restrictions applied to the data. The last two columns show the MAE for TT in minutes for each system. The first error column uses the average route length to calculate TT for radar. The second error column uses INRIX route length for radar TT calculation when comparing radar to INRIX, and similarly for HERE.

Based on the results in Table 5.5, Table 5.3, shows the speed experiments of radar vs. HERE. The average is shown for each variable over speed and time sub-categories. For example, the 0-40MPH row shows the average errors over all experiments under a speed range of 0-40MPH conditions. For example, the average TT MAE between radar and HERE is 4.16 minutes in 0-40 MPH, and 0.55 minutes across all time periods.

Based on the results of Table 5.5, Table 5.4 shows results for time experiments investigating radar vs. HERE.

Table 5.3
Average of Radar vs. HERE difference across all routes and speed experiments.

Speed	Radar vs. HERE MAE (in minutes) $d_{radar} = avg(d_{here}, d_{inrix})$	Radar vs. HERE MAE (in minutes) $d_{radar} = d_{here}$
All (any speed)	0.6	0.55
Outlier Removal	0.38	0.31
0 – 40 MPH	4.49	4.16
0 – 50 MPH	2.28	2.24

Table 5.4
Average of Radar vs. HERE difference across all routes and time experiments.

Time	Radar vs. HERE MAE (in minutes) $d_{radar} = avg(d_{here}, d_{inrix})$	Radar vs. HERE MAE (in minutes) $d_{radar} = d_{here}$
8 AM – 6 PM	2.26	1.97
All (any time)	1.82	1.75
Peak	2.0	1.93
Off-Peak	1.68	1.61

Table 5.5
Summary of TT comparison for all 9 routes across 16 experiments carried out between August 2021 and May 2022.

Experiment	Speed	Time	MAE (TT) in minutes $d_{radar} = avg(d_{here}, d_{inrix})$	MAE (TT) in minutes $d_{radar} = avg(d_{here}, d_{inrix})$	MAE (TT) in minutes $d_{radar} = avg(d_{here}, d_{inrix})$	MAE (TT) in minutes	MAE (TT) in minutes
			INRIX vs. Radar	INRIX vs. HERE	Radar vs. HERE	INRIX vs. Radar $d_{radar} = d_{inrix}$	**Radar vs. HERE** $d_{radar} = d_{here}$
1	All	8 AM – 6PM	0.68	0.61	0.67	0.72	0.61
2	Outlier Removal	8 AM – 6 PM	0.48	0.45	0.47	0.52	0.41
3	0-40MPH	8 AM – 6 PM	5.46	2.55	5.46	5.59	4.45
4	0-50MPH	8 AM – 6 PM	2.77	1.73	2.45	2.82	2.41
5	All	All	0.66	0.64	0.57	0.69	0.51
6	Outlier Removal	All	0.42	0.47	0.32	0.46	0.25
7	0-40MPH	All	4.98	2.45	4.15	5.1	4.04
8	0-50MPH	All	2.71	1.6	2.25	2.75	2.21
9	All	Peak	0.72	0.7	0.7	0.76	0.64
10	Outlier Removal	Peak	0.49	0.47	0.44	0.53	0.37
11	0-40MPH	Peak	5.35	2.37	4.45	5.48	4.33
12	0-50MPH	Peak	2.87	1.62	2.41	2.92	2.37
13	All	Off-Peak	0.61	0.59	0.48	0.64	0.43
14	Outlier Removal	Off-Peak	0.42	0.48	0.3	0.46	0.23
15	0-40MPH	Off-Peak	4.68	2.56	3.92	4.8	3.8
16	0-50MPH	Off-Peak	2.46	1.55	2.01	2.5	1.98

Based on the previous results, we can draw the following conclusions:

- In low speed (<50 MPH), radar TT estimation has an average absolute difference ranging from two to four minutes from HERE.
- In normal traffic flow, radar TT estimation has, on average, less than a one-minute average absolute difference from HERE.
- TT estimation has, on average, a two-minute average absolute difference from HERE across different time ranges (i.e., peak, off-peak, all, 8 AM-6 PM).
- Radar is deficient (i.e., high error) in the speed range 0-40 MPH particularly—low sample (data) size and inaccurate speed measurements. The average absolute difference increases significantly compared to free flow.

Finally, it is worth noting that radar has lower data density in lower speed ranges (i.e., 0 – 40 MPH). We have previously mentioned and shown this issue when comparing the speed distribution of radar and AVC (see Figure 4.16 and Figure 4.17), which indicates that radar does not detect motion as efficiently as AVC in lower speed ranges. To further understand the issue, we explored the results shown in Table 5.6. The number of data samples, per route, for each of the three systems (radar, INRIX, and HERE) in comparison to the remaining number of data rows at the 0–40 MPH speed range. In the table, "Any" means data in all speed ranges without filtering. Results include data from all hours without a time filter – including all available hours throughout the day rather than selecting specific periods such as peak hours. The table clearly shows the lack of data samples at lower speed ranges for the routes, the radar deficiency at this range is the most pronounced compared to HERE and INRIX.

Table 5.6
Effect of low-speed data filtering on data size.

Route	Radar	Radar	INRIX	INRIX	HERE	HERE
	Any	0-40MPH	Any	0-40MPH	Any	0-40MPH
1	4512	68	190084	7196	94955	2175
2	15844	710	511833	7994	257735	2285
3	19784	1351	242616	17458	135650	11630
4	14404	29	346676	6764	162780	1401
5	1536	24	50964	1217	27130	344
6	11428	2624	210839	19026	108520	6861
7	12868	0	116510	146	54260	5
8	15844	29	290225	1435	135650	222
9	12868	11	151918	1572	94955	328

Before wrapping up this section of the report on TT analysis, there are a couple more factors, which generally should have an impact on TT, that we would like to discuss. To be more specific, we would like to show the effect of the number of radars along a route and total route length on TT accuracy measured by MAE. Although these relationships may seem intuitive since more radars and shorter routes should theoretically lead to better TT estimates. However, it is useful to statistically test and prove these ideas.

5.5 Effect of number of radars on TT

To be able to understand the effect of the no. of radars on route length, the TT MAE should be compared for routes of different lengths. However, any discrepancies would be particularly highlighted if the comparison include of the same length but with different no. of radars. Then, observing the MAE (mean absolute error) of TT would show the impact of route length on TT accuracy. Out of the group of selected routes for this study, we have one route with one radar, five with two radars, and three with three radars. Yet, each group of routes that have the same number of radars varies in length.

That being said, we can still observe the effect of the no. of radars on TT by measuring the distance or length assigned per radar, this tells us how sparse the radars are located along a route. The distance per radar can be thought of as the segment length for each radar. The distance per radar is calculated by dividing the route length by the number of radars available on the route. For instance, in Table 5.7, the distance per radar for route 7 is obtained by dividing 4 miles of route length by the 2 radars, which results in 2 miles per radar. Higher "distance per radar" means that each radar will need to cover a larger portion of the route and provide speed data which is used for TT calculation. Similarly, lowering the distance per radar leads to a smaller coverage area, which should increase TT accuracy. Thus, adding new radars to a route leads to a lower "distance per radar" while eliminating a radar unit will increase this distance, this is assuming the whole route length (distance) is the same when new radars are added or eliminated.

Table 5.7 shows the calculated MAE (mean absolute error) for travel time regardless of speed range (free-flow, 0-40 MPH, etc.) or time period (peak, off-peak, etc.). The TT MAE is shown per route as well as the length of the route (miles), no. of radars along the route, and the length per radar (miles) – obtained by dividing the total route length by the number of radars along the route, number of INRIX segments, number of HERE segments, highway, and the city within which the route is located. The table is sorted according to the length per radar in ascending order.

Table 5.7
TT MAE per route

Route	Length	No. of Radars	Length per radar	No. of INRIX segments	No. of HERE segments	Highway	City	INRIX vs. HERE	INRIX vs. Radar	Radar vs. HERE
5	2	1	2	4	2	I-44	OKC	0.28	0.16	0.22
7	4	2	2	8	4	I-44	Tulsa	0.33	0.27	0.07
9	4	2	2	12	7	SH-51	Tulsa	0.45	0.42	0.17
1	5	2	2.5	13	7	I-35	OKC	0.31	0.53	0.33
6	6	2	3	16	8	I-44	OKC	0.95	1.22	1.33
2	9	3	3	35	19	I-40	OKC	0.6	0.86	0.46
8	9	3	3	20	10	I-44	Tulsa	0.78	0.81	0.47
3	7	2	3.5	17	10	I-40	OKC	0.81	0.84	0.82
4	12	3	4	24	12	I-40	OKC	1.21	1.1	0.71

Table 5.8 averages errors within each group of routes that have the same distance per radar. For example, we have three routes (5, 7, 9) with 2 miles per radar, the TT MAE for these three routes is averaged to provide an overall MAE that represents the TT error for this distance per radar. For instance, the MAE for INRIX vs. HERE for the three routes (5, 7, and 9) which have 2 miles per radar are 0.28, 0.33, and 0.45, respectively and the aggregated error for these is 0.35, shown in the subsequent Table 5.8. Comparing this calculated value to other MAE values at various other distances will show the effect of having more or fewer radars on TT accuracy.

Table 5.8
TT MAE per radar segment length (distance per radar along a route)

Length per radar	INRIX vs. HERE	INRIX vs. Radar	Radar vs. HERE
2	0.35	0.28	0.15
2.5	0.31	0.53	0.33
3	0.78	0.96	0.75
3.5	0.81	0.84	0.82
4	1.21	1.1	0.71

Notice, for example, that when length per radar is 3 miles the MAE for INRIX vs. HERE, INRIX vs. Radar, and Radar vs. HERE are 0.78, 0.96, and 0.75 respectively. However, if the distance is decreased to 2.5 which can be achieved by adding more radars, the TT MAE for INRIX vs. HERE, INRIX vs. Radar, and Radar vs. HERE drops to 0.31, 0.53, and 0.33 respectively. The error decreases by 2.5, 1.8, and 2.2 folds for INRIX vs. HERE, INRIX vs. Radar, and Radar vs. HERE respectively.

Figure 5.9 is a visualization of the previous Table 5.8 showing the progress of TT MAE as we increase the distance assigned per each radar along the route.

Table 5.9 Effect of number of radars on route TT

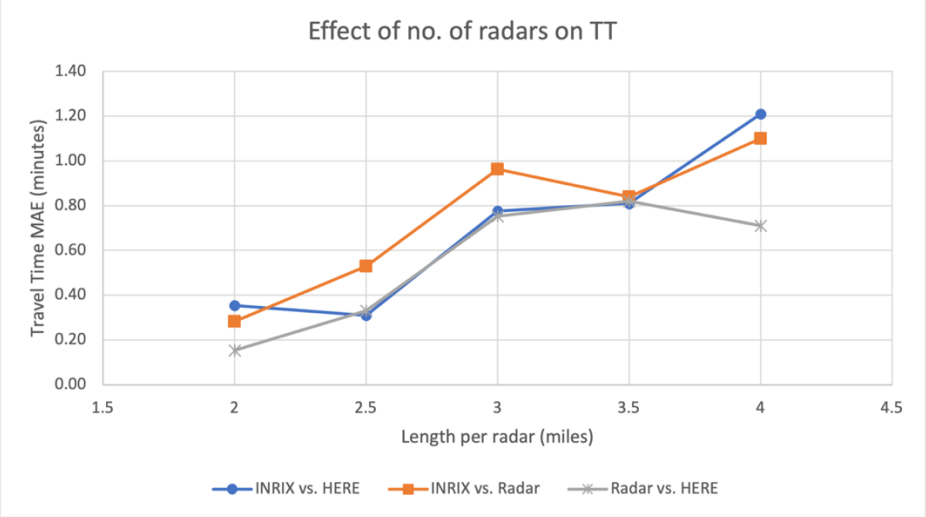

Notice that as the distance (length) assigned to each radar on a route increases, the TT MAE increases because sparsity increases. This is due to the fact that each radar will have a larger distance to cover which leads to lower accuracy in calculating TT.

To understand this, let us consider a route with a total length of 6 miles and has 2 radars, then the distance per radar is 6/2 which is 3 miles per radar. If a new radar along this route is added, then the length assigned to each radar will become 6/3 which is 2 miles per radar. We would expect the TT MAE for INRIX vs. HERE, INRIX vs. Radar, and Radar vs. HERE to drop by 2.2, 3.4, and 5 folds respectively based on the previous table.

5.6 Effect of route length on TT

To showcase the effect of variable route length on TT MAE, we need to observe the error for routes that have the same number of radars but have different total lengths. For example, routes 7, 9, 1, 6,

and 3 all have 2 radars but have the following lengths 4, 4, 5, 6, and 7 miles, respectively. Below, Figure 5.19, shows the TT MAE as we change the route length for these routes using the data presented in Table 5.7.

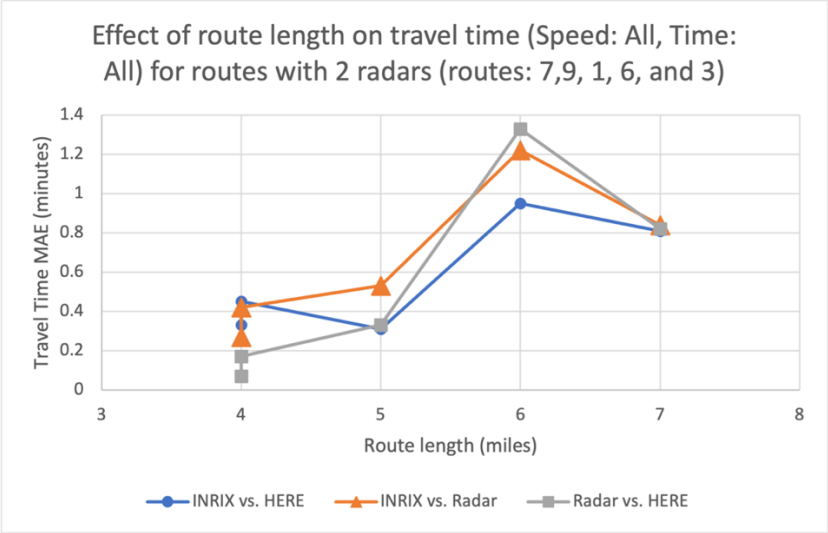

Figure 5.19 Effect of route length on TT

Observing Figure 5.19, we notice that the TT MAE has a general tendency to increase as the total route length increases; which is expected. It should be noted that there are many other factors that can impact the TT MAE for these routes other than route length as these routes are located in different regions (i.e., city, highway, location, etc..) which are observing different traffic behaviors. Yet, we still notice that the MAE increase for longer routes compared to shorter ones with the same setup – being the number of the radars.

5.7 Summary

In this section, we introduced the results of the TT comparison for both individual segments and routes. Routes start from DMS displays and end at nearby intersections; they have different length ranges (i.e., from 2 to 12 miles long). The first six routes are in OKC, and the last three are in Tulsa.

Experiments demonstrated a two-minute difference, on average, in TT estimation between radar and HERE across different time ranges (e.g., peak, off-peak, 8 AM–6 PM). Radar TT estimation has, on average, a one-minute variance from HERE in the free-flow speed range and a two to four minutes variance in the less than 50 MPH speed range. Radar is not as efficient as HERE in low-speed ranges.

Chapter 6: Volume Comparison

Next, we present volume comparison results between radar and AVC over two periods spanning September to December 2021, which included speed and volume data, as well as September 2021 to August 2022, which included only volume data. Comparison experiments used for volume comparison are the same as experiments (tests) designed for TT comparison (see the " Experiments" section).

Volume data for AVC during 2022 had a different format than data reported for 2021. Appropriate preprocessing and formatting were applied to AVC to extract volume data from 2022 and incorporate it with data from 2021. It is important to note that volume comparison is reported for radar and AVC sites, not for routes.

6.1 Results

Since the experimentation setup for time (e.g., peak, off-peak, etc.) and speed (e.g., traffic conditions) has been already introduced and discussed in the previous section, we can now report the results of volume comparison between radar and AVC.

Table 6.1 shows the results for AVC vs. Radar volume, per timestep of 15-minute intervals. Note that the time span for investigation is from September to December 2021. This is because AVC volume raw data for 2022 did not contain speed data. We preprocessed newly formatted volume data and merged it with volume data from a previous year. Table 6.1 shows MAE volume, the percentage of time in which radar's volume estimation was lower than AVC's, and average positive and negative volume differences as well as the number of data samples (size).

Table 6.1
Volume comparison: experiments results (AVC vs. radar) from Sept. to Dec. 2021.

Experiment	Speed	Time	**Volume MAE**	**Volume MAPE (%)**	% of time Radar volume < AVC volume	Avg. positive difference (radar is higher)	Avg. negative difference (radar is lower)	**Data Size**
1	All	8 AM – 6PM	33.01	18.03%	50.35%	43.06	23.1	399107
2	Outlier Removal	8 AM – 6 PM	31.76	17.55%	50.42%	41.92	21.77	384359
3	0-40MPH	8 AM – 6 PM	83.07	41.8%	50.8%	140.16	27.79	13056
4	0-50MPH	8 AM – 6 PM	32.71	18.29%	51.8%	47.79	18.67	73157
5	All	All	24.88	24.4%	47.44%	28.77	20.57	848613
6	Outlier Removal	All	24.41	22.31%	48.08%	28.88	19.59	771615
7	0-40MPH	All	64.73	49.45%	47.08%	98.33	26.95	20701
8	0-50MPH	All	22.8	24.57%	46.65%	28.73	16.01	149921
9	All	Peak	32.59	21.2%	47.82%	38.81	25.79	361887
10	Outlier Removal	Peak	30.77	20.38%	47.94%	37.44	23.53	338048
11	0-40MPH	Peak	83.92	44.8%	46.78%	127.84	33.95	10386

Experiment	Speed	Time	**Volume MAE**	**Volume MAPE (%)**	% of time Radar volume < AVC volume	Avg. positive difference (radar is higher)	Avg. negative difference (radar is lower)	**Data Size**
12	0-50MPH	Peak	31.92	20.36%	47.44%	42.45	20.25	64849
13	All	Off-Peak	21.61	25.39%	48.18%	24.04	18.99	631256
14	Outlier Removal	Off-Peak	21.76	23.14%	48.99%	24.75	18.65	573395
15	0-40MPH	Off-Peak	52.18	50.47%	48.16%	80.29	21.92	14128
16	0-50MPH	Off-Peak	18.4	25.87%	47.48%	22.1	14.31	110464

Table 6.2
Volume comparison: average of difference over speed experiments (AVC vs. Radar) (Sep. to Dec. 2021)

Speed	Volume MAE	MAPE (%)	% of time Radar volume < AVC volume	Avg. positive difference (radar is higher)	Avg. negative difference (radar is lower)
All	28.02	22.26%	48%	33.67	22.11
Outlier Removal	27.18	20.84%	49%	33.25	20.89
0 – 40MPH	70.98	46.63%	48%	111.7	27.65
0 – 50MPH	26.46	22.27%	48%	35.27	17.31

Table 6.3
Volume comparison. Average of difference over time experiments (AVC vs. radar) for Sep. to Dec. 2021.

Time	**Volume MAE**	MAPE (%)	**% of time Radar volume < AVC volume**	**Avg. positive difference (radar is higher)**	**Avg. negative difference (radar is lower)**
8 AM – 6PM	45.14	23.92%	51%	68.23	22.83
All	34.21	30.18%	47%	46.18	20.78
Peak	44.8	26.88%	47%	61.64	25.88
Off-Peak	28.49	31.22%	48%	37.8	18.47

Table 6.2 and Table 6.3 aggregate results shown in Table 11 to summarize the volume analysis for various speed ranges regardless of the time period and various time periods regardless of the speed range.

Based on Table 6.2 and Table 6.3 results:

- There exists around a 20% difference (Table 6.3) in volume in free-flow conditions between radar and AVC.
- In low-speed conditions, the difference increased to 46%. The difference is particularly recognized at < 40 MPH.

Table 6.4 shows the volume comparison results for the period spanning from September 2021 to August 2022. Looking at the results presented in Table 6.1 for the period from September to December 2021, we notice that the results are similar which shows that the results of the previous table were statistically representative. For instance, the MAE and MAPE for the 8 AM – 6 PM were 33.01, and 18.03%, respectively, in Table 6.1. The values of MAE and MAPE, Table 6.4, were 28.65, and 18.16%, respectively.

Table 6.4
Volume comparison for one year (September 2021 to August 2022)

Time	MAE (vehicles)	MAPE (%)
8 AM – 6PM	28.65	18.16%
All	21.99	24.92%
Peak	28.43	21.36%
Off-Peak	19.32	26.16%

Figure 6.1 shows mean absolute percentage error (MAPE) per site.

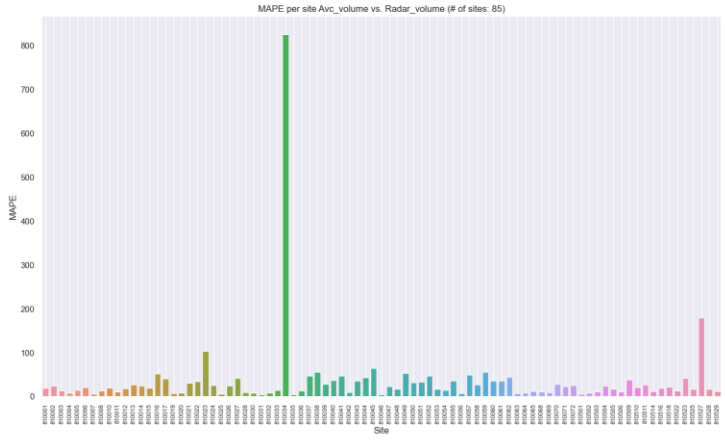

Figure 6.1. Volume MAPE per site Radar vs. AVC) from Sept. 2021 to Aug. 2022.

Where MAPE (mean absolute percentage error) is calculated as follows:

$$MAPE = \frac{100}{n}\sum_{i}^{n}\left|\frac{AVC_{volume} - Radar_{volume}}{AVC_{volume}}\right|$$

Figure 6.2 MAPE volume equation for AVC and Radar

Notice that in Figure 6.1 three sites (*810034, 810527, and 810023)* have relatively much higher differences than others. After removing these sites, a MAPE per site graph is shown in Figure 6.3.

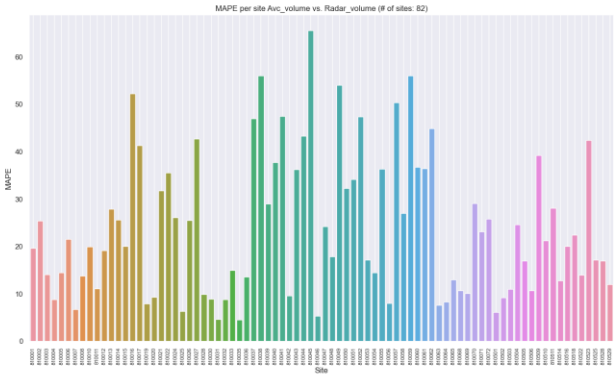

Figure 6.3. Volume MAPE per site (radar vs. AVC) from Sept. 2021 to Aug. 2022. Metric: MAPE, after removing 34,27, 23.

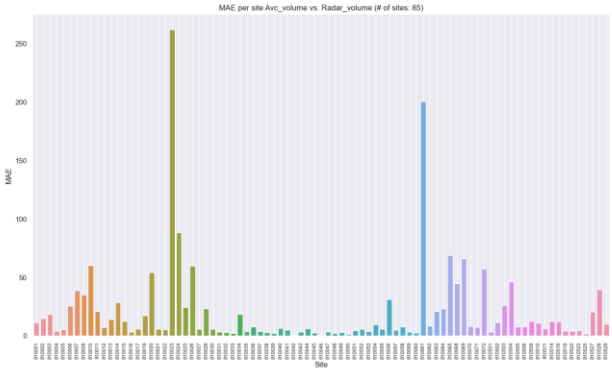

Figure 6.4. Volume MAE per site (radar vs. AVC) from Set.p 2021 to Au.g 2022. Metric: MAE.

The following shows the MAPE error per site for both directions.

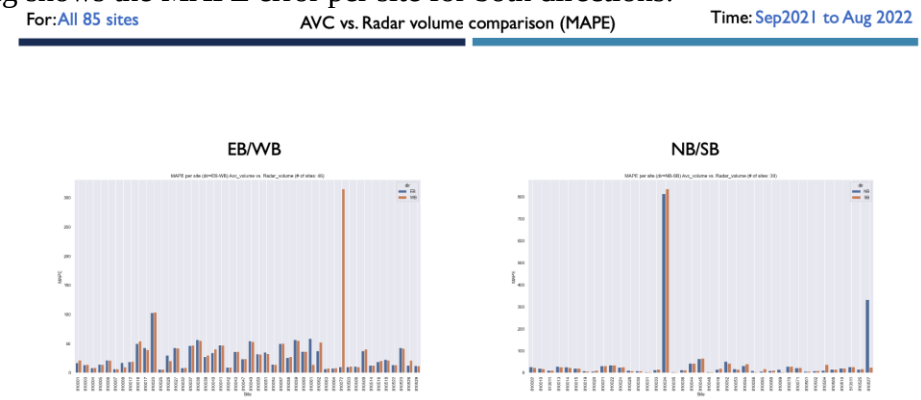

Figure 6.5. Volume comparison per site and direction (radar vs. AVC) from Sept. 2021 to Aug. 2021. Metric: MAPE.

In Figure 6.5, the graph on the left shows sites with EB/WB directions. The graph on the right shows sites with NB/SB directions. These visuals will aid in understanding whether the error for one direction is higher, which can explain the reason for the error. For example, site 8105127 has a much higher error for NB and a reasonable error for SB.

The following graph shows the sum volume over the whole period per site and direction for both systems.

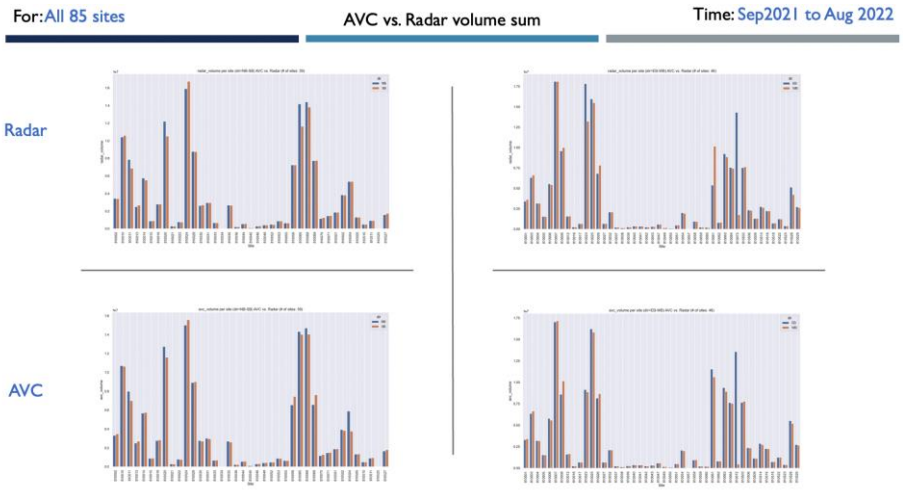

Figure 6.6. Volume comparison: sum over the whole period (radar vs. AVC) from Sept. 2021 to Aug. 2022.

6.1.1 Summary

In this section, we presented results for volume comparison between radar and AVC over the period from Sept. 2021 to Aug. 2022. Results demonstrated (see Table 6.2) a 27-vehicle difference between radar and AVC across different speed ranges. For lower speed ranges, specifically 0–40 MPH, the difference increases to 70. Comparison across different time ranges (see Table 6.3) showed 45 vehicles at peak times and 28 at off-peak with an overall count of 34 across all time ranges.

Chapter 7: Modeling Travel Time Estimation

The objective of this phase was to develop statistical schemes and machine learning models for leveraging radar data to estimate TT.

Two main types of models can be implemented: 1) estimation, in which models will estimate TT at the current moment, and 2) forecasting, in which models will estimate TT for the future (e.g., next hour). Although we are primarily interested in prediction models, we also experimented with forecasting models.

It should be noted that modeling was performed on data extracted from free-flow conditions since radar was found to be less efficient compared to HERE and INRIX at lower speeds. Issues at lower speeds were high MAE (mean absolute error) in speed measurements and, in turn, TT calculations as well as the low data sample size (i.e., number of data rows), especially at < 40 MPH.

7.1 Setup

Models are trained for each route, which means an appropriate dataset had to be built for modeling for each route under investigation.

Description of the dataset: A labeled dataset was built for each route. Features (i.e., data columns) are defined as data needed for the model to estimate the target label. In this case, features are speed measurements by the radars along the route in MPH as well as the distance per radar in miles. HERE TT, measured in minutes, was calculated for each of the routes and used to label the data rows of the constructed table.

Appropriate preprocessing and feature normalization and standardization were applied to the data.

Figure 7.1 shows an example of a dataset for a route with two radars.

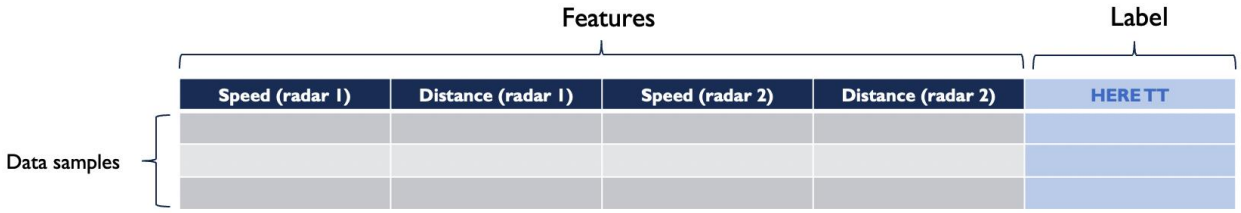

Figure 7.1. Dataset setup (shape) used for modeling a route with two radars.

Data split (i.e., data is randomly split into the following). **15%** of the data was reserved for the *test set (Never exposed to the model during training stages).* the other **85%** was divided into **90%** as the *training set* and **10%** as a *validation set*. The **Train set** is used to train the models and has a shape like in Figure 7.1. The **validation set** (i.e., development set) is used to periodically evaluate the model and steer the training procedure in the right direction. It is important for hyperparameter tuning, which is a process for searching and selecting the best model parameters based on values that yield superior results. The **test set** is used for final evaluation and to report model performance.

Although it is also common to divide data into only two datasets (training and testing), such a split might be locally optimized on the testing set, leaving us unable to detect performance bias. Hence, using a validation set for optimization and a test set for performance evaluation provides a top-quality estimate.

Performance metrics: error metrics, including MSE, MAE, and RMSE)**.** Difference ($actual - predicted$) error visualization across time. Analysis of error distribution difference was also performed.

Baseline model

To evaluate model performance on the test set, a baseline model must be available for comparison. Since this is a regression task, where we will get a regression error that is harder to interpret compared to classification metrics like accuracy. Therefore, we use a baseline model as a performance benchmark.

The chosen baseline model is one that always predicts the mean HERE TT (i.e., target column). We assume if the candidate model is performing better than a model that always yields average TT for a specific route, the model is learning meaningful representations of data.

To further explain how the baseline model works: after the data table is constructed per route using speed measurements from the radars along the route as well as the TT provided by HERE, the data is split into various sets for training, validation, and testing. Performance is evaluated and reported on the test set – the other two sets are used for training the ML models. The average HERE TT of the test set is calculated and the MAE is calculated for this value against all of the data samples (i.e., rows in 15-minute intervals), the average error across all rows in the test set is the MAE for the baseline model. To illustrate this, for instance, if you always estimate TT to be 6.49 minutes for route 6, in Table 7.1, you will get an MAE (mean absolute error) of 0.84 minutes.

Table 7.1
Average Absolute Difference as Compared to HERE TT Estimation.

Route	Average HERE TT (minutes)	Baseline model MAE (minutes)
1	4.53	0.1
2	8.15	0.27
3	7.51	0.32
4	10.87	0.27
5	1.62	0.04
6	6.49	0.84
7	3.08	0.07
8	7.71	0.16
9	3.75	0.06

The intuition behind choosing such a model for benchmarking stems from the idea that capable machine learning models should provide better estimations than the average TT for the route by capturing the statistical patterns from the speed dataset, thus exceeding the performance of the baseline model.

7.2 Models

We have experimented with and trained 14 different machine learning models/algorithms, including XGBoost, Linear Regression, Ridge Regression, Lasso Regression, Polynomial Regression, Support Vector Machines, ElasticNet Regression, Robust Regression (RANSAC, Huber, TheilSen), Regression Trees, Random Forest, Gaussian Process Regression, Neural Networks: standard (vanilla MLP).

Table 7.2 shows the MAE averaged across all nine routes for each of the algorithms on the test set (part of the data table which is not seen by the algorithms during learning processes). These should

be compared to the baseline MAE averaged for all routes which is calculated by taking the average value of the MAE column in Table 7.1, which results in 0.24 minutes. Therefore, algorithms, in Table 7.2, whose collective performance across the routes has a better (i.e., lower) MAE value than 0.24 minutes is considered acceptable. Note that these results are during free-flow conditions.

Table 7.2 Machine Learning Models used for TT Estimation and MAE across all routes.

Model	MAE (minutes)
Decision Tree	0.18
Elastic Net	0.23
Random Forest	0.18
Gaussian Random Process	0.20
Lasso Regression	0.20
Linear Regression	0.20
Neural Network	0.31
Polynomial Regression	0.19
Ridge Regression	0.20
Robust Huber	0.19
Robust Ransac	0.21
Robust Theil	0.26
Support Vector Machines	0.19
XGBoost	0.18

7.3 Clustering

Clustering was experimented with to boost model performance. Idea: cluster *data features* and train a separate model for each cluster.
Intuition: training a separate model for each data group (i.e., cluster) to create a marginally easier learning problem for ML models to fit, thus leading to *performance improvement*. Improvements were achieved but they were limited.

7.3.1 Method

The two-step procedure consists of clustering the data into sub-datasets and then developing regression models per sub-dataset to estimate TT The resulting model is an ensemble model of regression and clustering models.

Figure 7.2 visually details the model. The dataset is described in Figure 7.1, per route, and then processed through a clustering model (i.e., algorithm) to divide it into sub-datasets based on feature similarity between data samples. Most clustering algorithms require establishing the number of clusters K that corresponds to the number of sub-datasets. Figure 7.1 shows the results for $K = 3$, as an example.

Once sub-datasets are defined, an independent machine learning model can be built for each. This means, if there are three sub-datasets, each route will have three models.

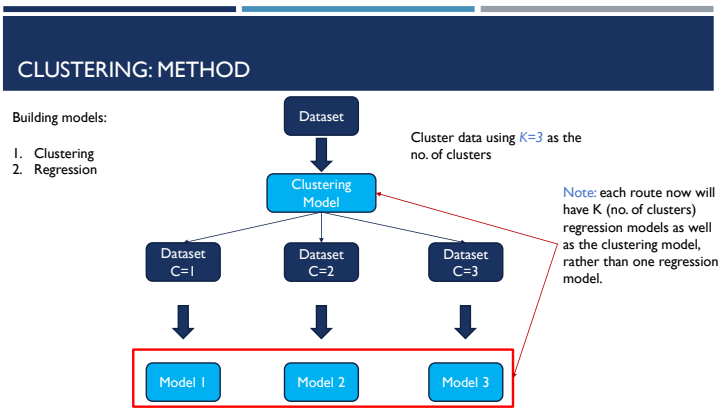

Figure 7.2. Clustering method: setup and training for example K=3.

After understanding how to train the models, it is important to understand how doing so is accomplished in inference time (i.e., when using models to make predictions/estimations on actual data).
Figure 7.3 explains the steps needed for inference. First, the input data sample (e.g., a row in Figure 7.1) is input into the clustering model previously trained on historical data for the designated route. Second, the clustering model will assign data to the appropriate cluster. Third, the data sample is input into the appropriate regression model trained to estimate TT for the designated cluster. Lastly, the regression model will yield an output.

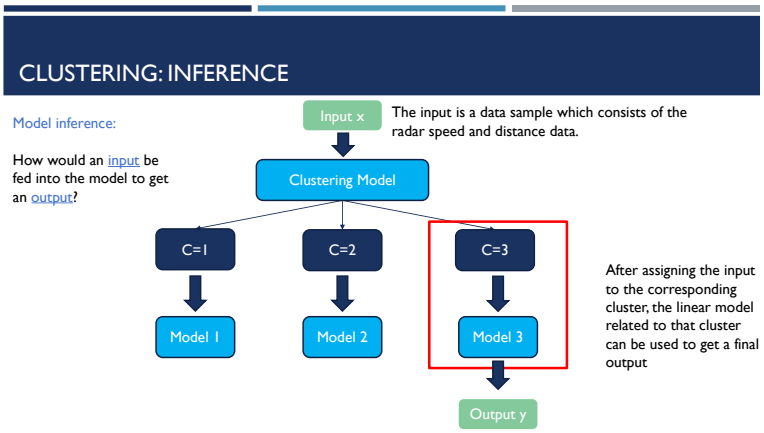

Figure 7.3 Clustering method: inference for example K=3.

The number of clusters affects performance significantly. Therefore, various methods widely adopted by the machine learning community were tested to determine the best possible K for the data.

Figure 7.4 shows the results for route 4 data (see Figure 5.13) when choosing K. The graph on the left shows results for the elbow method (i.e., lower is better), where a good value means that the SSE (sum of squared errors) begins plateauing at the point wherein the graph begins forming an elbow shape. The graph on the right shows the Silhouette coefficient method (i.e., higher is better). In this case, based on Figure 7.4, $K = 4$ was selected. Notably, $K = 3$ is also a viable choice.

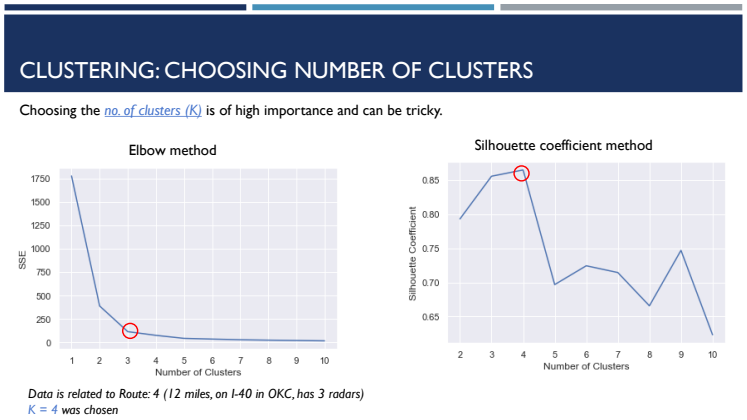

Figure 7.4. Clustering choosing K.

7.4 Neighboring radars

The goal for this section is improving models and performing data experimentation. Idea: Utilize data from radars surrounding the route to increase dimension size (i.e., number of features) and improve results. Intuition: Surrounding radars should be a contributing factor to the traffic condition of the route itself and, thus, have an impact on TT estimate. Note that only speed was used from the neighboring radar data. No additional distance columns were used. For example, given three neighboring radars for the route in Figure 7.1, there will be three additional feature columns for radar speed measurements.

Figure 7.5 shows an example route—the beginning point (green car) and end point (red car) of the route, on-route radars (blue circles), displays (pink circles), and neighboring radars (red circles) with three types of neighboring radars: “Before radars”, which proceed the route, with traffic feeding into the beginning of the route, “Middle radars”, in which traffic feeds into the middle of the route, and “After radars”, wherein the route feeds traffic into them.

For example, in Figure 7.5, the before-radar can be 811116, the middle-radar can be 811001, and the after-radar can be 811020.

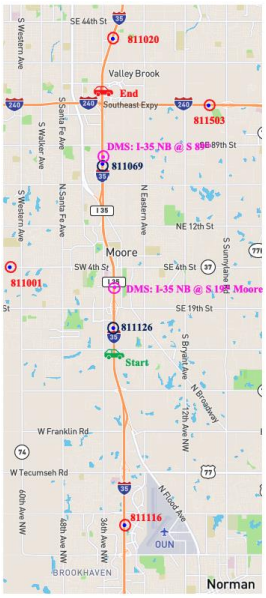

Figure 7.5. Route 1 on I-35 in OKC (~5 miles),

The list of the chosen radars as neighboring radars per route is as follows: Route 1: 811116, 811001, 811020, 811503. Route 2: 811066, 811112, 811023, 811056, 811008, 811020, 811111. Route 3: 811061, 811061, 811114, 811115. Route 4: 811056, 811110. Route 5: 811061, 811023, 811115. Route 6: 811061, 811115, 811007, 811112, 811072. Route 7: 811097, 811090. Route 8: 811104, 811096, 811105. Route 9: 811103, 811096, 811097, 811098.

7.5 Time Series Analysis

We have also experimented with models for predicting TT (future prediction) rather than providing instantaneous TT estimation.

Training models must incorporate time into TT estimation. Trained models use radar speed measurements as well as distance per radar along a route to predict TT with data provided by HERE.

Like previous modeling analyses, data were preprocessed, normalized, and standardized. Additionally, data was reshaped for transformation into a convenient format for the model.

A selected long short-term memory neural network (LSTM) model will utilize previous timesteps—each separated by 15 minutes—to predict TT for the upcoming time step. In other words, using data from the past 45 minutes can predict TT for the upcoming 15 minutes.

Doing so requires setting up the data in a way in which each data sample consists of data (feature representation) for the first, second, and third timestep

The target (i.e., value to predict) is the TT in minutes for the upcoming (i.e., fourth) timestep provided by HERE.

Feature representation is radar speed measurements *(MPH)* along a route, along with their corresponding distances *(length per radar measured in miles)*.

Training setup: the used model is an LSTM neural network – proven historical performance on time series data is the community standard choice. Two model architectures were experimented with, an architecture is what describes the neural network graph (i.e., the number of layers, neurons, and connections). Given the small data size, a small (i.e., shallow) architecture was chosen; larger models require much more data. Two architectures were tested. Architecture 1: two LSTM layers with four units, which use 'tanh' as an activation function and an output layer with one unit. Architecture 2: one-LSTM layer with four units, which uses 'tanh' as an activation function and an output layer with one unit. Architecture 2 (smaller) achieved better results on the test data. Because it has fewer parameters to learn, this architecture does not require as much data as Architecture 1.

Data split: data samples for each route were randomly split into **80%** for **training**, **10%** for **validation**, and **10%** for **testing**. Reported results are based on model predictions on the test data. The model was never exposed to test data while training. Background: training data was used to train the model and facilitate learning from the data. Validation data was used to evaluate the model's performance while training to tune and tweak the model hyperparameters and training setup to achieve improved performance. Testing data facilitates the final evaluation of model performance and result reporting.

Other setup choices include the number of training epochs which was 350, and the loss (objective function) which was MSE (other tracked metrics included MAE). To evaluate the performance of the models, each model's performance is evaluated on test data and compared to a baseline model. The baseline model is a naïve model that consistently predicts a constant value as TT. This value is the mean value of the target column (i.e., HERE TT).
Results are presented as a time series analysis rather than a results section. We present estimation models.

Results:
A trained recurrent neural network (LSTM) on route 4 (Figure 5.13) data is presented below.

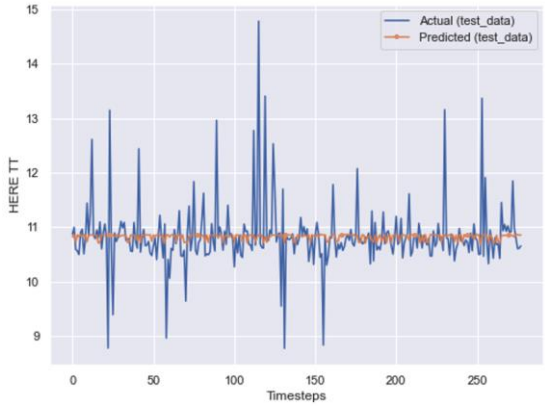

Figure 7.6. Actual vs. predicted TT over time (LSTM) for route 4.

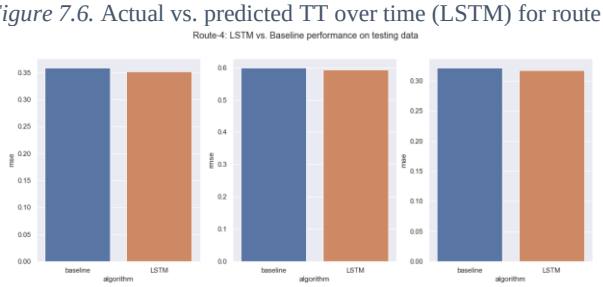

Figure 7.7. LSTM vs. baseline performance on test set.

The results of the LSTM model were only slightly better (i.e., lower error) than the baseline model on the test set. Training a recurrent neural network like LSTM is a data-intensive process that requires large amounts of data to train and yield good performance. Nonetheless, the effort was worth experimenting with the data.

7.6 Correlation Analysis

The goal was to understand the relationship between data from radars and the TT, as well as the overall effect of the results.

Correlation analysis between radar speed data (e.g., neighboring and on-route) and TT was performed to better understand the relationship with and contribution of neighboring radars to overall results.

The following is performed for each route. Pearson's Correlation was applied to speed data columns and TT. P-values were calculated to measure the statistical confidence of the correlation. Heatmap visualizations were generated. The distance between the radars (neighboring and on-route) was calculated. The distance between the radars and starting point of the route was calculated.

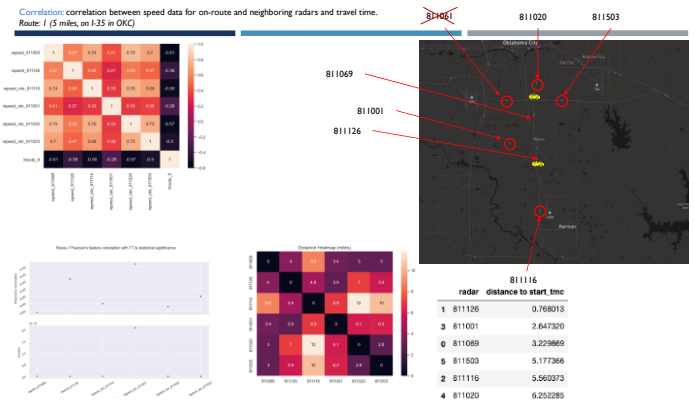

Figure 7.8. Correlation analysis on route 1.

In Figure 7.8, correlation analysis results for route 1 are shown. Plots by position include: (Top left): correlation between speed and TT. (Bottom left): correlation between speed and TT with P-value (i.e., statistical confidence); the lower the p-value the more confidence in correlation values. Low p-values correspond to having a large enough data sample to support the correlation claim. (Middle bottom): heatmap of distances between all radars (e.g., neighboring and on-route). (Top right): route with neighboring and on-route radars, as well as the starting and ending points of the route. (Bottom right): table showing, in ascending order, the distance (in miles) from each radar to the starting point of the route, which acts as a reference point

From the correlation plot (see Figure 7.8), notice that the correlation between speed columns and TT is negative, which is expected because time decreases as speed increases.

Issue: notice that radar site **811061** is removed. After looking at the correlation between the speed column for this radar and itself, we notice speed values were constant over time. Raw data file for this radar was examined to discover that the radar always reported 65MPH for EB and 63MPH for WB. (Refer to Figure 7.9 to see route 1 before removing 811061.)

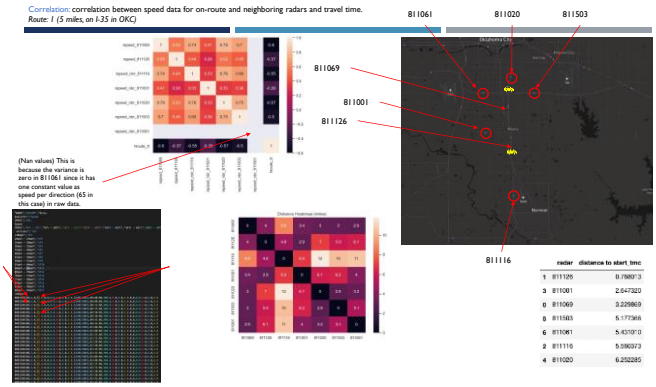

Figure 7.9. Correlation analysis on route 1, including 811061.

Further experiments were carried out to further understand the relationship between the data and TT.

First, visualizing the weights of a linear regression model: Each feature has a corresponding weight in [-1,1]; the closer to 1 or -1, the more important the feature. For example, the weights of two models for route 4 are shown in Figure 7.10, Note that ridge regression is a variation of linear regression. Both models agree on the importance of the features.

The second is “feature dropout” in which we compare model errors on the test set using all features (e.g., data columns). Then, at each iteration, drop a column representing radar speed data and measurement error. This example aids in understanding how removing data from one radar will impact overall model performance. Experiment results for route 1 are shown in Figure 7.11.

Third, “Feature Importance + Random Features”: Four new randomly generated features of different properties were added as data columns. Doing so aid in understanding when original features outperform random features, which means original features actually have a meaningful representation improving model performance. To measure the importance of feature columns, one can look at the corresponding weights of the linear regression model. Weights are in the range [-1,1], and the closer the weight to 1, the higher the importance of the feature. Notably, the sign refers to the nature of correlation, whether positive or negative. 0 indicates the feature is useless. Here is the list of added data columns (features) 1) Gaussian (mean=0, std=1), 2) Binary, 3) Uniform (low=0, high=1), 4) Integer (low=0, high=100). Regarding the experimental results for route 1, notice that random features have the lowest weights, meaning that other features (e.g., speed neighboring and on-route and distances) are more essential for the decision-making process of the model. This also means that the model figured out that this added Gaussian (random) feature is not of interest and can be classified as noise, this acts as a sanity check to validate the results of models.

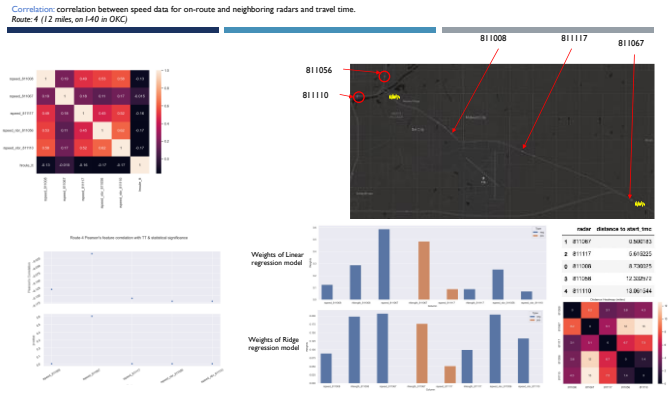

Figure 7.10. Correlation analysis: feature importance on route 4.

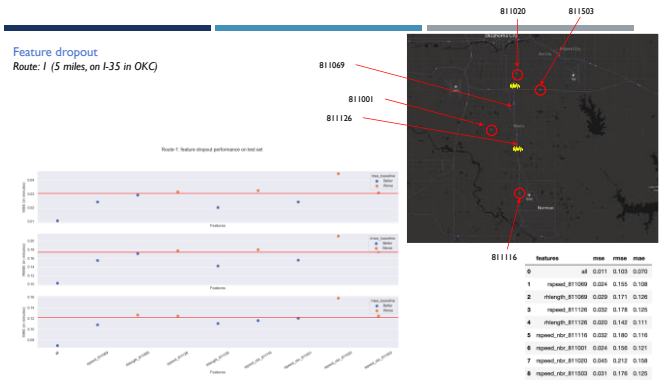

Figure 7.11. Correlation analysis for feature dropout on route 1.

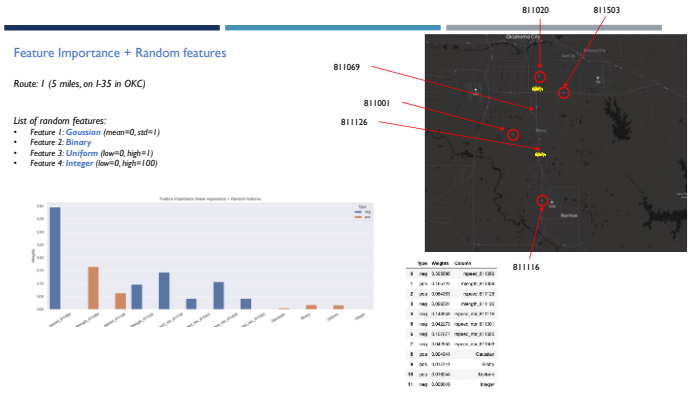

Figure 7.12. Correlation analysis examines feature importance + random features.

7.7 Results

Most models converged to improved performance on the test set for all routes compared to the baseline model, as shown in Table 7.2.

Figure 7.13 is a visual illustration of the performance results of models on training and testing sets for route 1 on I-35 in OKC. The red line corresponds to the baseline model performance. Each corresponds to one algorithm/model. Models performing better (i.e., lower) than the baseline model are highlighted in blue, while models that did not converge to good performance are shown in orange.

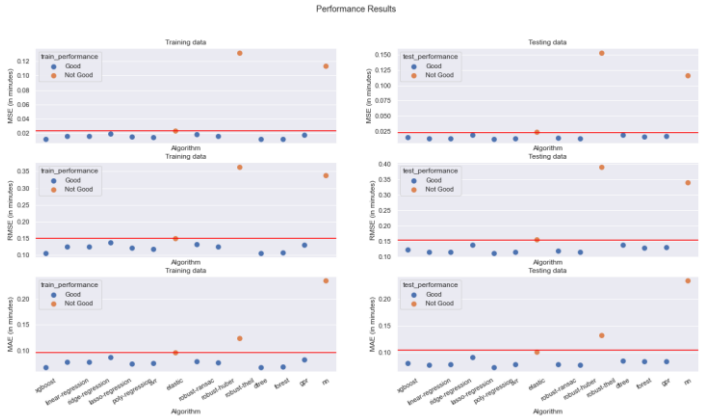

Figure 7.13. Performance results of models on training and test sets. Metrics: MAE, MSE, RMSE.

The following plot shows that the testing data is representative of the training data (i.e., displays a similar distribution/pattern).

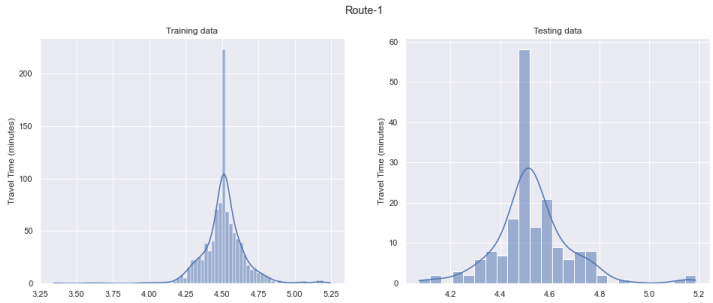

Figure 7.14. TT data distribution for training and test sets for route 1.

Figure 7.14 shows that the testing data is indeed representative of the training data, only on a smaller scale. Given that test data distribution is quite different from the original data, performance results are not trustworthy. In fact, the opposite is quite true.

Figure 7.15 shows estimations and actual TT over time indicated by a model that converged on the data. Notice that the model is not overfitting by not following the unusually large spikes in the training data (see left graph). This makes overall model performance good, which is indicated by test set performance, wherein estimations (in orange) follow the trend smoothly without overfitting.

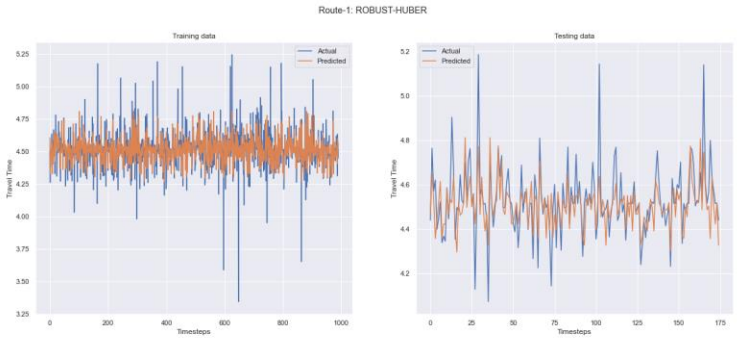

Figure 7.15. Predictions vs. actual over time for robust-huber.

Figure 7.15 shows an error as the difference between estimated TT and actual TT per time step over time (see left graph) for both training and test sets. The last two columns describe the error distribution; the second column is a boxplot, and the third is a histogram. No significantly noticeable patterns are visible in the error, neither temporally nor in distributions. Instead, distributions have a shape similar to a Gaussian, which is expected since the data has a similar distribution.

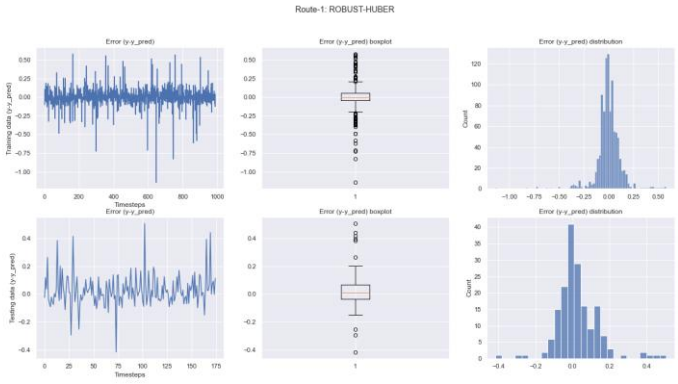

Figure 7.16. Error (y – y_pred) distribution over time.

Table 7.3
Summary of routes and statistics of the testing data.

Route	Length (miles)	Radars	INRIX	HERE	Count (data size)	TT (mean in min)	TT (std in min)	Baseline (MSE)	Baseline (MAE)
1	5	2	13	7	175	4.53	0.15	0.02	0.1
2	9	3	35	19	590	8.15	0.43	0.19	0.27
3	7	2	17	10	647	7.51	0.41	0.17	0.32
4	12	3	24	12	642	10.87	0.59	0.35	0.27
5	2	1	4	2	88	1.62	0.04	0.001	0.04
6	6	2	16	8	623	6.49	1.30	1.67	0.84
7	4	2	8	4	651	3.08	0.09	0.008	0.07
8	9	3	3	10	655	7.71	0.21	0.04	0.16
9	4	2	12	7	603	3.75	0.08	0.007	0.06

Table 7.3 is a summary table of test data results to provide a bird's eye view of the routes, the nature of the test dataset, and the baseline model used for comparison with developed models.

Chosen ML models learned from training data and generalized well to test data, outperforming the baseline model.

Results for modeling with neighboring radars

In Figure 7.17, performance results are shown for training and testing sets for all models on route 4 data. Models beat baseline model performance on both datasets.

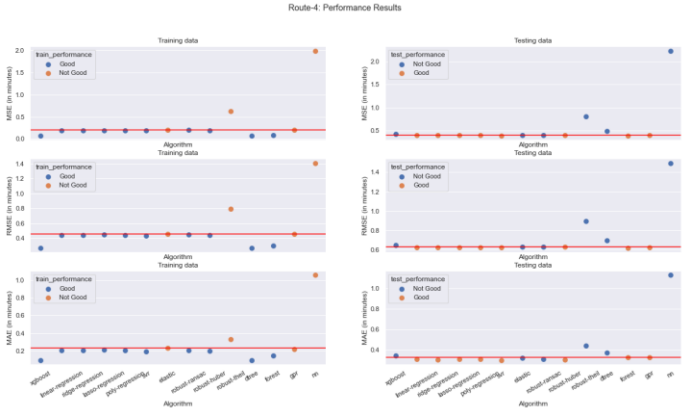

Figure 7.17. Performance results of models on training and test sets for neighboring radars (Metrics: MAE, MSE, RMSE).

This section aids in better understanding how useful data from neighboring radars is compared to using only data from on-route radars for model development.

In Figure 7.18, model performance was improved when training with neighboring radars + on-route radars, Notably, there was an 8.08% error improvement (for MSE) when compared to the baseline model.

In Figure 7.19, the performance of models trained on on-route radars data showed only a 4.85% error improvement (for MSE) when compared to the baseline model.

Figure 7.18. Performance improvement with linear-regression vs. baseline for route 4 with neighboring radars.

Figure 7.19. Performance improvement with linear regression vs. baseline for route-4.

Based on results indicated in Figure 7.19 and Figure 7.19, one can expect a 4% MSE error improvement when using data from neighboring radars compared to using only on-route radars. This is because the percentage improvement of MSE when using neighboring radars, shown in Figure 7.19, was 8.08% while was only 4.85% , in Figure 7.19, when using only on-route radars.

Although using data from neighboring radars improved model performance on the test set, improvement was not substantial.

Correlation analysis experiments indicated the following results.

- Radars near the route end had the greatest effect (in most cases) on TT.
    - For routes 1, 2, 4, 5, 6, and 7, radars near the end (on-route and/or neighboring) were most correlated to TT based on Pearson's Correlation.
- Neighboring radars feeding traffic into the middle of the route had minimal effect on TT.
    - For routes 1, 2, 3, and 6 with middle neighboring radars, radars that feed traffic into the middle of the route had a minimal correlation with TT.
- Speed correlation between radars is based on spatial proximity, as expected.
- There was a negative relationship between radar speed and TT.
- There was no distinguished, generalized pattern that relates radar distances—between each other or to the route starting point—with TT.

7.8 Summary

In this section, we introduced the modeling setup and datasets for routes; the algorithms used, and the various experiments implemented to improve results and better understand relationships and correlations between the data. Some experiments were guided by intuition (i.e., clustering and using neighboring radars data), and others by systematic statistical approaches to analyze data and results (e.g., correlation analysis). Results demonstrated that it is possible to train models that estimate TT with relatively low error using radar data.

Chapter 8: Geospatial and Temporal Analysis

This chapter investigates the spatial and temporal correlation between different speed measurement systems.

The presented results and experiments of this chapter were carried out by OSU (Oklahoma State University)

First, the basic units of investigated systems were visualized in the Oklahoma map and compared to infer the causation of speed differences. Then a similarity checking was conducted on paired sites to quantify the difference between various speed measurements. Subsequently, a panel data analysis was performed to correlate the speeds provided by different measurements.

8.1 Data Description and Processing

The data in this chapter was provided by OU and covered information from two aspects: 1) geospatial paring between Radar/AVC sites and the corresponding HERE & INRIX TMCs or segments; 2) metadata of the four-speed measurement systems. A description of the four-speed measurement systems was summarized in Table 3.2.

Before the data processing, the locations of paired sites and segments were visualized on the map. The matched sites and segments (provided by OU) were visualized in Figure 8.1. The AVC (marked with a circle) and RADAR (star) were site-based measurement systems, while the INRIX (blue lines) and HERE (orange lines) were segment-based systems. It can be observed that the measurement sites of AVC and RADAR generally overlapped. However, the segments of INRIX and HERE were different. The differences in the basic units may cause variations in speed results.

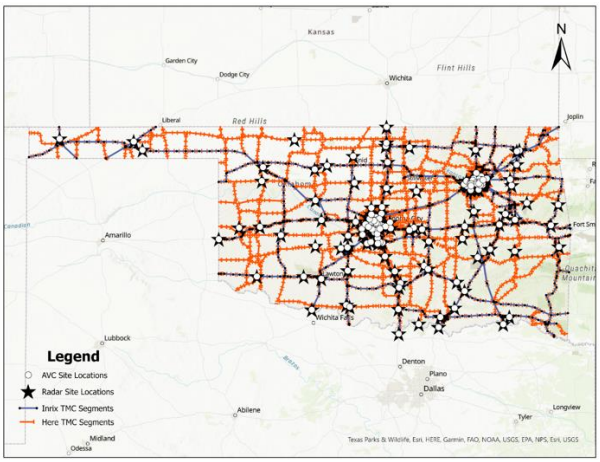

Figure 8.1 GeoMap of sites of four systems

Then the speed measurement data were averaged by day. For RADAR and AVC data, a weighted average was adopted based on vehicle occurrences in different speed bins. It should be noted that volume was not available for INRIX and HERE. Figure 8.2 shows the processed speed and volume in different systems. It was observed that the period across different systems was not consistent. For unknown reasons, the speed from Nov 10th to Dec 4th, 2021, was constant in the HERE system.

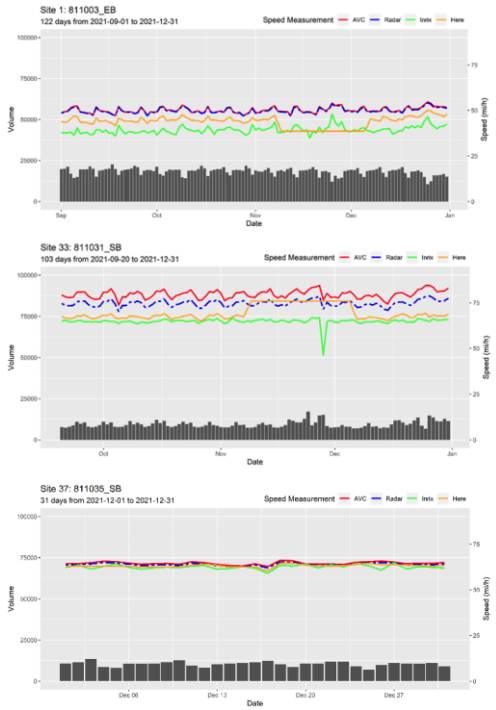

Figure 8.2 Speed and Volume provided by AVC, RADAR, INRIX and HERE. (Using Three Sites as Example)

Figure 8.3 summarizes the distribution of all average speeds on all sites in AVC, RADAR, INRIX, and HERE systems. The figure provided a general impression of the differences between different speed measurement systems. The difference may result from the unit difference shown in Figure 8.1. It may also result from the monitoring mechanisms of different systems summarized in Table 3.2. The INRIX and HERE measurements were based on probe data, while the AVC and RADAR measurements used on-site speed monitoring. The measured sample in probe data is different from on-site monitoring. Moreover, the speeds reported in different bin widths may also cause differences between AVC and RADAR. For example, 17 speeds at the RADAR system may be divided into 12 bins in AVC, resulting in a precision difference when reporting the speed on the same site.

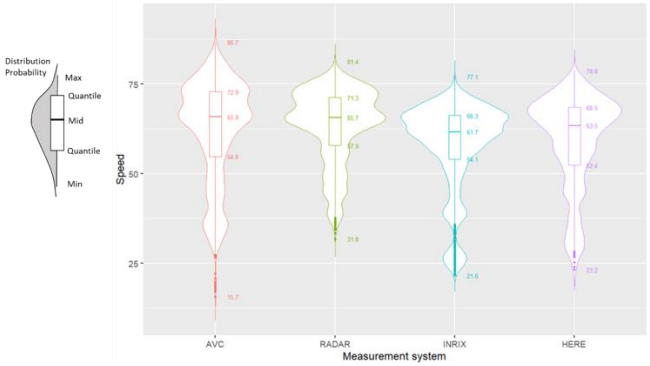

Figure 8.3 Speed Distribution in AVC, RADAR, INRIX, and HERE.

8.2 Comparison between Measurement Systems using Similarity Checking

After geospatial paring, speed measurements from four measurement systems on paired sites and segments were filtered out. Similarity checking was conducted using an index called similarity factor (Xu and Beard 2021). The similarity factor indicates the variation and magnitude of two sequences. Given two speed sequences $(v_{11}, v_{12}, v_{13}, \cdots, v_{1t})$ and $(v_{21}, v_{22}, v_{23}, \cdots, v_{2t})$, where t stands the number of timestamps, the origin similarity factor can be calculated following:

$$OriginSim(v_1, v_2) = \frac{\sum_{j=1}^{C}\left(1 - Abs\left(lev(v_{1j}) - lev(v_{2j})\right)\right)}{|v_1 \cup v_2|}$$

Figure 8.4 Origin Similarity Function

Where:

$$lev\left(v_{1j}\right) = \frac{v_{1j}}{v_{1j}+v_{2j}}, lev\left(v_{2j}\right) = \frac{v_{2j}}{v_{1j}+v_{2j}}$$

Figure 8.5 Lev function

The similarity factors were then transferred using:

$$Sim = 2e^{\frac{OriginSim-1}{1.44}} - 1$$

Figure 8.6 Similarity function

After transformation, the similarity factor Sim ranges in $[-1,1]$, where a value of one stands for the two sequences being the same, and the difference between two sequences is acceptable when the similarity factor is larger than 0. The larger the similarity factor, the closer the speed measurements are. Figure 8.7 shows the similarity factors between measurement systems across matched sites. The similarity factors were colored from red (resembles -1) to green (resembles 1). A positive similarity factor resembles the speed measurements at the same magnitude. It is observed that a): only a few sites had similar speed measurements across 4 systems; b): AVC and RADAR were more likely to have comparable measurements; 3) even the AVC to RADAR correlation was not stably comparable on several sites.

sitedir	A_R	A_I	A_H	R_I	R_H	I_H
811003_EB	0.88	-0.84	-0.56	-0.83	-0.53	-0.37
811003_WB	0.85	-0.71	-0.03	-0.72	-0.03	-0.43
811006_EB	0.69	-0.96	-0.91	-0.96	-0.93	-0.30
811006_WB	0.44	-0.94	-0.92	-0.96	-0.94	0.35
811007_EB	-0.16	-0.03	-0.58	0.56	-0.01	-0.13
811007_WB	-0.29	-0.05	-0.61	0.47	0.11	-0.17
811008_EB	-0.83	-0.50	-0.02	-0.34	-0.66	-0.08
811008_WB	-0.99	-0.94	-0.96	-0.84	-0.76	-0.06
811010_NB	-0.03	-0.55	-0.08	-0.07	0.65	-0.02
811010_SB	0.06	-0.58	-0.29	-0.21	0.34	0.09
811011_SB	0.84	-0.14	0.58	-0.07	0.49	-0.30
811013_NB	0.82	-0.96	-0.91	-0.96	-0.90	-0.31
811014_NB	0.29	-0.91	-0.82	-0.94	-0.88	-0.19
811014_SB	0.37	-0.82	-0.49	-0.88	-0.65	-0.32
811017_EB	-0.94	-0.96	-0.96	-0.80	-0.81	0.18
811017_WB	-0.95	-0.94	-0.96	-0.81	-0.62	-0.39
811020_NB	0.46	0.41	-0.16	0.76	-0.15	-0.12
811020_SB	0.71	0.54	0.17	0.62	0.15	0.11
811023_EB	-0.96	-0.97	-0.99	0.12	-0.43	-0.12
811023_WB	-0.99	-0.99	-1.00	-0.28	0.23	-0.33
811024_NB	0.09	-0.14	-1.00	0.56	-1.00	-1.00
811024_SB	0.53	0.33	-1.00	0.10	-1.00	-0.99
811025_EB	0.63	-0.30	0.22	-0.14	0.45	0.10
811025_WB	0.36	-0.42	0.15	-0.14	0.61	0.01
811026_EB	0.70	-0.43	0.19	-0.47	0.08	-0.05
811027_EB	0.56	-0.46	0.39	-0.45	0.44	-0.31
811027_WB	0.36	-0.46	-0.14	-0.24	0.22	0.25
811028_NB	0.42	-0.35	0.10	-0.08	0.28	-0.06
811028_SB	-0.16	-0.69	0.15	-0.27	0.32	-0.51
811030_NB	0.73	-0.62	-0.53	-0.66	-0.58	0.52
811030_SB	0.73	-0.72	-0.56	-0.68	-0.49	0.26
811031_NB	-0.05	-0.81	-0.72	-0.60	-0.41	0.19
811031_SB	-0.36	-0.94	-0.80	-0.80	-0.47	-0.34
811033_NB	0.90	-0.64	-0.80	-0.65	-0.81	0.06
811033_SB	0.68	-0.27	-0.45	-0.38	-0.54	0.32
811035_NB	0.25	-0.58	0.29	-0.32	0.65	-0.37
811035_SB	0.71	0.24	0.45	0.43	0.68	0.58
811041_EB	0.53	-0.88	-0.68	-0.85	-0.58	-0.35
811041_WB	0.11	-0.70	-0.64	-0.47	-0.34	0.20
811042_EB	0.65	-0.87	-0.89	-0.84	-0.86	0.34
811042_WB	0.88	-0.79	-0.95	-0.78	-0.94	-0.48
811044_NB	0.52	-0.34	-0.01	-0.15	0.28	-0.18
811044_SB	-0.07	-0.12	0.26	0.15	-0.22	-0.28
811048_NB	0.70	-0.12	-0.08	-0.14	-0.09	0.60
811048_SB	-0.97	-0.92	-0.91	-0.34	-0.49	0.48
811052_NB	0.57	-0.11	-0.66	-0.29	-0.74	-0.26
811052_SB	0.20	-0.17	-0.74	0.31	-0.56	-0.36
811053_NB	0.81	-0.68	-0.86	-0.65	-0.84	-0.10
811053_SB	0.47	-0.91	-0.80	-0.88	-0.73	-0.14
811054_EB	-0.36	-0.74	-0.99	-0.18	-0.97	-0.94
811055_NB	0.51	-0.55	-0.10	-0.42	0.16	0.00

sitedir	A_R	A_I	A_H	R_I	R_H	I_H
811055_SB	0.39	-0.74	-0.45	-0.62	-0.20	-0.06
811056_NB	-0.97	-0.95	-0.98	0.22	0.53	-0.05
811058_EB	-0.10	-0.90	-0.90	-0.78	-0.78	0.67
811058_WB	0.86	-0.83	-0.63	-0.82	-0.61	-0.06
811059_EB	0.90	-0.81	-0.91	-0.81	-0.91	-0.16
811059_WB	0.39	-0.95	-0.95	-0.93	-0.93	-0.20
811062_EB	0.43	-0.43	-0.07	-0.22	0.23	0.21
811062_WB	0.27	-0.48	-0.31	-0.67	-0.56	-0.09
811063_EB	0.58	-0.21	0.63	-0.38	0.29	-0.04
811063_WB	0.15	-0.64	0.17	-0.38	0.64	-0.43
811064_EB	0.73	-0.02	0.33	0.13	0.53	0.40
811064_WB	0.66	-0.31	0.26	-0.16	0.41	-0.14
811065_NB	0.87	0.07	0.39	0.09	0.43	0.25
811065_SB	0.93	-0.53	0.70	-0.53	0.70	-0.56
811069_NB	0.35	0.70	0.12	0.30	0.36	0.05
811069_SB	0.68	0.38	0.30	0.25	0.54	0.14
811070_NB	0.77	-0.78	-0.24	-0.75	-0.14	-0.41
811070_SB	0.69	-0.92	-0.28	-0.90	-0.16	-0.77
811072_EB	0.81	0.14	0.69	0.10	0.72	0.24
811072_WB	-0.86	-0.79	-0.62	0.32	-0.27	0.11
811501_NB	0.61	-0.70	-0.29	-0.62	-0.13	-0.14
811501_SB	0.92	-0.72	0.32	-0.72	0.31	-0.57
811502_NB	-0.35	-0.78	-0.69	-0.33	-0.05	0.41
811502_SB	-0.39	-0.86	-0.66	-0.53	0.11	-0.15
811503_EB	0.82	-0.09	0.68	-0.17	0.55	0.07
811503_WB	0.42	0.30	0.60	-0.07	0.71	0.08
811504_NB	-0.55	-0.60	-0.33	0.73	0.33	0.18
811504_SB	-0.56	-0.84	-0.72	-0.26	0.28	0.16
811506_EB	-0.31	-0.68	-0.54	-0.09	0.34	0.36
811509_EB	-0.18	-0.55	-0.17	-0.08	0.74	-0.09
811509_WB	0.71	-0.48	-0.09	-0.48	-0.11	0.07
811510_NB	0.45	-0.38	-0.22	-0.15	0.07	0.59
811510_SB	-0.33	-0.68	-0.56	-0.05	0.32	0.44
811511_NB	0.65	-0.98	-0.92	-0.99	-0.93	-0.57
811511_SB	0.25	-0.94	-0.92	-0.90	-0.88	0.46
811514_EB	-0.28	-0.70	-0.45	-0.17	0.53	0.09
811514_WB	0.07	-0.68	-0.50	-0.41	-0.07	0.27
811516_EB	0.22	-0.45	-0.31	-0.10	0.14	0.56
811516_WB	0.16	-0.35	-0.08	0.13	0.59	0.41
811518_EB	0.66	0.08	0.08	0.10	0.09	0.79
811518_WB	0.48	-0.11	-0.04	0.13	0.20	0.73
811523_EB	0.28	0.64	0.69	0.28	0.52	0.56
811523_WB	0.66	0.11	0.38	0.28	0.66	0.46
811525_NB	0.89	-0.09	-0.07	-0.04	-0.03	0.70
811525_SB	0.72	-0.26	-0.24	-0.14	-0.12	0.74
811527_NB	-0.44	-0.88	-0.59	-0.57	0.47	-0.42
811527_SB	-0.18	-0.78	-0.41	-0.47	0.43	-0.27
811528_EB	0.09	-0.77	-0.16	-0.58	0.55	-0.46
811528_WB	-0.09	-0.81	-0.26	-0.58	0.63	-0.48
811529_EB	-0.12	-0.50	-0.24	0.14	0.72	0.32
811529_WB	-0.11	-0.74	-0.53	-0.43	0.05	0.10

Figure 8.7 Similarity factors between measurement systems on matched sites Note: A: AVC; R: Radar; I: INRIX; H: HERE.

The similarity factors in Figure 8.7 were summarized in Figure 8.8 using AVC as the reference system. Preferred similarity factors should be centralized in the positive area. The higher the distribution is, the better similarity it resembles. The similarity factors between AVC and RADAR were much better than the AVC-INRIX and AVC-HERE pair. This observation was consistent with the former inference in Figure 8.3, and Figure 8.7, as the AVC and RADAR were site-based monitored systems, while the INRIX and HERE were probe-based measurement systems.

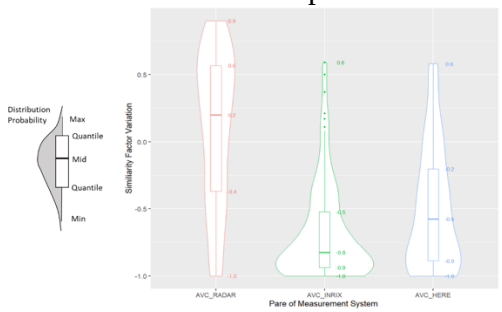

Figure 8.8 Similarity Factor Distribution using AVC as Reference.

Figure 8.9 visualizes the similarity factors in Figure 8.7 on the map. On each site, the similarity factors in Figure 8.7 were labeled with six dots in two rows. It can be observed that only a small proportion of sites had all six dots in green, representing a good similarity between all measurement systems. Compared with the site location in Figure 8.1, it is inferred that when AVC and RADAR were located close to the middle of INRIX and HERE segments, the similarity factors were likely to be high.

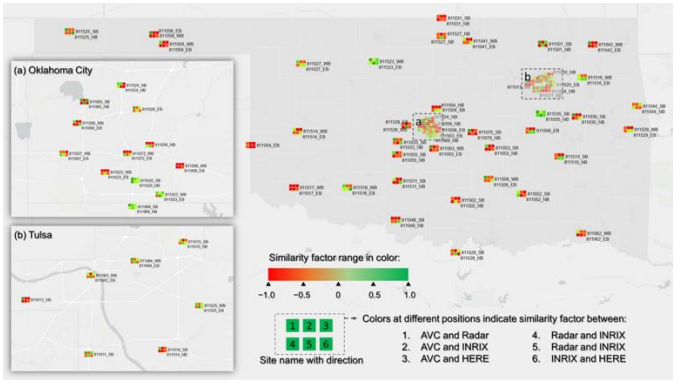

Figure 8.9 Similarity Factors on Different Sites GeoMap

Figure 8.10 plotted the speed and volume (in the AVC system) of site 811035 SB, one of the few sites with positive speed similarity factors across all pairs in the four-speed measurement systems. Figure 8.7 and Figure 8.10 shows that the similarity factor only provided a general description of the level of similarity, and further investigation into the correlation between different measurement systems was required.

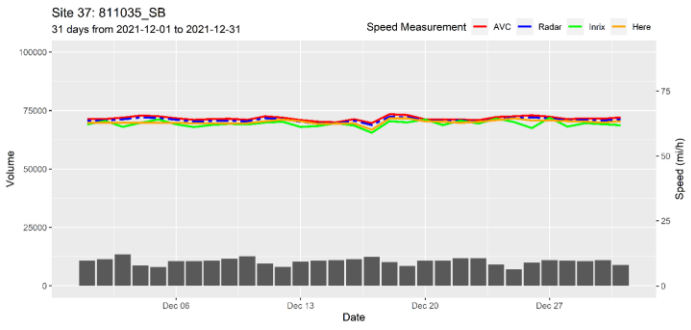

Figure 8.10 Speed comparison on site 811035 (SB)

8.3 Speed Correlation using Panel Data Regression

As the similarity factors indicate that the four speed measurement systems rarely had stable similarity on the matched sites, it is of interest to investigate the correlation between different systems. First, an Ordinary Least Squares regression (OLS) was conducted using all data on all sites. The OLS predicted AVC speed using the RADAR speed following:

$$v_{AVC} = \alpha + \beta v_{RADAR\ i,t} + \epsilon_{i,t}$$

Figure 8.11 OLS predicted AVC speed

where constant α and coefficient β are constant across groups and time. All differences in the groups were modeled in the error term $\epsilon_{i,t}$. Figure 8.8 shows the predicted AVC speed vs. the Radar speed. The blue line plotted the predicted AVC speed at different Radar speeds. Different colors resemble speed pairs measured on different sites. Although an R-square of 0.70 was achieved, several groups of speeds located apart away from the regression line and do not follow the prediction trend.

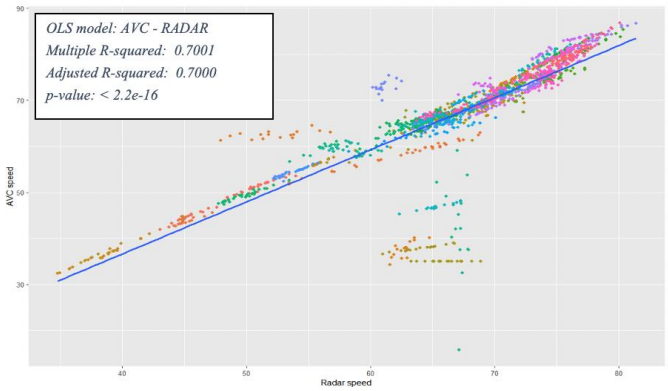

Figure 8.12 Speed comparison on site 811035 (SB)

Noticing the heterogeneity across sites, Panel data regression was adopted in this research to conduct temporal-spatial analysis. Panel data contains observations about different cross-sections across time (Croissant and Millo 2008). It combines the advantages of time series and cross-sectional data. The central idea of panel data addresses the likely dependence across data observations within the same group (Eric 2019). The panel data regression with fixed effect uses the following equation:

$$v_{AVC} = \alpha_{i,t} + \beta v_{RADAR\ i,t} + \epsilon_{i,t}$$

Figure 8.13 Panel data regression with fixed effect speed equation

Where coefficient β is constant across groups and time (that is the meaning of "fixed effects"), but the intercept $\alpha_{i,t}$ can be different across different groups.

Figure 8.14 visualizes the fixed model on AVC speed and RADAR speed. The points resemble observed results, while the lines resemble the regression results. Different sites are marked with different colors. The dashed blue line plots the former established OLS model. The colored lines show the fixed effect regression results, which use a set of parallel lines to reveal the correlation between AVC and RADAR. The fixed model has an adjusted R square of 0.9855 and a quite small p-value, indicating high confidence in the model. In a word, **Error! Reference source not found.**

shows that the fixed effects panel data regression model achieved good performance on almost all sites.

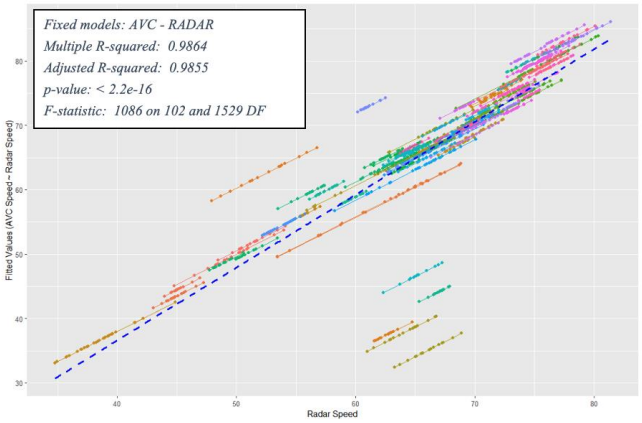

Figure 8.14 AVC-RADAR Speed Correlation using Panel Data Regression

Figure 8.14 and Figure 8.15 show the fixed effects panel data regression model that predicts AVC speed using INRIX and HERE, respectively. It was observed that the R-square of all fixed effects models were higher than 0.95, and their p-values were small. This observation indicates that on the paired sites, the AVC speed can be predicted well using fixed effects panel data regression from other speed measurement systems. Further, the correlation is time-independent, meaning the prediction formula is seldom affected by time. Thus, transportation agencies can build the panel data regression model on their preferred reference measurement system.

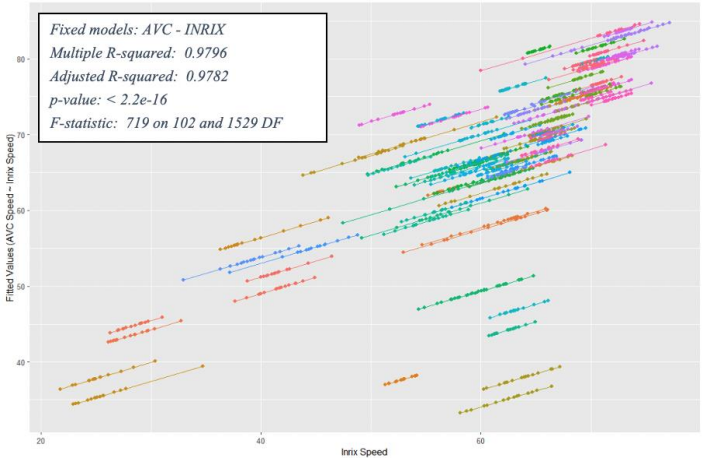

Figure 8.15 AVC-INRIX Speed Correlation using Panel Data Regression.

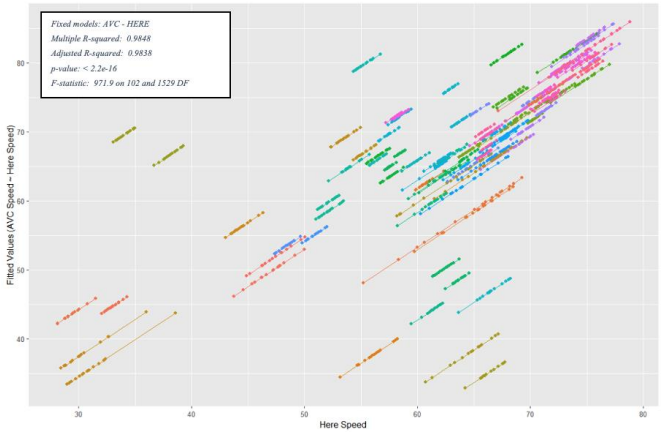

Figure 8.16 AVC-HERE Speed Correlation using Panel Data Regression.

8.4 Summary

This chapter investigated the spatial and temporal correlation between different speed measurement systems. Key findings can be summarized as follows:

- The speed variations among AVC, RADAR, INRIX, and HERE systems may result from their differences in basic units and measurement mechanisms. AVC and RADAR were site-based monitoring systems and recorded speed with different bin widths. INRIX and HERE were probe-based systems and adopted different basic segments.
- Similarity factors gave a general site-by-site comparison between various speed measurements. The similarity factors between AVC and RADAR were much better than the AVC-INRIX and AVC-HERE pair. However, even the AVC to RADAR correlation was not stably comparable on several sites
- A reliable prediction of AVC speed can be achieved using panel data analysis considering fixed effects. The fixed effects model has an R square higher than 0.95, and the correlation is time-independent. Transportation agencies can build the panel data regression model on their preferred reference measurement system.

The resulting findings regarding speed measurements displayed in the higher agreement between AVC vs. Radar compared to AVC vs. (INRIX or HERE) align with the results found in Table 4.1.

Chapter 9: Conclusion

Oklahoma Department of Transportation (ODOT) has access to and uses four different sources of datasets for their traffic analysis and roadway designs. Some degree of variability among the collected data exists. This project will investigate and quantify the variability among the four datasets by comparing their collected data against traffic speed and volume measurements; as well as evaluate travel time (TT) estimation for nine routes whose TT are currently being monitored and determined in real-time using speed data obtained by HERE—one of the four sources. Traffic conditions (free-flow or congestion) under which variability increases or decreases are identified and highlighted. The project also investigates the potential use of radars to provide real-time TT estimation for the nine routes. This makes the network of radars a backup system that ODOT may use when the real-time (RT) speed data streaming provided by a contractor is disrupted; otherwise, radar data could potentially be augmented to the RT data to improve TT accuracy or be used to validate RT speed data.

The two sources of datasets are obtained by a network of collocated radars and automatic vehicle counts (AVC) sites. Both systems are sensor-based and deployed across Oklahoma National Highway System (NHS). They are owned and operated by ODOT. The remaining two sources are probe-based systems—HERE and INRIX—that employ traveling passengers' cellphone data or in-vehicle transponders installed in commercial vehicles. While HERE is contracted by ODOT to provide the RT speed data streaming used to calculate the TT for the nine routes, INRIX data is provided monthly by FHWA. Table 9.1 summarizes the characteristics of each of the data sources in terms of type, sampling rate, data availability, speed measurement type, and source. The speed and vehicle volume analysis is conducted using data from 85 radar and AVC sites.

Table 9.1
Radar, AVC, HERE, INRIX Systems Characteristics

System	Type	Sampling Rate	Data availability	Speed	Source
Radar	Sensor	1 min	Real-time	17 bins	ODOT
AVC	Sensor	15 min	Daily	12 bins	ODOT
INRIX	Probe	5 min	Monthly	Average	Outsourced
HERE	Probe	5 min	Real-time	Average	Outsourced

Vehicle Speed Analysis: In order to obtain accurate speed comparisons among all four systems, it is necessary the identify highway locations shared among all four systems. It was easy to find many

sites where Radars and AVCs are collocated. Using these locations, the research team determined the HERE and INRIX highway segments within which the radar/AVC sites are located. Analyses are carried out under free-flow and low-speed (congested) flow conditions. The speed comparison results for free- and congested flows are presented in Table 9.2 and Table 9.3, respectively. Data used for the analysis was obtained between August and December 2021. The tables present mean absolute error (MAE) in miles per hour (MPH), the percentage of time in which one system is measured with lower speed, the average positive difference, and the average negative difference.

Table 9.2
Speed Comparison under Free-Flow Traffic Condition.

Systems	**MAE** (MPH)	**Time with lower speed (%)**	**Avg. pos diff** (MPH)	**Avg. neg diff** (MPH)
AVC vs. RADAR	**3.02**	Radar was **60.22%** of the time lower than AVC	3.66 (radar is higher)	2.61 (radar is lower)
AVC vs. HERE	**6.7**	HERE was **77.8%** of the time lower than AVC	6.77 (HERE is higher):	6.69 (HERE is lower):
AVC vs. INRIX	**7.1**	INRIX was **84.1%** of the time lower than AVC	5.37 (INRIX is higher)	7.45 (INRIX is lower)
Radar vs. INRIX	**5.6**	Radar was **16%** of the time lower than INRIX	6.0 (radar is higher)	3.86 (radar is lower)
Radar vs. HERE	**5.7**	Radar was **26.52%** of the time lower than HERE	6.65 (radar is higher)	3.44 (radar is lower)
INRIX vs. HERE	**4.5**	INRIX was **70.77%** of the time lower than HERE	3.67 (INRIX is higher)	4.87 (INRIX is lower)

Table 9.3
Speed Comparison under Low-Speed (<40MPH) Traffic Conditions.

Systems	**MAE** (MPH)	**Time with lower speed (%)**	**Avg. pos diff** (MPH)	**Avg. neg diff** (MPH)
AVC vs. RADAR	**3.36**	Radar was **13.05%** of the time lower than AVC	3.35 (radar is higher)	3.39 (radar is lower)
AVC vs. HERE	**8.77**	HERE was **56.39%** of the time lower than AVC	7.13 (HERE is higher)	10.04 (HERE is lower)
AVC vs. INRIX	**12.6**	INRIX was **88.71%** of the time lower than AVC	6.54 (INRIX is higher)	13.83 (INRIX is lower)
Radar vs. INRIX	**11.89**	Radar was **7.94%** of the time lower than INRIX	12.6 (radar is higher)	3.73 (radar is lower)
Radar vs. HERE	**9.79**	Radar was **11.6%** of the time lower than HERE	10.54 (radar is higher)	3.44 (radar is lower)
INRIX vs. HERE	**5.55**	INRIX was **72%** of the time lower than HERE	4.13 (INRIX is higher)	6.11 (INRIX is lower)

Before drawing any conclusion, it should be pointed out that speed data per system under evaluation is collected and calculated differently. Radar and AVC collect speed data per vehicle; then it places vehicles' speeds in their respective 5 mph bins. To calculate an average speed per

site, it is assumed that vehicles, whose speeds are placed in one bin, travel at a speed equal to the midpoint. Using midpoint speeds, number of vehicles per bin, and total number of vehicles, an average speed per site location is calculated. Unlike radar and AVC, HERE and INRIX provides their speed or TT data, respectively, averaged for a highway segment whose length is provided and may vary per radar site, affecting its average calculation. Longer segments will have a higher averaging effect. Furthermore, HERE and INRIX average speed calculation is highly affected by the number of reporting vehicles since they are probe-based systems. Lower vehicle count will render biased average speed calculations.

The results depicted in the preceding tables indicate the following observations.

- Average speeds measured by sensor-based (radar, AVC) sites are on average within 4 mph, regardless of traffic conditions.
- Average speeds measured by probe-based (HERE, INRIX) sites are on average within 5 mph, regardless of traffic conditions. This could be to different segment lengths and numbers of reporting vehicles.
- Speed measurements determine by sensor-based systems (radar, AVC) are always higher than those of probe-based systems (HERE, INRIX). This could be a result of averaging speed over a length of the segment while the radars measure the speed at discrete sites.
- Speed differences between sensor- and probe-based systems grew at least one-fold under traffic congestion conditions (<40mph). This could be explained that radar and AVC are known to have less accurate measurements for low-speed traffic. While HERE and INRIX are anticipated to have better accurate measurements since vehicles spend more time to travel their segments; hence reporting more measurements.

Table 9.4 compares the speed among radar, HERE, and INRIX for a period of one year (Aug. 2021 to July 2022). This analysis is carried out under free-flow traffic conditions for the same sites and segments used in Table 9.2 and Table 9.3. The table shows that average speeds measured by radars are within 5 mph to those measured by HER and INRIX, confirming the results presented in Table 9.2.

Table 9.4
Speed Comparison between Radar, HERE, and INRIX for one year.

Systems	**MAE** (MPH)	**Time with lower speed (%)**	**Avg. pos diff** (MPH)	**Avg. neg diff** (MPH)
Radar vs. INRIX	**5.24**	Radar was **18.74%** of the time lower than INRIX	5.39 (radar is higher)	4.58 (radar is lower)
Radar vs. HERE	**5.08**	Radar was **27.82%** of the time lower than HERE	5.69 (radar is higher)	3.5 (radar is lower)
INRIX vs. HERE	**4.35**	INRIX was **70.37%** of the time lower than HERE	3.54 (INRIX is higher)	4.7 (INRIX is lower)

Travel Time (TT) Analysis: This section concludes the feasibility of utilizing the radar speed measurement for travel time (TT) estimations. Nine routes (corridors) situated along major interstate highways in metropolitan areas of Oklahoma City and Tulsa are selected and evaluated for TT accuracy. TT estimation using radars is compared to those calculated using probe-based systems, namely HERE and INRIX. This comparison was performed under various traffic conditions, including different time periods and speed ranges to gain insights into the inherent differences and capabilities of the radar in TT estimations. These routes commenced at a location near a DMS display and terminated at a nearby intersection. The chosen nine routes vary in length

from one to twelve miles and are equipped with one to three radar units; but constructed with many HERE or INRIX segments, as shown in Table 9.5.

The analysis includes various time periods, constituting a range of peak and off-peak periods; as well as diverse speed ranges that cover both traffic conditions: free-flow and low-speed congestion. The analysis includes the following periods: all hours, 8 AM-6 PM, peak hours (morning 6-10 AM and afternoon 4-8 PM), and Off-peak hours (10 AM-4 PM and 8 PM-6 AM). Furthermore, the speed ranges considered in the analysis include free-flow conditions while filtering out all sites identified erroneously, all speed ranges with no Filtering, speed ranges between 0 to 40 mph, and speed ranges between 0 to 50 mph.

Table 9.5
Nine Selected Routes to Study TT Using the Radars.

Route	Length (miles)	Number of Radars	Number of INRIX segments	Number of HERE segments	Highway	City
1	5	2	13	7	I-35	OKC
2	9	3	35	19	I-40	OKC
3	7	2	17	10	I-40	OKC
4	12	3	24	12	I-40	OKC
5	2	1	4	2	I-44	OKC
6	6	2	16	8	I-44	OKC
7	4	2	8	4	I-44	Tulsa
8	9	3	20	10	I-44	Tulsa
9	4	2	12	7	SH-51	Tulsa

Travel time analyses are presented in Table 9.6. It shows absolute differences between TT calculated using radar measurements versus HERE and/or INRIX. A total of 16 tests were conducted for various periods and speed ranges. Processed data were collected between August 2021 to May 2022. The time shown in Table 9.6 is the differences averaged across all nine routes.

Table 9.6
TT Absolute Difference Comparison among Radar, HERE, INRIX.

Test	Speed range	Time period	MAE (TT) in minutes	MAE (TT) in minutes	MAE (TT) in minutes
			INRIX vs. HERE	**INRIX vs. Radar**	**Radar vs. HERE**
1	All	8 AM – 6PM	0.61	0.72	0.61
2	Outlier Removal	8 AM – 6 PM	0.45	0.52	0.41
3	0-40MPH	8 AM – 6 PM	2.55	5.59	4.45
4	0-50MPH	8 AM – 6 PM	1.73	2.82	2.41
5	All	All	0.64	0.69	0.51
6	Outlier Removal	All	0.47	0.46	0.25
7	0-40MPH	All	2.45	5.1	4.04
8	0-50MPH	All	1.6	2.75	2.21
9	All	Peak	0.7	0.76	0.64
10	Outlier Removal	Peak	0.47	0.53	0.37
11	0-40MPH	Peak	2.37	5.48	4.33
12	0-50MPH	Peak	1.62	2.92	2.37

Test	Speed range	Time period	MAE (TT) in minutes	MAE (TT) in minutes	MAE (TT) in minutes
13	All	Off-Peak	0.59	0.64	0.43
14	Outlier Removal	Off-Peak	0.48	0.46	0.23
15	0-40MPH	Off-Peak	2.56	4.8	3.8
16	0-50MPH	Off-Peak	1.55	2.5	1.98

Table 9.7 and Table 9.8 aggregate results shown in Table 9.6 to summarize the TT differences for different speed ranges regardless of period and different periods regardless of the speed range.

Table 9.7
TT Difference between Radar and HERE Data at Different Speed Ranges

Speed range	Radar vs. HERE MAE (in minutes)
All (any speed)	0.55
Outlier Removal	0.31
0 – 40 MPH	4.16
0 – 50 MPH	2.24

Table 9.8
TT Difference between Radar and HERE for Different Time Periods.

Time	Radar vs. HERE MAE (in minutes)
8 AM – 6 PM	1.97
All (any time)	1.75
Peak	1.93
Off-Peak	1.61

The TT calculations presented in the last three tables may lead to the following observations.

- Under free-flow traffic conditions, TT estimation using radar speed is on average within one minute from the TT calculated using HERE speed data, regardless of route length, number of radar units within a route, and speed range. Noting, HERE data is the data streaming that ODOT uses for RT travel time calculations displayed on highway displays.
- Under slow-speed traffic conditions, the absolute TT difference on average grows two folds to within 4 minutes, especially at lower speeds (<40mph). This large difference is due to two factors: the radar's elevated speed measurement inaccuracy during congestions and the low sample size used for the calculations.
- Radar TT estimations are on average within two minutes of that of HERE's, regardless of the time period.

Travel Time Estimation using Machine Learning Models: multiple machine learning (ML) algorithms are developed to assess the potential of providing improved TT estimation accuracy as compared to the results achieved using HERE data. A data table is constructed for training the ML models. This table includes speed measurements per route under free-flow traffic conditions and route length. This table was then labeled using HERE travel time estimations summed for all route segments to generate a total TT per route. The final table is used for training the models and testing their prediction accuracy per route. Various ML algorithms are trained using a partial dataset obtained randomly from the table and tested on the remaining unused dataset. The ML models used for the TT estimation are listed in Table 10.

Table 9 shows the absolute differences per route between the baseline model and the deviation from the baseline per route. The baseline is calculated by averaging TT values per route using HERE data. For example, route one requires on average 4.53 minutes to completely travel. Its deviation using real-time speed data under free-flow conditions is averaged to 0.1 minutes. This developed baseline will be used as the basis to evaluate the accuracy of the ML-based predictors shown in Table 9.10.

Table 9.9
Average Absolute Difference as Compared to HERE TT Estimation.

Route	HERE Baseline TT (minutes)	MAE (minutes)
1	4.53	0.1
2	8.15	0.27
3	7.51	0.32
4	10.87	0.27
5	1.62	0.04
6	6.49	0.84
7	3.08	0.07
8	7.71	0.16
9	3.75	0.06

Table 9.10 shows the mean absolute error (MAE) averaged across all nine routes using various ML algorithms. The baseline model shows an average of 0.24 minutes (obtained by averaging MAE in Table 9.9 across all routes). Hence, every ML model listed in Table 9.10 and whose MAE is lower than the average 0.24 is considered a better predictor of TT than the HERE baseline.

Table 9.10
Machine Learning Models used for TT Estimation.

Model	MAE (minutes)
Decision Tree	0.18
Elastic Net	0.23
Random Forest	0.18
Gaussian Random Process	0.20
Lasso Regression	0.20
Linear Regression	0.20
Neural Network	0.31
Polynomial Regression	0.19
Ridge Regression	0.20
Robust Huber	0.19
Robust Ransac	0.21
Robust Theil	0.26
Support Vector Machines	0.19
XGBoost	0.18

Attempts to improve the performance of the ML models were conducted. One such attempt was to incorporate into the original training table speed measurements collected by radars located in neighboring interstate highways. These neighboring radars are strategically selected on segments of the roadways that either feed vehicles into the routes under evaluation or take them away. Speed correlation analysis was conducted between the two sets of radars (within and neighboring the route). Measurements that were found highly correlated were not included in the new training data table. The improvements achieved after enhancing the table were observed limited.

No ML models were developed under traffic congestions, due to the fact that the data sample size was small, preventing the models to converge to accurate TT predictors.

In conclusion, the results demonstrate that machine learning models can be trained to leverage radar data for travel time estimations. Nonetheless, it should be noted that there exist inherent differences in speed measurements between radar data and HERE data, as previously illustrated in the comparison results. Such differences may be particularly pronounced in low-speed conditions and should be taken into consideration when interpreting the models' output.

Vehicle count (volume) Analysis: The PI and his research team conducted a volume analysis between the radar sites collocated with the AVC sites. The analysis will show the sample size of speed measurements used in the aforementioned analysis and modeling. It highlights the small size of speed measurements collected during congestion periods, that lead to poor TT estimation performance. Table 9.11 presents volume comparison results between radar and AVC sites of data collected over a period spanning September to December 2021. Volume analyses were conducted under sixteen different scenarios to capture volume discrepancies under various traffic conditions (free-flow, low-speed) and time periods (peak, off-peak, etc.). The table presents the mean absolute difference per unit time of 15 minutes between the radar and AVC across all sites. It also presents mean absolute percentage error– showing the portion of vehicles.

Table 9.11
Vehicle Volume Comparison Analysis per Speed group and Per Time Group (September to December 2021)

Experiment	Speed	Time	**Volume MAE**	**Volume MAPE (%)**	% of time Radar volume < AVC volume	Avg. positive difference (radar is higher)	Avg. negative difference (radar is lower)
1	All	8 AM – 6PM	33.01	18.03%	50.35%	43.06	23.1
2	Outlier Removal	8 AM – 6 PM	31.76	17.55%	50.42%	41.92	21.77
3	0-40MPH	8 AM – 6 PM	83.07	41.8%	50.8%	140.16	27.79
4	0-50MPH	8 AM – 6 PM	32.71	18.29%	51.8%	47.79	18.67
5	All	All	24.88	24.4%	47.44%	28.77	20.57
6	Outlier Removal	All	24.41	22.31%	48.08%	28.88	19.59
7	0-40MPH	All	64.73	49.45%	47.08%	98.33	26.95
8	0-50MPH	All	22.8	24.57%	46.65%	28.73	16.01
9	All	Peak	32.59	21.2%	47.82%	38.81	25.79
10	Outlier Removal	Peak	30.77	20.38%	47.94%	37.44	23.53
11	0-40MPH	Peak	83.92	44.8%	46.78%	127.84	33.95
12	0-50MPH	Peak	31.92	20.36%	47.44%	42.45	20.25
13	All	Off-Peak	21.61	25.39%	48.18%	24.04	18.99
14	Outlier Removal	Off-Peak	21.76	23.14%	48.99%	24.75	18.65
15	0-40MPH	Off-Peak	52.18	50.47%	48.16%	80.29	21.92

Experiment	Speed	Time	**Volume MAE**	**Volume MAPE (%)**	% of time Radar volume < AVC volume	Avg. positive difference (radar is higher)	Avg. negative difference (radar is lower)
16	0-50MPH	Off-Peak	18.4	25.87%	47.48%	22.1	14.31

Table 9.12 and Table 9.13 aggregate results shown in Table 9.11 to summarize the volume analysis for various speed ranges regardless of time period and various time periods regardless of speed range.

Table 9.12
Vehicle Volume aggregated during Different Periods.

Speed	MAE (vehicles)	MAPE (%)
All (any speed)	28.02	22.26%
Outlier Removal	27.18	20.84%
0 – 40 MPH	70.98	46.63%
0 – 50 MPH	26.46	22.27%

Table 9.13
Vehicle Volume aggregated for All Speed Ranges.

Time	MAE (vehicles)	MAPE (%)
8 AM – 6 PM	45.14	23.92%
All (any time)	34.21	30.18%
Peak	44.8	26.88%
Off-Peak	28.49	31.22%

The previous results demonstrate around a 20% difference in volume in free-flow conditions between radar and AVC. However, in low-speed conditions, the difference increased to 46%.

Table 9.14 shows the volume comparison results for the period spanning from September 2021 to August 2022. Looking at the results presented in Table 9.11,Table 6.1 for the period from September to December 2021, we notice that the results are similar which shows that the results of the previous table were statistically representative. For instance, the MAE and MAPE for the 8 AM – 6 PM were 33.01, and 18.03%, respectively, in Table 6.1. The values of MAE and MAPE, Table 6.4, were 28.65, and 18.16%, respectively.

Table 9.14
Vehicle Volume Comparison Analysis for one year (September 2021 to August 2022) Per Time Group

Time	MAE (vehicles)	MAPE (%)
8 AM – 6PM	28.65	18.16%
All	21.99	24.92%
Peak	28.43	21.36%
Off-Peak	19.32	26.16%

Chapter 10: References

[1] Lu, C., & Dong, J. (2018). Estimating freeway travel time and its reliability using radar sensor data. *Transportmetrica B: Transport Dynamics, 6*(2), 97-114.

[2] Li, R., Rose, G., & Sarvi, M. (2006). Evaluation of speed-based travel time estimation models. *Journal of Transportation Engineering, 132*(7), 540-547.

[3] Wang, H., Tang, X., Kuo, Y. H., Kifer, D., & Li, Z. (2019). A simple baseline for travel time estimation using large-scale trip data. *ACM Transactions on Intelligent Systems and Technology (TIST), 10*(2), 1-22.

[4] Van Lint, J. W. C. (2008). Online learning solutions for freeway travel time prediction. *IEEE Transactions on Intelligent Transportation Systems, 9*(1), 38-47.

[5] Ban, X. J., Li, Y., Skabardonis, A., & Margulici, J. D. (2010). Performance evaluation of travel-time estimation methods for real-time traffic applications. *Journal of Intelligent Transportation Systems, 14*(2), 54-67.

[6] Croissant, Y., & Millo, G. (2008). Panel data econometrics in R: The plm package. Journal of statistical software, 27(2).

[7] Gentili, M., & Mirchandani, P. B. (2018). Review of optimal sensor location models for travel time estimation. *Transportation Research Part C: Emerging Technologies, 90,* 74-96.

[8] Xu, F., & Beard, K. (2021). A Unifying Framework for Analysis of Spatial-Temporal Event Sequence Similarity and Its Applications. ISPRS International Journal of Geo-Information, 10(9), 594.